2017

Comprehensive Structural, Thermal and Toxicological Characterization of 1-Ethyl-3-Methylimidazolium Alkylbenzenesulfonate Ionic Liquids

Hiranmayee Kandala
South Dakota State University

COMPREHENSIVE STRUCTURAL, THERMAL AND TOXICOLOGICAL CHARACTERIZATION OF 1-ETHYL-3-METHYLIMIDAZOLIUM ALKYLBENZENESULFONATE IONIC LIQUIDS

BY

HIRANMAYEE KANDALA

A dissertation submitted in partial fulfillment of the requirement for the

Doctor of Philosophy

Major in Chemistry

South Dakota State University

2017

COMPREHENSIVE STRUCTURAL, THERMAL AND TOXICOLOGICAL CHARACTERIZATION OF 1-ETHYL-3-METHYLIMIDAZOLIUM ALKYLBENZENESULFONATE IONIC LIQUIDS

This dissertation is approved as a creditable and independent investigation by a candidate for the Doctor of Philosophy degree and is acceptable for meeting the dissertation requirements for this degree. Acceptance of this dissertation does not imply that the conclusions reached by the candidate are necessarily the conclusions of the major department.

Douglas E. Raynie Date
Dissertation Advisor
Head, Chemistry & Biochemistry

Dean, Graduate School Date

I dedicate this dissertation

to the strongest woman I have ever known,

my mom, Swarna Kandala

ACKNOWLEDGEMENTS

As in Helen Heyes quote, ‘The expert in anything was once a beginner’, my journey to doctoral life began with a storm of scattered thoughts. It was my research advisor, Dr. Doug Raynie, who mentored me in shaping my thoughts into a meaningful sculpture. I remember he used to say something like, “you should know when to put a period to your work”. This sentence not only guided me academically but also supported me emotionally to get through the rough road while completing the final chapters of my dissertation. He gave me enough freedom and moral support that I need to move on and transition into an independent research scientist. I would like to convey my deepest appreciation to my mentor Dr. Raynie for his patience, support and his very own way of teaching me cutting edge research.

Teaching is my passion, which I believe I inherited from my grandpa and then from my mom. However, Dr. Matthew Miller introduced me to non-traditional and creative teaching. He is a very energetic and enthusiastic person and I feel that his way of teaching is contagious. Thank you Dr. Miller for motivating me to think outside the box with your inspiring teaching methodologies. When it comes

to teaching, I would definitely thank Dr. Ronald Hirko, who has a big contribution in shaping my teaching brain. Dr. Fathi Halaweish is one of the smartest people I know and his projects introduced me to the real roots of structural determination of unknown compounds. I am grateful to Dr. Halaweish for many insightful scientific discussions and suggestions about life after grad school.

I thank Dr. Chandradhar Dwivedi, distinguished professor and pharmacy department head emeritus, for being very supportive of me when I the president of Indian Students Association. Thank you Dr. Dwivedi ji and it was simply an honor knowing you. I also thank Dr. Kasiviswanathan Muthukumarappan for providing me ample access to all thermal analysis instrumentation in the Department of Agriculture at SDSU.

I thank Dr. James Rice for teaching me all do’s and don’ts about presentation and how to present my work to a scientific audience. I thank all staff and my colleagues at South Dakota State University, specially Stephanie Jensen and Jaque Mann for always being so helpful and friendly. I will forever be thank full to my lab mates George Gachumi, Vinod Bathula, Vara Sakampally, Victor Essel, Tunde Dioszegi, John Kiratu, Sampson Asare, Priya Sarvanan, Tanvir Amit, Raj Bhandari, Joseph Dzisam, and Randy Jackson

for all the laughs and good times that we shared in our chemistry journey. I specially thank Vara Sakampally for being a wonderful friend and for all the road trips and fun activities we've been together. Your friendship is invaluable to me.

I was lucky to have a good support system and people around me who helped me in staying sane. I thank my backpacking friends Balaji Venuthurumilli, Siva Maddineni, Akash Reddy Challa, Vinod Kallam, Sasi Rajulapati and Anusha yalavarthi, for all the good memories at SDSU. I thank Kelly, the janitor. I like to think of her as the guardian angel, as she was the person looking after me when I was working late preparing for exams or writing up dissertation. She used to get me little cookies as late night snack and talked about all non-science things in the world that kept me awake and going without coffee even after she left.

I extend my deepest acknowledgements to Anay Kudire, who has been there with me during my roughest doctoral road run. He has always been there for me as great supporter and friend in need with his never fading smile and super positive attitude. I thank you for being so patient with me and for sticking by my side even in my tough times.

My Family has always been my strength and the hope to keep moving further. My father and mother always had faith in me even in times when I lost faith in myself. It's their continuous support and encouragement that fuelled me these past years. I feel that their unconditional love and confidence in me made me walk that extra mile. My sister Amuktha Harathi, has always been my best friend all my life. I thank my BIL, Dinesh Harathi for all his advices and supportive talks that got me through the toughest times. Special thanks to the newest additions to my family, my nieces, Aanya and Ameya Harathi, who have been constantly setting high standards for me to inspire them. I love my family and dearly thank them for all their support and faith in me. All together, we made it!!

TABLE OF CONTENTS

ABSTRACT

COMPREHENSIVE STRUCTURAL, THERMAL AND TOXICOLOGICAL CHARACTERIZATION OF 1-ETHYL-3-METHYLIMIDAZOLIUM ALKYLBENZENESULFONATE IONIC LIQUIDS

HIRANMAYEE KANDALA

2017

Synthesis and characterization of 1-ethyl-3-methylimidazolium alkylbenzenesulfonate ionic liquids for extraction of lignin from prairie cord grass have been studied. The ionic liquids (ILs) 1-ethyl-3-methylimidazolium benzenesulfonate (EBS), 1-ethyl-3-methylimidazolium toluenesulfonate (ETS) and 1-ethyl-3-methylimidazolium xylenesulfonate (EXS) have been synthesized in this research. An extensive structural, physical, thermal and toxicological characterization has been performed to understand the behavior of these ionic liquids.

The reaction yield for the synthesis of EBS, ETS, and EXS ionic liquids was determined to be 91.2 ± 1.5 %, 96.1 ± 0.7 %, 99.0 ± 0.5 % respectively. Spectral analysis using NMR and FTIR confirms the structure of these ionic liquids. The Kamlet-Taft properties of these ionic liquids have been

determined using solvatochromic probes limited to Reichardt's dye, 4-nitroaniline and N,N-diethyl-4-nitroaniline. Viscosity, polarity and hydrogen bond acidity of EBS, EEBS, ETS, and EXS ILs was found to increase with increasing methylation and anion size in the following order EBS < ETS < EXS.

Thermal analysis of the ILs has been performed using DSC and TGA. Study of the glass transition and mesomorphic phases has been analyzed using DSC. The TGA has been used to determine thermal stability of the ILs. The EBS and EEBS were found to have decomposition onset around 349 °C, which is higher than the decomposition onset of ETS and EXS at 331 °C and 319 °C respectively. Thermal behavior of the ILs has been studied at different nitrogen flow rates, where the significant mass loss after 300 °C was attributed to thermal decomposition of ILs.

Toxicological studies were performed using LDH, MTT and Ames assays. The EXS exhibited highest cytotoxicity and genotoxicity followed by ETS and then EBS. The optimal temperature in the lignin extraction study was found to be at 90 °C for 3 hours without addition of water or steam-pretreatment. The percent lignin extracted from PCG using EBS, EEBS, ETS and EXS ILs was found to be 17.5±0.28, 17.4±0.53, 19.6±0.07 and 21.9±0.05 respectively.

CHAPTER 1

INTRODUCTION AND BACKGROUND

1.1. Biomass as a Renewable Energy Source

Biomass is an extremely valuable and potentially clean renewable source of energy. Biomass is an abundant source of sustainable energy, which is generally carbon neutral. To make it truly carbon neutral, we need to keep up a continuous cycle of cultivating biomass and using it as fuel, so that the carbon is reabsorbed in the cycle. There is a large variety of biomass available, ranging from corn stalks, soy, grasses, and wood to animal fat. Use of abandoned land reduces the pressure on land use and using grasses instead of corn may address the food versus fuel issue.

1.1.1. Need for Fossil Fuel Alternative: Biofuel

There is a huge demand for fuel to keep the transportation connecting the entire world intact and this demand is expected to grow drastically in the future. With the rate that the fossil fuels are being depleted, there is a growing concern for the search of alternative fuels. Biofuels derived from corn, sugarcane, grasses, and wood are high in octane levels and can be used in gasoline

blends. Most of these biofuel and gasoline blends exhibit increased oxidative stability and lubricity.[1] The other advantages of biofuels are very low sulfur levels and reduced emissions.

Due to the rapid rate of fossil fuel depletion, it is necessary to transition toward renewable carbon bio-resources. Energy experts predict a 35% upsurge in the worldwide demand for petroleum and a 25% increase in U.S. alone by the year 2025 compared to current needs.[2] The fossil-fuel energy challenge has a strong relationship with greenhouse gases and global climate stability. The energy crisis of the 1970s ignited interest in the potential of biofuels to decrease energy dependence.

This shift from petroleum to renewable bioresources is a significant step toward development of a sustainable future. The United States Department of Energy (DOE) aims at replacing around 30% of petroleum fuels and 25% of industrial organic chemicals used currently with biomass-derived products by the year 2025.[3,4] Now the major challenges would be to develop crops with suitable physical and chemical traits and to develop designer solvents to extract specific biomass components like cellulose and lignin.

1.2. Lignin is the Missing Link

Around 40—50 million tons of lignin is being produced as noncommercial waste around the world every year.[2] Lignin is the second most abundant organic polymer and hence lignin is nothing but waste comprising about 37% of the natural carbon content on earth. Lignin is a renewable source of energy and a potential source of biofuel that can be a good alternative to fossil fuel. Lignin is made of phenylpropanoid units and has less oxygen content compared to cellulose. Therefore, biofuel from the pyrolysis of lignin would have higher oxidative stability that would aid in achieving longer shelf-life and better quality transportation fuel.

Cellulose can be hydrolyzed to ethanol and lignin from left-over biomass residue can be isolated to produce biofuel like high octane jet fuel or turn it into high-value organic compounds like vanillin. This makes the biorefinery more efficient and profitable. Lignin is a complex polymer and its structure makes it difficult to isolate qualitatively from biomass. This study focuses on selective extraction of linin from prairie cordgrass using 1-ethyl-3-methylimidazolium alkylbenzenesulfonate ionic liquids.

1.3. Conventional Methods to Isolate Lignin

There are several methods available for lignin isolation but none of them can be used for quantitative analysis. Table **1** shows some common methods used in the isolation of lignin.[5] Milled-wood lignin (MWL) is most preferred in qualitative analysis as it is considered to be an appropriate representation of proto-lignin. Milled-wood enzyme lignin (MWEL) is similar to MWL but involves treatment with polysaccharidase enzymes to solubilize carbohydrates. The MWEL residue contains a large content of lignin but has about 10-12% of residual carbohydrates from the covalent linkages between lignin and polysaccharide fragments.[5] Due to the high molecular weight of MWEL, it is not soluble in common lignin solvents such as dioxane and dimethyl sulfoxide (DMSO).[5]

Some of the other lignin-treatment methods include hydrochloric acid lignin, periodate lignin, enzymatically liberated lignin, alcohol-HCl lignin, thioglycolic acid lignin, acetic acid lignin, dioxane-HCl lignin, phenol lignin, and hydrogenolysis lignin.[6] The Braun's native lignin has a very low molecular weight which is neither suitable for qualitative nor structural analysis.[7]

Table 1. Lignin isolation methods[5] (Table adopted from reference 5).

Preparation	Methodology	Remarks
Milled-wood lignin (MWL)	Aqueous dioxane extraction of finely milled-wood	About 20% yield considered to be representation of original lignin
Milled-wood enzyme lignin	Residue left after polysaccharidase hydrolysis of carbohydrates in finely milled-wood	95% yield but contains around 10-12% carbohydrates. Not completely soluble in normal lignin solvents.
Cellulase enzyme lignin (CEL)	Solvent fraction of MWEL	Similar to MWL
Braun's native lignin	Ethanol extract of ground wood	Lower yield and lower molecular weight than MWL
Brown rot lignin	Ethanol or aqueous dioxane extract of brown-rotted wood	Not severely altered but some demethylation of methoxyls and oxidation of side chains has occurred
Chemical lignin (Kraft and sulfite)	Dissolution of lignin at high temperature and pressure with chemicals	Not representative of original lignin. Major by-products in pulp production to make paper
Klason lignin	Insoluble, condensed residue left after hydrolysis of polysaccharides with sulfuric acid	Not representative of original lignin. Often used as a measure of lignin content

The yield for MWL, Braun's and Brown-rot (Table **1**) processes is very low when compared to the traditional commercial processes like Kraft and sulfite. All these methods also involve tedious pretreatment steps with a

variety of solvents for lignin extraction. Kraft and sulfite are the two common chemical pulping processes. In both these methods, lignin is highly modified and can only be used as industrial by-products. Most of the above-mentioned methods are not economically viable and involve use of hazardous solvents for the pretreatment and isolation processes. The yield of lignin is either too low or the lignin structure is extremely modified.[8]

1.3.1. Need for Alternative Lignin Solvents: Green Solvents

Specific isolation of lignin without high modification to its structure with traditional solvents is very rare. Most portions of lignin are generally not accessible to catalysts due to its structural arrangement. However, enzymatic isolation of lignin after pretreatment of biomass is possible, but results in fragments of lignin with at least 10% polysaccharides.[5]

The conventional methods of lignin isolation from biomass requires a huge amount of toxic organic solvents, along with hazardous, and hot, strong acids and bases such as HCl, H_2SO_4 and NaOH. Isolation of lignin is difficult due to its complex structure and therefore, most of the unpurified lignin from the cellulose extraction is used as a calorific resource that is to burn it for heat. Hence, there is a need for greener and more efficient solvents[9] to

specifically isolate lignin from biomass without major modifications to its structure.

1.4. Ionic Liquids

Walden reported the first description of a new class of liquids called ionic liquids in 1914, where the physical properties of ethylammonium nitrate were studied at room temperature.[10] This ionic liquid was synthesized by a neutralization reaction between ethylamine and concentrated nitric acid. The classical definition of ionic liquids has been derived from Walden's work; ionic liquids are defined as materials that are composed of anions and cations that melt at or below 100 °C.[10] Technically, due to the presence of neutral species at room temperature in ethylammonium nitrate, this salt cannot be considered as a true ionic liquid.[11]

Later on, there were a couple of studies on ionic liquids applied towards isolation of cellulose[12] and electrodeposition[13] $AlCl_3$ but more intense work on ionic liquids did not begin until late 1990's. Wilkes and Hussey studied the correlation between the LUMO energies and extant reduction potentials of around sixty heterocyclic cations and concluded that the 1, 3-dialkylimidazolium cations are more stable to reduction than the 1-alkylpyridinium compounds.[14,15]

Moisture associated with ionic liquids is a very important parameter as it interferes with many solvent properties. During the cellulose or lignin extraction from biomass, water associated with ionic liquids causes poor hydrogen bonding, resulting in an inefficient isolation. For instance, hexaflurophosphate ionic liquids produce HF if they are exposed to water and can then no longer be used as a medium in electrochemistry studies.[16] Wilkes and Zaworotko proposed a new class of ionic liquids in 1992, which were less corrosive and more stable in air and water when compared to the previously reported ionic liquids. These were made up of 1-ethyl-3-methylimidazolium cation and inorganic anions such as NO_3 and BF_4.[17]

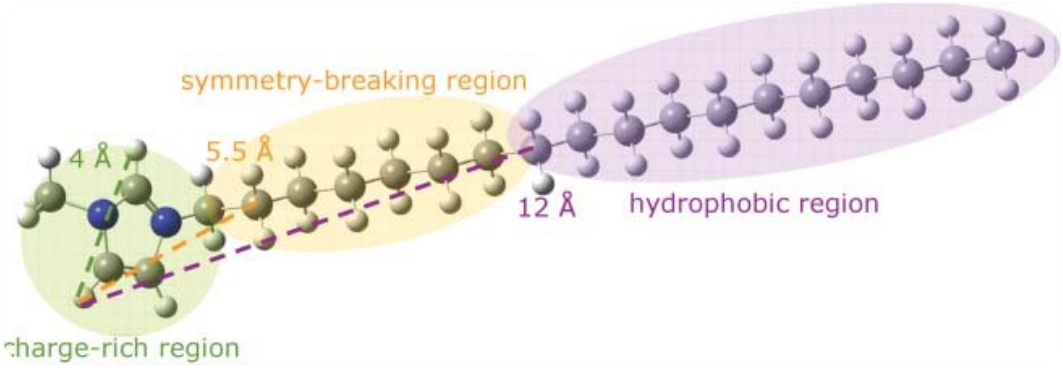

Figure 1. The structure of 1-methyl-3-octadecylimidazolium cation showing a charge rich region near 4 A° and a hydrophobic region at 12 A°.[17]

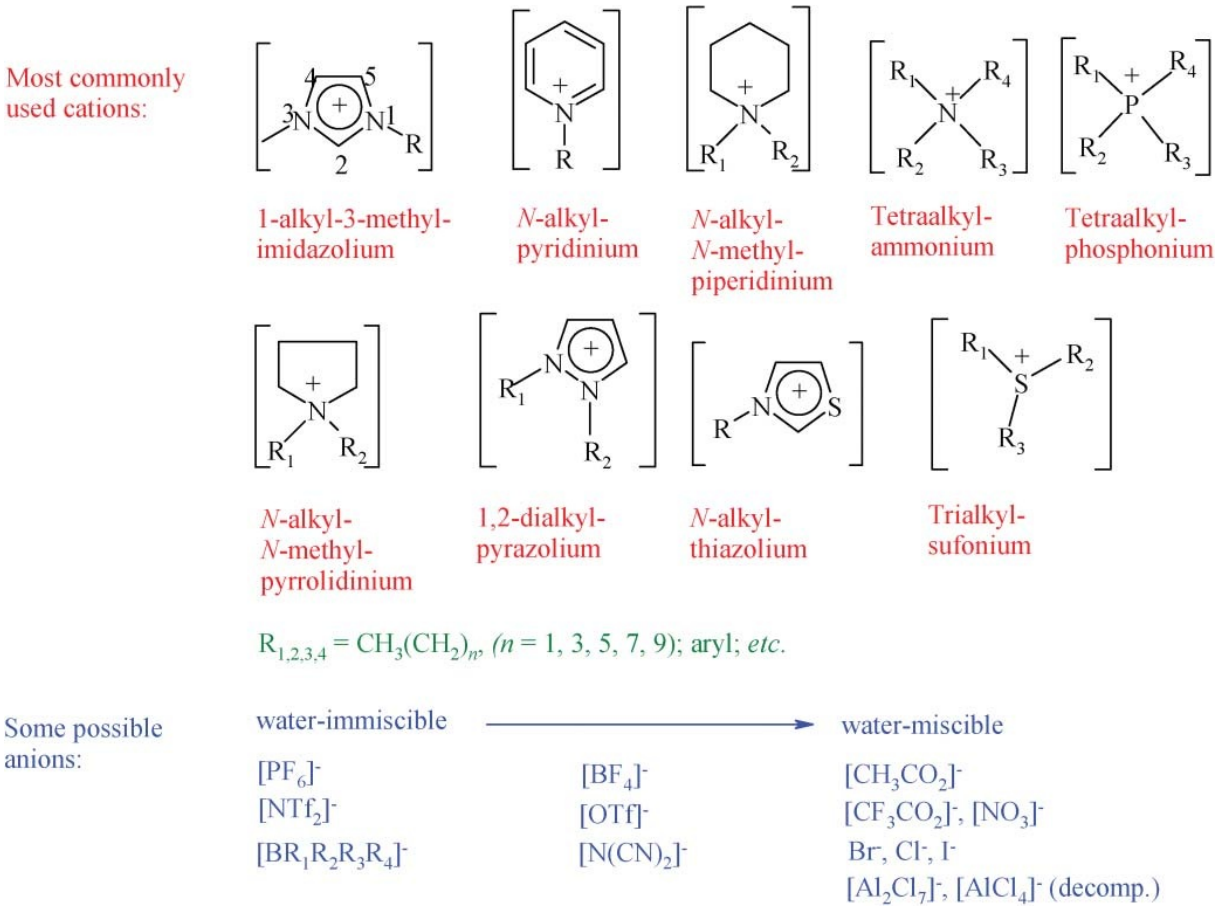

Figure 2. Commonly used cations and anions in design of ionic liquids[20] (Figure adapted from reference 20).

The importance of the symmetry of cations came into discussion in 2004 when Gui et al. studied the relationship between asymmetry and melting points of ionic liquids.[18] The 1-butylpyridinium cation has a C_{2v} symmetry and melts 100 °C above the melting point of a more asymmetrical cation like

1-butyl-3-methylimidazolium.[18] An optimized structure of 1-methyl-3-octadecylimidazolium cation is shown in Figure 1. The lack of symmetry at 5.5 A° is the reason for the decrease in melting point. The hydrophobic region increases the melting point due to van der Waals interactions.[17]

The resonance and charge distribution over a large volume on a larger asymmetric cation is the major reason for ionic liquids to be molten at lower temperatures when compared to the inorganic salts like sodium chloride, which is solid at room temperature. Figure 2 displays some of the common ions used for ionic liquid synthesis. In cases of long aliphatic side chains, we can expect to observe a prominent glass transition temperature instead of a clear melting point.

Another concept that affects the melting point is the hydrogen bonding capacity in the structures. Longer carbon chains in the cation results in the formation of higher hydrophobic regions that are responsible for increasing the melting point due to Van der Waals interactions.[19]
The data presented in Table 1 is a brief comparison of typical values and is not a comprehensive study.

Table 2. Comparison of organic solvents and ionic liquids.[21]

Property	Organic Solvents	Ionic Liquids
Number of solvents	>1000	>1,000,000
Applicability	Single function	Multifunction
Catalytic ability	Rare	Common and tunable
Chirality	Rare	Common and tunable
Vapor Pressure	Generally high	Negligible
Flammability	Usually flammable	Usually nonflammable
Solvation	Weakly solvating	Strongly solvating
Polarity	Conventional polarity	Variable polarity
Tune-ability	Limited tunable solvents	Designer solvents
Cost	Normally cheap	More expensive
Recyclability	Green imperative	Economic imperative
Viscosity (cP)	0.2 - 100	22 – 40,000

Table 1 shows that approximately 10^3 conventional organic solvents can be compared to at least 10^6 simple primary ionic systems, which makes 10^{12} binary combinations and about 10^{18} ternary ionic liquid combinations that can be synthesized.[22] Currently there are around 300 commercialized ionic liquids developed by companies like BASF and that leaves us a large proportion of ionic combinations that can be explored to make designer solvents for specific needs. A lot of properties of ionic liquids and their combinations

are yet to be discovered, making them exciting compounds for applicative studies.

The cations in the ionic liquids largely contribute to their physical properties such as viscosity, melting points and thermal conductivity, whereas anions play a major role in their overall chemical reactivity. Hence, both the physical and chemical properties of the ionic liquids can be tuned by synthesizing a binary solvent with the required combination of ions. Ternary solvent systems may also be developed to fine tune the efficiency of ionic liquids, making them truly designer solvents.

Compared to the classic organic solvents, ionic liquids have very low or negligible vapor pressure that makes it impossible for them to evaporate under normal conditions. When using an ionic liquid as a solvent in catalytic reactions, due to the extremely low vapor pressure of ionic liquids, the solvent and catalyst can be retained quantitatively in the distillation process resulting in thermal removal of the products.

This property of ionic liquids helps reduce atmospheric contamination and also mitigates the amount of solvent required for a process. Hence, it is one of the properties that make ionic liquids green. However, other parameters like its toxicity, biodegradability and its life

cycle analysis have to be considered before deeming an ionic liquid ‘green’. For instance, in some cases, ionic liquids might consist of ions with very low toxicity that are edible, like in sweeteners[23] and in other cases, they might be composed of highly toxic ions such as cyanide.

In recent years, there is a serious consideration for alternative solvents with environmental and technological advantages. There is a need for a class of solvents that are more flexible in terms of their physical and chemical properties when compared to traditional organic solvents. With the increase in green consciousness, the research in solvents is taking a wide turn towards eco-friendly and sustainable compounds suitable for selective functions. Such a class of alternative solvents is ionic liquids. The physiochemical properties of ionic liquids can be altered to achieve higher efficiency in terms of a specific task. For instance, changing the anion in a binary ionic liquid can change the solvating ability from cellulose dissolution to lignin dissolution.

Ionic liquids are salts existing in the liquid state at temperatures near or below 100 °C and some of these salts are liquids below 0 °C. These are also referred to as molten salts. Following are characteristics of ionic liquids, which make them an emerging choice of solvent systems.

- The possibility of designing an ionic liquid with specific fine tunable properties makes them attractive not only on a pilot scale, but also as an industrial solvent.
- Ionic liquids can dissolve a wide range of organic, organometallic and inorganic materials as they can behave as both polar and non-polar solvents.
- Ionic liquids have very negligible vapor pressures due to the strong ionic interactions, making them almost impossible to evaporate, mitigating air pollution due to VOC's and reducing the need for large amounts of solvent for chemical processes.
- Ionic liquids are generally made up of large cations and weakly coordinating anions.
- Ionic liquids are usually nonflammable, therefore decreasing the chance of accidents.
- These solvents have high thermal, mechanical and electrochemical stability.
- Ionic liquids have low interphase tension and can form a biphasic system with a secondary organic solvent.[24]
- In a chemical process, IL can be designed to behave as a solvent or a catalyst or a solvent-catalyst system or a solvent-ligand system.[25]

- These solvents have a large window of applications such as chromatographic stationary phases, background electrolyte additives, electrolytes for electro-deposition of metals etc. Intense research is also going on in optical, electrochemical and biochemical sensor technology.

Functionality of ILs is dependent on the specific composition of ions, where these ions exhibit properties such as dissolution of biopolymers, which is extremely difficult using conventional solvents. The dissolution of cellulose is a good example, where the ion-dipole attraction between chloride ions in an ionic liquid and hydroxyl groups of the cellulose results in dissolution of the biopolymer in an efficient way when compared to the organic solvents.

There are multiple types of interactions in IL's that are generally responsible for the melting point or their functionality. In addition to covalent, ionic, hydrophobic, and Vander wals interactions, hydrogen bonding and π-stacking are found in ILs, which are mostly uncommon in traditional solvents. The effect of these interactions on the properties on ILs may differ based on the composition of different ILs. It is essential to understand the

structure-functional relationship in an ionic liquid architecture to truly develop designer ILs.

1.4.1. Types of Ionic Liquids

The common cations used for ionic liquid synthesis are imidazolium, pyridinium, ammonium, phosphonium, and pyrrolidinium. Apart from these, there are triazolium-, thiazolium- and glycoside-based ionic liquids that are becoming an attractive ionic architecture in the recent times.[25] In a binary ionic liquid system, the cations pair with weakly coordinating anions resulting in molten salts or ionic couples. The most commonly studied anions reported in the literature are chloride (Cl^-), bromide (Br^-), tetrafluoroborate $[BF_4]^-$, hexaflurophosphate $[PF_6]^-$, trifluromethanesulfonyl $[CF_3SO_2]^-$, dicyanamide $[N(CN)_2]^-$ and alkylsulfate anions $[C_nSO_4]^-$.[25]

Imidazolium-based ionic liquids are proven to have great potential in biomass processing such as the task-specific isolation of cellulose or lignin. Of the heterocyclic aromatic ionic liquids, pyridinium has been shown to have a great potential as a solvent in organic synthesis.[26] There are more studies in the literature that examine the biodegradability of pyridinium ILs when compared with the imidazolium ILs. The pyridinium ILs are also commonly used as biocatalysts in chemical reactions.[26,27]

For dye-sensitized solar cell (DSSC) studies, pyrrolidinium cations are the choice for ILs.[28]

Deep eutectic solvents are the class of ionic liquids that are the easiest to make. Choline chloride is a naturally occurring quaternary ammonium salt generally used in chicken feed. This salt has a high melting point at 302 °C. When choline chloride is mixed with urea (melting point around 133 °C) in a simple 1:2 mole ratio, a freezing point depression is observed and the newly formed mixture of choline chloride—urea has a melting point of 12 °C.[29] Metal salts and strongly hydrogen bonding compounds, such as cellulose and sugars, are also extremely soluble in this choline chloride-urea deep eutectic ionic liquid.[30]

Ionic liquids can also be classified based on acidity and basicity. These parameters impart certain physical and chemical properties to designing ionic liquids. The anions, which are neutral or very weakly basic, form weak electrostatic interactions with cations in ionic liquids. As a result, they have high thermal and electrochemical stability along with low melting points and viscosities.[31] Neutral types of ionic liquids are generally used as inert solvents.[32]

The hexaflurophosphate, tetrafluoroborate, methanesulfonate, and thiocyanate are some common examples of neutral pH anions. Slightly acidic ionic liquids would be those that exhibit Lewis acid character. Ionic liquids that have $AlCl_3$ in excess are a good example of those with acidic character.[33] The protic ammonium, pyrrolidinium and imidazolium cations can also be exemplified as common acidic ionic liquids.[34]

Some of the common anions forming basic ionic liquids are lactate, acetate, dicyanamide, and phosphonium.[35] The dicyanamide and phosphonium salts have low viscosity. Hence they are readily available in the market. Basic ionic liquids generally exhibit a variety of solubilizing and catalytic properties. These ionic liquids can be tuned to have higher thermal stability if a compatible basic cation and anion couple is designed.[36] The ionic liquids with the possibility to both accept and donate protons such as hydrogen sulfate (H_2SO_4) and dihydrogen phosphate (H_2PO_4) are amphoteric ionic liquids.[37]

1.4.2. Dissolution of Cellulose in Ionic Liquids

Cellulose is the most abundant biopolymer available on earth with an annual estimated production of 9.0×10^{10} metric tons.[38] Hence, cellulose is a large renewable source

that can be directed towards fuel production or can be functionalized to produce a variety of organic compounds. It is a highly ordered polymeric structure present in biomass. This complex structure makes finding a suitable solvent that can aid in the solubility of cellulose challenges. The hunt for a solvent started in 1920s. Despite the expensive and harsh conditions for cellulose dissolution, these traditional solvents suffered from poor solvating power and high toxicity.[39]

Since the application of ionic liquids towards cellulose dissolution in the past couple of decades, there has been a moderation of extreme conditions required for the process, along with other attractive incentives such as solvent recovery and efficient dissolution. The stability of the cellulosic structure is due to the strong hydrophobic nature of the glycosidic bonds and the high extent of inter- and intramolecular hydrogen bonding. Therefore, the primary characteristics of ILs that influence dissolution of cellulose are the polarity and hydrogen bonding capacity.

The common ionic liquids that are used for efficient cellulose dissolution include methylimidazolium and methylpyridinium cations with allyl, ethyl and butyl side

chains.[40] The dissolution of cellulose has been discussed in a few publications where carbon and chloride NMR studies showed that the dissolution of cellulose in ionic liquids such as 1-butyl-3-methylimidazolium chloride occurs when the hydrogen bonding network of the cellulose is disrupted. The chloride ion interacts 1:1 mole ratio with the hydroxyl groups of sugar moieties.[41]

1.4.3. Dissolution of Lignin in Ionic Liquids

Though there were a couple of studies done to isolate lignin using ILs in the 1990s, promising results were not out until the late 2000s. Most of the studies involving dissolution of lignin were aimed at the imidazolium class of ionic liquids with chloride, bromide, acetate, tetrafluoroborate, and methylsulfonate anions.[42] Polycyclic amidine bases such as 1,8-diazabicyclo[5.4.0]undec-7-enium cation with a variety of anions, like acetate, thiocyanate, hydrogen sulfate, methanesulfonate, lactate, and tosylate were also found to be good solvents for the isolation of lignin at a range of temperatures from 50 to 150 °C.[43]

Equally efficient solvents for isolation of lignin, such as 1-butyl-3-methylimidazolium trifluoromethanesulfonate,[44] 1,3-dimethylimidazolium methylsulfate,[45] 1-butyl-3-methylimidazolium methylsulfate,[42]

1-ethyl-3-methylimidazolium acetate,[44] and 1-allyl-3-methylimidazolium chloride[44] were published in the years 2007 through 2009. The raw materials for these studies were mostly kraft lignin, softwood kraft pulp lignin, or sugarcane bagasse.[42-45] The 1-benzyl-3-methylimidazolium chloride is reported as a poor solvent.[44] In spite of having a benzyl ring with unsaturated bonds mimicking lignin, and thereby theoretically increasing solvent-lignin interaction, there was no significant improvement reported in the lignin extraction.

Some of the other poor solvents for the dissolution lignin in literature include alkylimidazolium cation moieties along with anions such as bromide, acetate, tetrafluoroborate, and hexafluorophosphate.[42-45] Hence it can be said that the large noncoordinating anions such as Br^-, BF_4^- and PF_6^- are not good choices of anions for lignin isolation from biomass.[45] There is not much data on the mechanism of lignin dissolution until now.

1.5. Choice of Feedstock – Prairie Cordgrass

The choice of feedstock for this study was prairie cordgrass (PCG). Prairie cordgrass grows tall to about 6-8 feet.[46] It is a robust and native grass seen all over in U.S. It grows in the Northeast, Great Lakes, and Midwest

states as well as most other states in the country. PCG has strong rhizomes that provide the ability to grow 5-10 feet per year, which is a distinctive feature of this warm season grass.[46] PCG is a drought-resistant type of grass that grows well on seasonally dry sites and tolerates alkaline conditions.

The PCG seedling has a very fast development stage as this character dodges it from frosting issues on wet soils.[46] This grass grows on wasteland and around marshes, and has no management needs. As shown in the Figure 3, PCG is composed of 41% cellulose, 33% hemicellulose, 17% lignin, 3% crude protein, and 6% other components such as small portions of resins, fats and fatty acids, phenolics, phytosterols, salts, and minerals. These percentages are based on PCG total-dry biomass basis.[47]

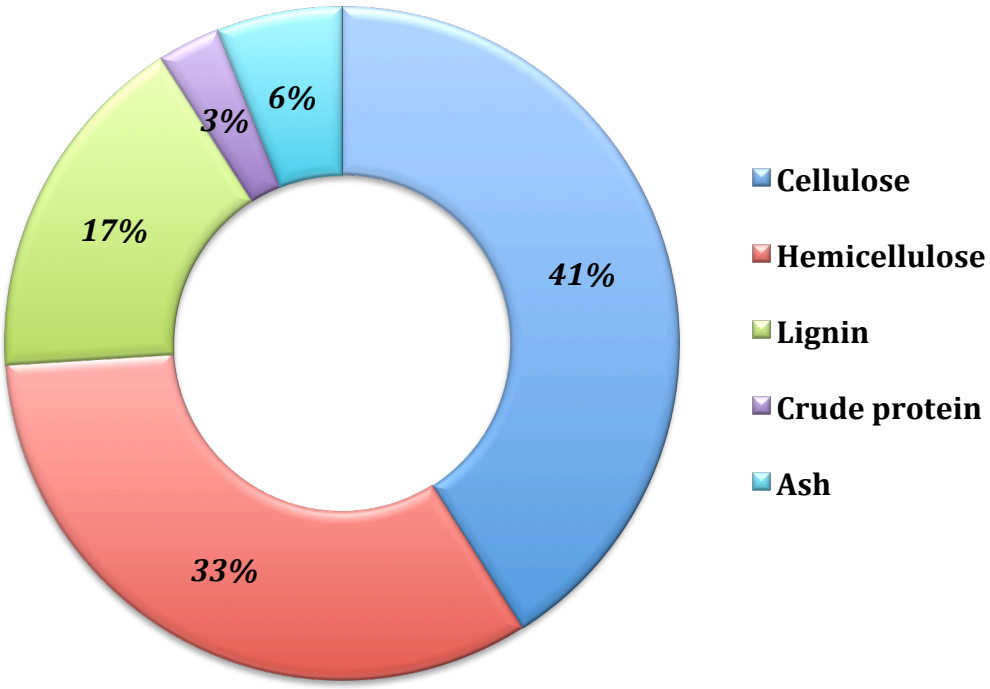

Figure 3. Composition of Prairie cordgrass (PCG).[47] PCG is composed of mainly cellulose (41%), hemicellulose (33%), lignin (17%) and 9% protein and other components.

1.6. LIGNIN

1.6.1. Lignin uses

Lignin is the second most abundant organic polymer, constituting around 30% of the earth's organic carbon. Lignin accounts for about 15-35% of the total weight of biomass depending on the type of biomass taken into consideration.[48] Hence lignin is a potential source of renewable energy for biofuels and a wide variety of

aromatic chemicals. It has biological significance in plant regulatory processes and provides the mechanical strength and structural support needed for the plant to stand upright. The hydrophobic nature of lignin facilitates efficient water conduction and transportation of nutrients through the xylem tracheary elements in plants.[48]

The lignin component in lignocellulosic material also acts as a barrier between the plant cell wall and microorganisms, preventing the destruction of the cell wall.[48] Therefore, the interactions between lignin and cellulose have to be broken to isolate lignin from biomass. Lignin also aids in mitigating the degradation of structural polysaccharides by restricting hydrolytic enzymes and thereby limits the bioconversion of forages into animal products or liquid fuels.[49,50] Due to the progressive lignification of the primary and secondary cell walls in plants, increased hydrophobicity, and excessive cross-linkage of lignin with other matrix structures, the degradability of the structural components of stems and leaves drastically decreases as the plant reaches its physiological maturity.[51] Lignin plays an important role, not only in plants but in humans also, by maintaining gastrointestinal function.[52]

1.6.2. Lignin Structure

Lignin is a complex structure, which has not been fully established. It is made up of a set of tridimensional, cross-linked, highly branched systems of phenolic polymers that are present in the plant cell wall. These polymers are formed as a result of extensive polymerization of three types of phenylpropanoid moieties involving C-C and ether linkages.[53] Carbon fixation by the energy gained during photosynthesis is an important step for the biosynthesis of lignin in plants. As shown in the Figure 4, lignin in forages is composed primarily of *p*-hydroxyphenyl (H), guaiacyl (G) and syringyl (S) structures.[54]

The coniferyl alcohol copolymerizes with small amounts of *p*-coumaryl alcohol in the initial stages of lignification. This polymerization occurs in the primary wall to form mixed G and H lignins.[55] The coniferyl alcohol and high amounts of sinapyl alcohol copolymerizes to form G and S lignins during the secondary wall development process.[8] Depending on the environment such as soil pH and weather, the H, G and S monomer composition varies in lignin.[56-59]

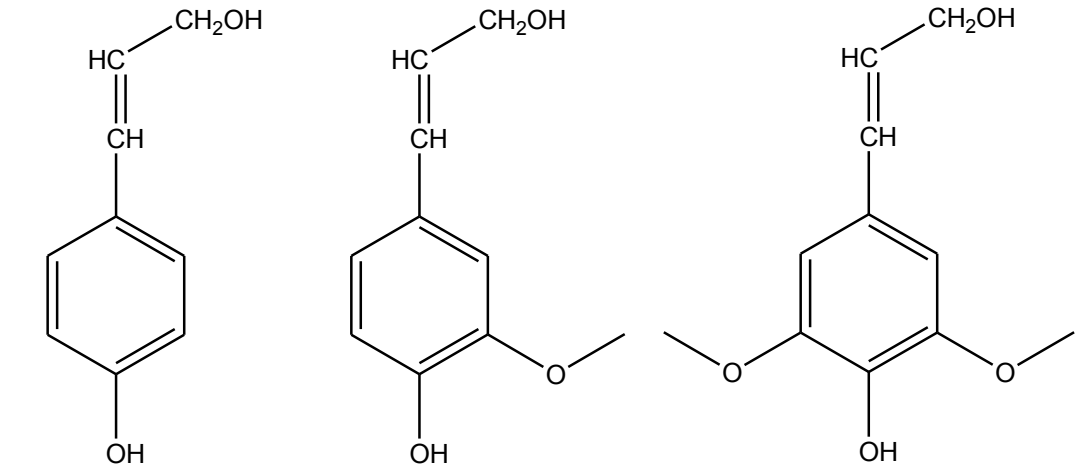

Figure 4. Structures of three basic lignin monomers.[54]

Generally, grass lignins are composed of mainly *p*-hydroxyphenyl (H) units along with guaiacyl (G) and syringyl (S) units. Hardwood lignin has high guaiacyl (G) and syringyl (S) units.[60] As shown in Figure 5, high guaiacyl (G) moieties are present in softwood and all the aromatic monomers are connected by propane side chains called phenylpropanoid monomeric units in the softwood lignin polymeric structure. If the enzymes in the lignin biosynthesis pathway are altered by mutations or genetic engineering, then high levels of unusual phenylpropane units were observed along with the normal H, G and S units in lignin.[61]

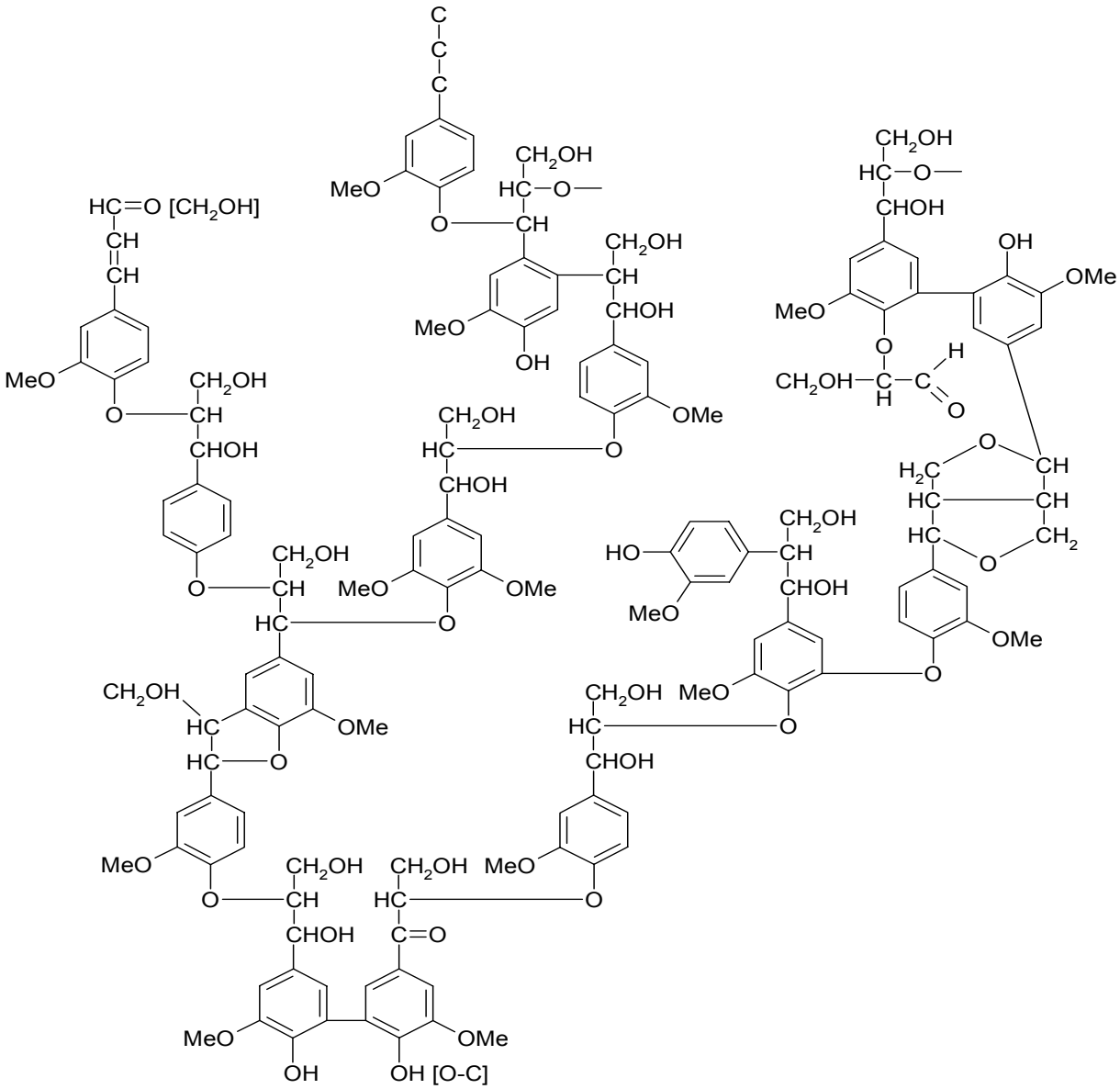

Figure 5. Structure of lignin from softwood.[54]

The rate of lignin monomer secretion into the apoplast affects the interactions of lignin with the matrix and possibly influences the structure of lignin. Rapid “bulk” polymerization in primary wall results in a highly branched polymer with more C-C linkages of monomers. Slow and constant “end-wise” polymerization in secondary walls favors exceedingly linear polymers in the lignin structure.[62] Primary walls in lignified grass tissue are less degradable when compared to the secondary. Based on this study, it has been reported that the highly branched lignins show more inhibition towards the degradation of cell walls.[63]

1.7. Purpose of this Research

This aim of this study is to synthesize and comprehensively characterize ionic liquids that can selectively isolate lignin from PCG because lignin is not soluble in conventional solvents. This set of ionic liquids is the 1-ethyl-3-methylimidazolium alkylbenzenesulfonates. An extensive physical, chemical, structural, thermal, and toxicological characterization of these ionic liquids is done to understand the properties of this solvent system. Preliminary characterization of lignin is performed to prove the hypothesis of isolation of lignin using ionic

liquids and to understand the modifications of the isolated lignin.

1.8. References

1. Kandala, H. *The Study of Variations in the Properties of Biodiesel on Addition of Antioxidants.* Master's Thesis & Specialist Projects. **2009**, p 93. http://digitalcommons.wku.edu/theses/93 (accessed June 10, 2010)
2. Lovins, A. B. In *Winning the Oil Endgame: Innovation for Profits, Jobs, and Security.* Aranow, B. T. Ed.; Rocky Mountain Institute, Snowmass, CO, 2004; pp.1-122.
3. Chum, H. L.; Overend, R. P. *Adv. Solar Energy.* **2003**, *15*, 83.
4. Parikka, M. *Biomass Bioenergy.* **2004**, *27*, 613.
5. John, R. O., and Kent, K. T. Isolation of Lignin. In *Methods in enzymology — Biomasspart, Lignin, Pectin and Chitin.* Wood, W. A.; Kellogg, S. T., Ed.; Academic Press Inc., San Diego, CA, 1988; 161, pp 3-12.
6. Fengel, D.; Wegener, G. *Wood, Chemistry, Ultrastructure, Reactions;* deGruyter: Berlin, Federal Republic of Germany, 1983; p. 50.
7. Brauns, F. E. *The Chemistry of Lignin;* Academic Press: New York, 1952; p. 51.

8. Freudenberg, K.; Neish, A. C. *Constitution and Biosynthesis of Lignin;* Springer-Verlag: Berlin and New york, 1968; p. 52.
9. Anastas, P.; Warner, J. In *Green Chemistry: Theory and Practice;* Oxford University Press, New York, 1998.
10. Walden P. *Acad. Imp. Sci*. **1914**, 405.
11. Greaves T.L.; Drummond C.J. *Chem. Rev*. **2008**, *108*, 206.
12. Graenacher C. Cellulose solution. US Patent 1,943,176, 1934.
13. Hurley F. H. Electrodeposition of Aluminum. US Patent 4,446,331, 1948.
14. Wilkes J. S. *In Ionic liquids: Industrial Applications to Green Chemistry*; Rogers, R. D., Seddon, K. R., Eds.; *ACS Symp. Ser;* American Chemical Society:Washington, DC, 2002; *4,* pp 73-80.
15. Wallach O. *Ber. Chem. Dtsche. Ges. **1884**, 16,* 535.
16. Bonhote, P.; Dias, A. P.; Papageorgiou, N.; Kalyanasundaram, K.; Gratzel, M. *Inorg. Chem.* **1996**, *35*, 1168-1178.
17. Wilkes, J. S.; Zaworotko, M. J. *J. Chem. Soc. Chem. Commun.* **1992**, 965-967.
18. Seddon, K. R. *Kinet. Catal.* **1996**, *37*, 743-748.
19. Lopez-Martin, I.; Burello, E.; Davey, P. N.; Seddon, K. R.; Rothenberg, G. *ChemPhysChem,* **2008**, *8*, 690-695.

20. Stark, A.; Seddon, K. R. in *'Kirk-Othmer Encyclopaedia of Chemical Technology'*, ed. A. Seidel, John Wiley & Sons, Inc., Hoboken, New Jersey, **2007**, *26*, 836-920.
21. Lide, D. R. 'CRC Handbook of Chemistry and Physics', ed. CRC Press, Boca Raton, 73rd ed., 1992.
22. Abdul-Sada, A. K.; Seddon, K. R.; Stewart, N. J. Ionic Liquids of Ternary Melts, World Patent WO 95 21872, 1995.
23. Freemantle, M. *Chem. Eng. News*, **2004**, *82*, 10.
24. Van Doorslaer, C.; Schellekens, Y.; Mertens, P.; Binnemans, K.; DeVos, D. *Phys. Chem. Chem. Phys.* **2010**, *12*, 1741.
25. Magna, L.; Olivier-Bourbigou, H.; Morvan, D. *Appl. Catal.* **2010**, *373*, 1.
26. Zhao, H.; Malhotra, S. V. *Aldrichimica Acta*. **2002**, *35*, 75.
27. Docherty, K. M.; Dixon, J. K.; Kulpa, C. F. Jr. *Biodegradation*. **2007**, *18*, 481.
28. Johansson, P.; Fast, L. E.; Matic, A.; Appetecchi, G. B.; Passerini, S. *J. Power Sources*. **2010**, *195*, 2074.
29. Andrew P. A.; Glen C.; David L. D.; Raymond K. R.; Vasuki T. *Chem. Commun*. **2003**, 70—71.
30. Abbott, A. P.; Bell, T. J.; Handa, S.; Stoddart, B. *Green Chem.* **2005**, *7*, 705-707.

31. Bonhote, P.; Dias, A. P.; Papageorgiou, N.; Kalyanasundaram, K.; Graetzel, M. *Inorg. Chem.* **1996**, *35*, 1168.

32. Yukihiro, Y.; Koji, M.; Akihiro, O.; Gunzi, S.; Masahide, T.; Toshinobu, Y. *Inorg. Chem.* **2004**, *43*, 1458.

33. Martins, M. A. P.; Frizzo, C. P.; Moreira, D. N.; Zanatta, N.; Bonacorso, H. G. *Chem. Rev.* **2008**, *108*, 2015.

34. Hajipour, A. R.; Azizi, G.; Ruoho, A. E. *Synth. Commun.* **2009**, *39*, 242.

35. MacFarlane, D. R.; Pringle, J. M.; Johansson, K. M.; Forsyth, S. A.; Forsyth, M. *Chem. Commun.* **2006**, 1905.

36. Henriksson, M.; Berglung, L. A.; Isaksson, P.; Lindstroem, T.; Nishino, T. *Biomacromolecules.* **2008**, *9*, 1579.

37. Heinze, T.; Leibert, T. *Prog. Polym. Sci.* **2001**, *26*, 1689.

38. Feng, L.; Chen, Z. *J. Mol. Liq.* **2008**, *142*, 1.

39. Remsing, R. C.; Swatloski, R. P.; Rogers, R. D.; Moyna, G. *Chem. Commun.* **2006**, *12*, 1271-1273.

40. Pu, Y.; Jiang, N.; Ragauskas, A. J. *J. Wood Chem. Technol.* **2007**, *27*, 23-33.

41. D'Andola, G.; Szarvas, L.; Massonne, K.; Stegmann, V. Ionic Liquids for Solubilizing Polymers. WO Pat. 2008/043837, 2008.

42. Lee, S. H.; Doherty, T. V.; Linhardt, J. S. *Biotechnol. Bioeng.* **2009**, *102 (5)*, 1368-1376.

43. Lee, S. H.; Lee, S. B. *Chem. Commun.* **2005**, 3469-3471.

44. Swiderski, K.; McLean, A.; Gordon, C. M.; Vaughan, D. H. *Chem. Commun.* **2004**, 2178-2179.

45. Maki-Arvela, P.; Amugwom, I.; Virtanen, P.; Sjoholm, R.; Mikkola, J. P. *Industrial Crops and Products.* **2010**, *32*, 175-201.

46. United States Department of Agriculture, Plant Guide. http://plants.usda.gov/plantguide/pdf/pg_sppe.pdf (accessed December 05, 2014).

47. Sungrant initiative, Composition of herbaceous biomass feedstock. http://ncsungrant.sdstate.org/uploads/publications/SGINC1-07.pdf (accessed December 05, 2014).

48. Iiyama, K.; Lam, T. B. T.; Stone, B. *Plant Physiol.* **1994**, *104*, 315-320.

49. Jung, H. J. G. *Phytochemistry.* **2003**, *63*, 543-549.

50. Brown, A. *J. Appl. Biochem.* **1985**, *7*, 371-387.

51. Wilson, J.; Hatfield, R. *J. Agric. Res.* **1997**, *48*, 165-180.

52. Ferguson, L. R.; Chavan, R. R.; Harris, P. J. *Nutr. Cancer.* **2001**, *39*, 155-169.

53. Feldman, D. Lignin and its polyblends. In Reviews in Chemical Modification, Properties, and Usage of Lignin; Hu, T. Q., Eds.; Kluwer Academic/Plenum Publishers: New York, 2002; pp 81-99.

54. Adler, E. *Wood Sci. Technol.* **1977**, *11*, 169-218.

55. He, L.; Terashima, N. *J. Wood Chem.* **1990**, *4*, 435-459.

56. Baucher, M.; Bernard, M. A.; Chabbert, B.; Besle, J. M.; Opsomer, C.; Van, M. M.; Botterman, J. *Plant Mol. Biol.* **1999**, *39*, 437-447.

57. Jung, H. G.; Casler, M. D. *Anim. Feed Sci. Technol.* **1991**, *32*, 63-68.

58. Jung, H. J. G.; Ni, W. T.; Chapple, C. C. S.; Meyer, K. *J. Sci. Food Agric.* **1999**, *79*, 922-928.

59. Jung, H. J. G.; Buxton, D. R. *J. Sci. Food Agric.* **1994**, *66*, 313-322.

60. Vanholme, R.; Demedts, B.; Morreel, K.; Ralph, J.; Boerjan, W. *Plant Physiol.* **2010**, *153*, 895.

61. Boerjan, W.; Ralph, J.; Baucher, M. *Annu. Rev. Plant Biol.* **2003**, *54*, 519-546.

62. Jurasek, L. Experimenting with virtual lignins. In *Lignin and Lignan Biosynthesis;* Lewis, N. G. and Sarkanen, S., Ed.; ACS Symposium Series, No. 697,

American Chemical Society, Washington, DC, 1998; pp 276-293.

63. Jung, H. G. and Deetz, D. A. Cell wall lignification and degradability. In *Forage cell Wall Structure and Digestability*; Jung, H. G. et. Al., Ed.; ASA, CSSA, and SSSA, Madison, WI, 1993; pp 315-346.

CHAPTER 2

SYNTHESIS AND COMPREHENSIVE STRUCTURAL AND PHYSICAL CHARACTERIZATION OF 1-ETHYL-3-METHYLIMIDAZOLIUM ALKYLBENZENESULFONATE IONIC LIQUIDS

2.1. Synthesis of 1-ethyl-3-methylimidazolium alkylbenzenesulfonate ionic liquids

The conventional methods of lignin isolation from biomass requires a huge amount of toxic organic solvents, along with hazardous, and hot, strong acids and bases such as HCl, H_2SO_4 and NaOH. Isolation of lignin is difficult due to its complex structure and therefore, most of the impure lignin from cellulose extraction is used as a calorific resource that is to burn for heat. Hence, there is a need for greener and more efficient solvents[1] to specifically isolate lignin from biomass without major modifications to its structure.

The cations in the ionic liquids largely contribute to their physical properties such as viscosity, melting points and thermal conductivity, whereas anions play a major role in their overall chemical reactivity. Hence, both the physical and chemical properties of the ionic liquids can be tuned by synthesizing a binary solvent

with the required combination of ions. The choice of solvent plays an important role in chemical processes.

In this study, a set of 1-ethyl-3-methylimidazolium (EMIM) alkylbenzenesulfonate (ABS) ionic liquids were synthesized that can specifically isolate lignin from the plant material.[1] Ionic couples consisting of EMIM cation and ABS anions were chosen and the synthesis was done through metathesis reaction. Figure 6 shows the ionic liquids were synthesis using benzenesulfonate, toluenesulfonate and xylenesulfonate as the anions.

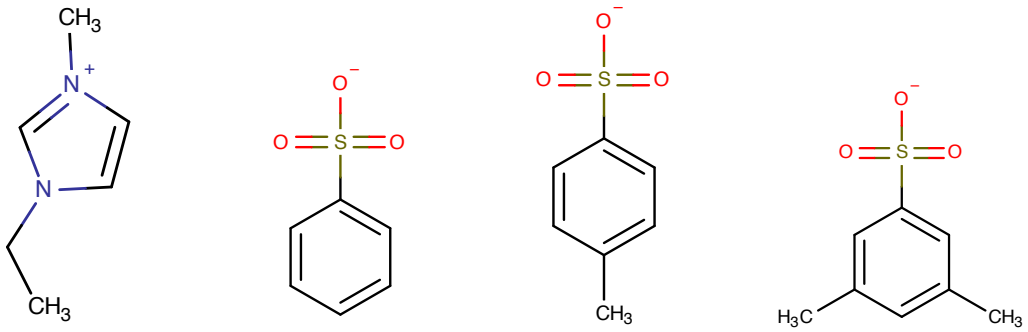

[A] [B] [C] [D]

Figure 6. Structures of ions used in this study, including A. 1-ethyl-3-methylimidazolium, B. benzenesulfonate, C. toluenesulfonate, D. xylenesulfonate

2.1.1. Materials

The materials used in the synthesis of 1-ethyl-3-methylimidazolium alkylbenzenesulfonate (EMIM–ABS) ionic

liquids are presented in Table 3, along with CAS numbers, purity, molecular weight, and supplier.

Table 3. Materials used in the synthesis of EMIM–ABS ionic liquids.

Chemical/Material	Purity (%)	CAS	Molecular weight	Supplier
1-Ethyl-3-methylimidazolium acetate	97	143314-17-4	170.21	Sigma Aldrich
Sodium xylenesulfonate	93	1300-72-7	208.21	Pfaltz & Bauer
Sodium toluenesulfonate	99	657-84-1	194.19	MP Biochemicals
Sodium benzenesulfonate	96	515-42-4	180.15	TCI America
Ethyl benzenesulfonate	99	515-46-8	186.23	Acros
Acetone	99.5	67-64-1	58.08	Sigma Aldrich
Water	HPLC Grade	7732-18-5	18.02	Sigma Aldrich
Glass Fiber Filter	N/A	N/A	N/A	Fisher Brand

2.1.2. Experimental

The synthesis of 1-ethyl-3-methylimidazolium alkylbenzenesulfonate ionic liquids involves two steps. The first step comprises a metathesis reaction between anion

and cation and the second is a byproduct-removal step. Water is used as a solvent in the synthesis procedure and acetone is used as a solvent in the removal of the byproduct (sodium acetate). The 1-ethyl-3-methylimidazolium acetate (EMIM–AC) is used as the cation source in the synthesis of all ionic liquids in this study.

Table 4. Weights of the materials used in synthesis of ionic liquids.

Ionic Liquid	EMIM-AC (411.3 mmol)	ABS (411.3 mmol)	Water (mL)	Acetone (mL)
EXS	70 g	85.63 g	150	200
ETS	70 g	79.86 g	150	200
EBS	70 g	74.09 g	150	200
EEBS	70 g	76.59 g	150	200

The anions in EMIM xylenesulfonate (EXS), EMIM toluenesulfonate (ETS) and EMIM benzenesulfonate (EBS) are derived from the respective sodium sulfonates of xylene, toluene and benzene. The EMIM benzenesulfonate synthesized using anion from the Ethyl benzenesulfonate is denoted as EEBS in this study. The reaction materials, solvents and

their respective weights used in the synthesis of ionic liquids are displayed in Table 4. As the synthesis of ionic liquids is a metathesis (double displacement) reaction, equimolar concentrations (411.3 mmol) of the cation and anion are used.

2.1.2.1 Synthesis of 1-ethyl-3-methylimidazolium xylenesulfonate (EXS) ionic liquid

The 1-ethyl-3-methylimidazolium acetate and the sodium xylenesulfonate were dissolved in water and allowed to react overnight at room temperature with moderate agitation on a flask shaker. Figure 7 shows the metathesis reaction resulting in the formation of EXS ionic liquid. A rotary evaporator was used to remove water under vacuum at 55 °C. The yellowish-white solid obtained after the evaporation of water was dissolved in acetone. A white precipitate of sodium acetate was formed at this point, which was removed through filtration using a glass-fiber filter.

The flask containing the synthesized EXS ionic liquid and acetone was left in a refrigerator at 4 °C overnight to help precipitate fine sodium acetate crystals. The sodium acetate forms sharp transparent spikes at the bottom of the flask. This sodium acetate was removed by filtration and the filtrate now consists of the ionic liquid dissolved in acetone. The acetone was removed using a rotary evaporator

and the ionic liquid was dried at 70 °C for 12 hours. Care was taken to avoid bubbling of the contents in the round-bottom flask during the rotary evaporation. The synthesized ionic liquid was stored in a labeled, airtight, amber container and placed in a desiccator.

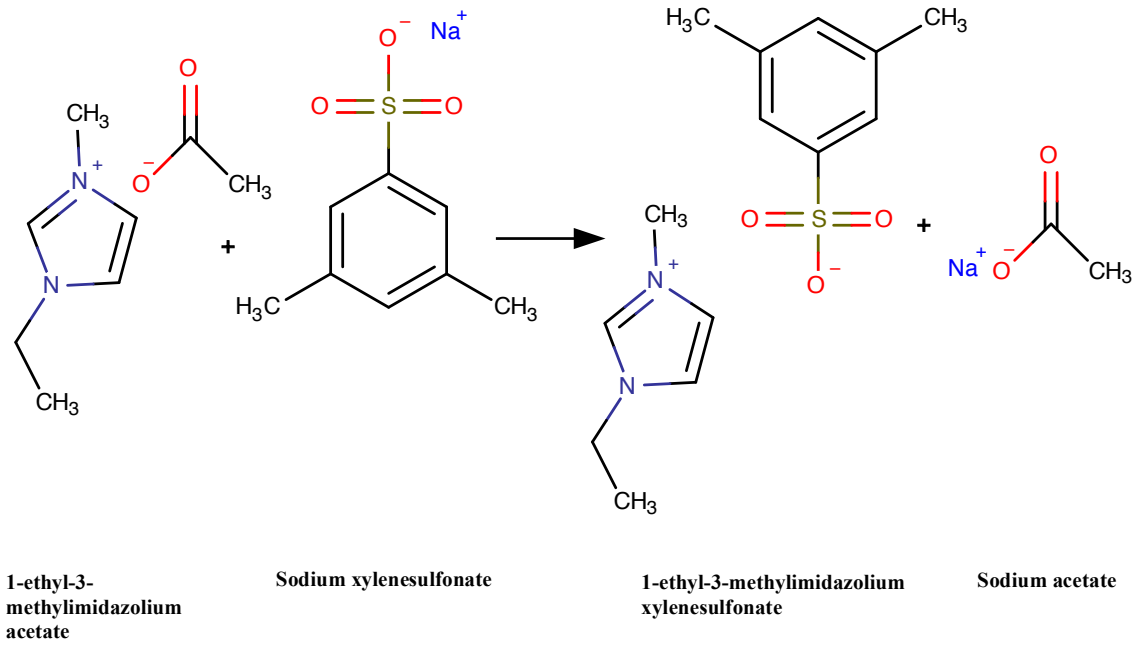

Figure 7. A reaction showing the synthesis of 1-ethyl-3-methylimidazolium xylenesulfonate (EXS) ionic liquid. The water is used as a solvent in this reaction. Sodium acetate is formed as a byproduct.

2.1.2.2. Synthesis of 1-ethyl-3-methylimidazolium toluenesulfonate (ETS) ionic liquid

EMIM acetate and sodium toluenesulfonate were dissolved in water in a conical flask and allowed to react

overnight at room temperature with moderate agitation on a flask shaker. The rest of the 1-ethyl-3-methylimidazolium toluenesulfonate (ETS) synthesis is similar to that of the 1-ethyl-3-methylimidazolium xylenesulfonate (EXS) in Section 2.3.1. Figure 8 display the metathesis reaction involved in the synthesis of ETS ionic liquid.

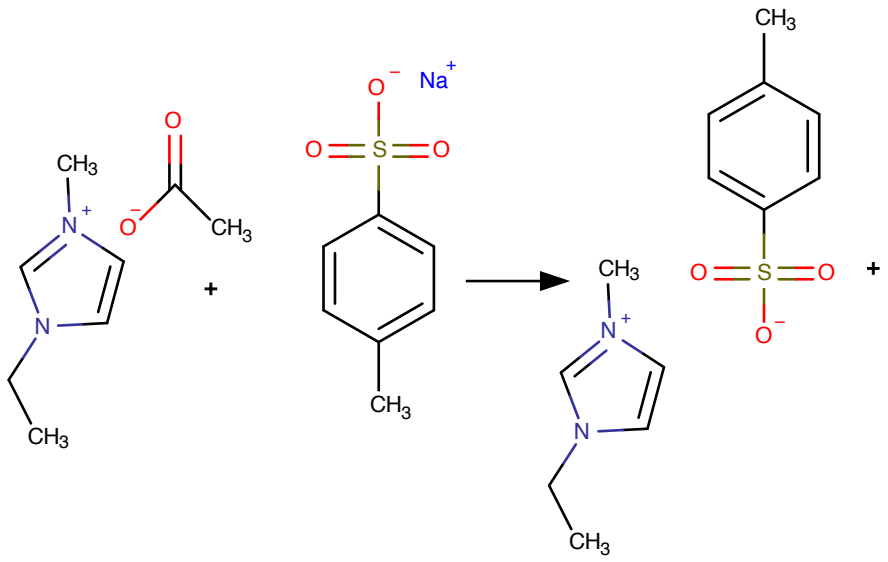

1-ethyl-3-methyl imidazolium acetate

Sodium toluenesulfonate

1-ethyl-3-methyl-imidazolium toluenesulfonate

Sodium acetate

Figure 8. A reaction showing Synthesis of 1-ethyl-3-methylimidazolium toluenesulfonate. The water is used as a solvent in this reaction. Sodium acetate is formed as a bi-product.

2.1.2.3. Synthesis of 1-ethyl-3-methylimidazolium benzenesulfonate ionic liquids

This study involves synthesizing EMIM benzenesulfonate from two different anion sources, sodium benzenesulfonate and ethyl benzenesulfonate.

2.1.2.3.1. Synthesis of 1-ethyl-3-methylimidazolium benzenesulfonate ionic liquid using sodium benzenesulfonate

The Water was used as a solvent to dissolve EMIM acetate and sodium benzenesulfonate. The rest of the 1-ethyl-3-methylimidazolium benzenesulfonate (EBS) synthesis is similar to that of the 1-ethyl-3-methylimidazolium xylenesulfonate (EXS) in Section 2.1.2.1. Figure 9 displays the metathesis reaction involved in the synthesis of EBS ionic liquid from sodium benzenesulfonate.

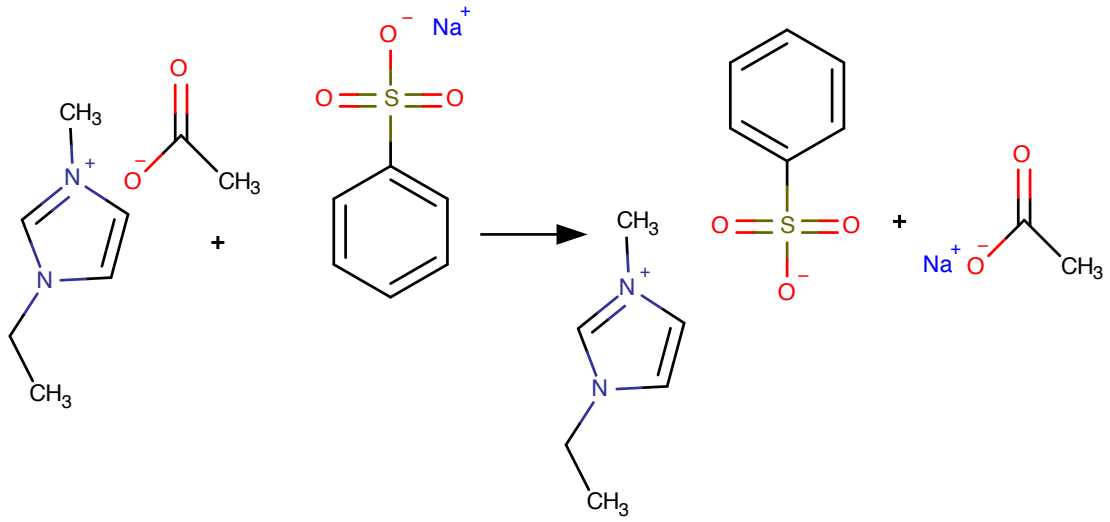

Figure 9. A reaction showing the synthesis of 1-ethyl-3-methylimidazolium benzenesulfonate using sodium benzenesulfonate as the parent anion.

2.1.2.3.2. Synthesis of 1-ethyl-3-methylimidazolium benzenesulfonate ionic liquid using ethyl benzenesulfonate

This reaction required no solvents as both the EMIM acetate and ethyl benzenesulfonate were liquids. When EMIM acetate and ethyl benzenesulfonate were mixed together, an exothermic reaction occurred. Two layers of products were formed after the reaction and ethyl acetate was removed by rotary evaporation leaving behind EMIM benzenesulfonate

ionic liquid. Figure 10 displays the metathesis reaction involved in the synthesis of EBS ionic liquid from ethyl benzenesulfonate. The temperature recorded during the synthesis of EEBS was ~81.5 °C and the reaction was completed in an hour.

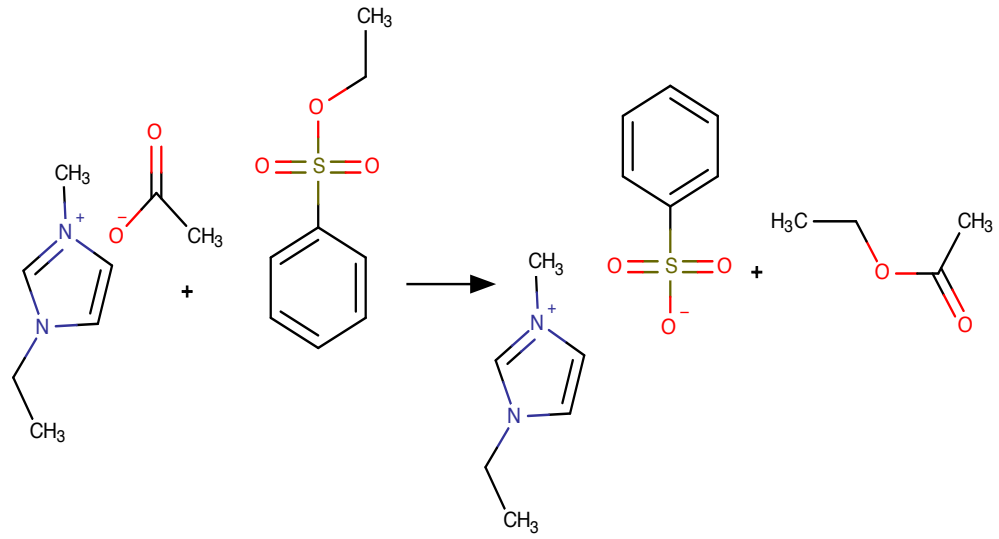

1-ethyl-3-methyl imidazolium acetate

Ethyl benzenesulfonate

1-ethyl-3-methyl-imidazolium benzenesulfonate

Ethyl acetate

Figure 10. A reaction showing the synthesis of 1-ethyl-3-methylimidazolium benzenesulfonate using ethyl benzenesulfonate as the anion.

2.1.3. Results and Discussion

The synthesis of the 1-ethyl-3-methylimidazolium alkylbenzenesulfonate ionic liquids is a metathesis

reaction, where a double displacement of the anion and cation occurs resulting in the synthesis of the products. The product yield obtained in this reaction is calculated by dividing the actual yield of the ionic liquid obtained by the theoretical yield of the ionic liquid. Table 5 shows the actual yield, the theoretical yield and the calculated percent yield for the synthesis of EBS, EEBS, ETS and EXS ionic liquids. The reaction yield for the synthesis of EBS, EEBS, ETS, and EXS ionic liquids was determined to be 91.2 ± 1.5 %, 99.2 ± 0.2 %, 96.1 ± 0.7 %, 99.0 ± 0.5 % respectively. The EBS and ETS had lower % yield when compared to the EXS and EEBS.

Table 5: Actual, theoretical and % yields of the EBS, EEBS, ETS, and EXS Ionic liquids.

Ionic Liquids	**Actual Yield (g)**	**Theoretical Yield (g)**	**% Yield**
EBS	100.8±1.7	110.6	91.2±1.5
EEBS	109.7±0.3	110.6	99.2±0.2
ETS	111.8±0.9	116.3	96.1±0.7
EXS	121.1±0.5	122.1	99.0±0.5

Sodium acetate is formed as a byproduct that is removed from the reaction. Sometimes there is a small amount of sodium acetate that remains in the ionic liquid

and forms sharp, transparent crystals at the bottom of the container. In such cases, the ionic liquid was dissolved in acetone and refrigerated overnight at 4 °C. Sodium acetate formed a white precipitate that was removed through filtration and acetone was removed using a rotary evaporator, which was followed by drying of the ionic liquid.

The presence of sodium acetate alters the physical and behavior of the ionic liquids. Hence it is important to make sure that the sodium acetate is completely removed from the synthesized ionic liquid. To monitor the completion of reaction, thin-layer chromatography (TLC) was run after 12 hours on a silica gel TLC glass plate, where a solution of 15% methanol-dichloromethane was used as a solvent. Structural confirmation was done using proton and carbon nuclear magnetic resonance (NMR) and fourier-transform infrared (FTIR) spectroscopies. Ionic liquids notoriously absorb a lot of moisture. Hence the synthesized ionic liquids were always stored in a desiccator. For all the filtrations involving ionic liquids, only glass-fiber filter papers were used.

2.2. Structural Characterization of 1-ethyl-3-methylimidazoilum alkylbenzenesulfonate ionic liquids

The structural determination of the synthesized ionic liquids is very important to investigate the purity and to determine the hypothesized structure of the compounds being studied. Since the synthesis of EBS, EEBS, ETS, and EXS ILs involved a simple metathesis reaction, it is crucial to ensure complete removal of the solvent and the byproducts from the reaction. The major byproducts in the synthesis of these ILs are sodium acetate and ethyl acetate. Sodium acetate is a white solid, which is precipitated in the synthesis of EBS, ETS and EXS ILs. Ethyl acetate is evaporated using rotary evaporation from EEBS IL synthesis products.

Analytical techniques such as fourier transform infrared spectroscopy (FTIR) and proton nuclear magnetic resonance spectroscopy (^{1}H NMR) have been used for the structural determination study of these ILs. As both byproducts contain acetate, it is very important to observe the absence of acetate in FTIR and NMR. The ethyl functional group is also monitored in EEBS to ensure complete removal of any leftover reactants and to achieve purity of the EEBS IL.

2.2.1. FTIR Spectroscopic Analysis of Ionic Liquids

A broad part of the electromagnetic spectrum that lies between the electromagnetic and the microwave regions is termed the infrared (IR) region.[1] All organic and some of the inorganic molecules absorb light in the infrared region causing bond vibrations which are detected as the IR spectra. The vibrational-rotational bands occurring in the region of 4000 and 400 cm^{-1} gives us the information about functional groups in the compounds. This analytical technique is generally used to determine the functional groups and molecular composition of surfaces.[2]

2.2.1.1. Experimental

A Nicolet 380 FTIR spectrometer from Thermo-Scientific (Bridgewater, NJ) was used to obtain the FTIR spectra of the ILs in this study. The FTIR spectra were obtained with an 8 cm^{-1} resolution in the range 4000-700 cm^{-1} with 100 scans frequency. The spectral interpretation was done using the OMNIC analysis software supplied with the spectrometer.

2.2.1.2. Results and Discussion

A stretching absorption band is found in all four ILs at around 3500 cm^{-1} showing the characteristic absorption of N-H stretching from the heterocyclic ring of the imidazolium cation. The FTIR spectra of the EBS, EEBS, ETS and EXS ILs are shown in Figures 11–14 respectively. The

bands at 3500 cm^{-1} are widened due to the high concentration of ILs that were used. Ring stretching vibrations (C=C and C=N) occur in the general region between 1600 and 1300 cm^{-1} for aromatic heteroatoms and these bands are seen at 1572 and 1444 cm^{-1} for the imidazolium cation in all ILs.[3]

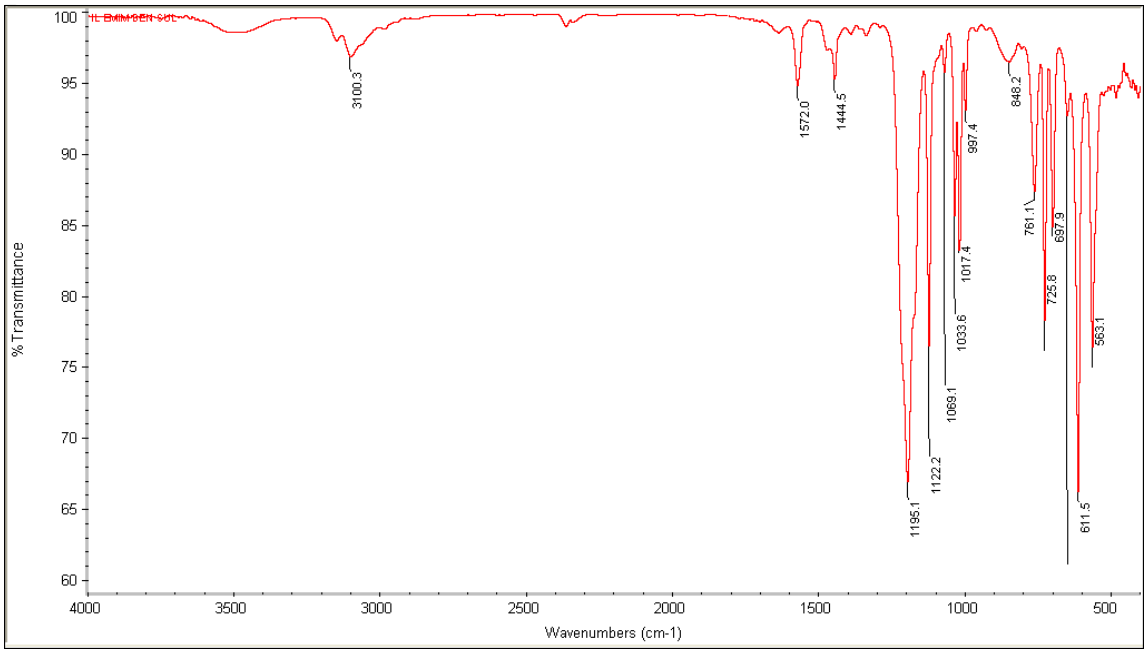

Figure 11. The FTIR spectra of 1-ethyl-methylimidazolium benzenesulfonate (EBS) ionic liquid synthesized from sodium benzenesulfonate and 1-ethyl-methylimidazolium acetate.

An aromatic C-H stretching band is found near 3100 cm^{-1} showing the characteristic aromatic ring nature of the anions EBS, ETS and EXS in Table 6. The vibration absorption frequency between the sulfur and oxygen bonds is seen around 1352 and 1122 cm^{-1}. The sulfonate in all the anions

from this study shows an asymmetric stretch as a doublet at 1352 cm^{-1}.

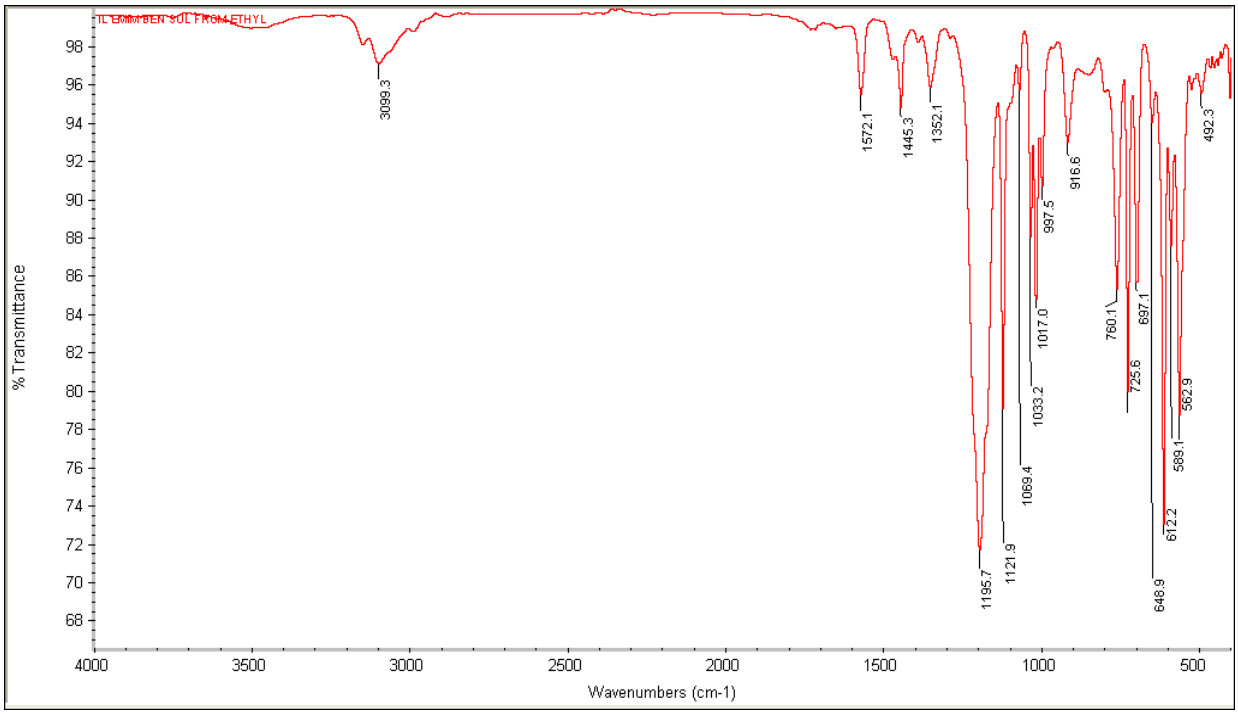

Figure 12. The FTIR spectra of 1-ethyl-methylimidazolium benzenesulfonate (EEBS) ionic liquid synthesized from ethyl benzenesulfonate and 1-ethyl-methylimidazolium acetate.

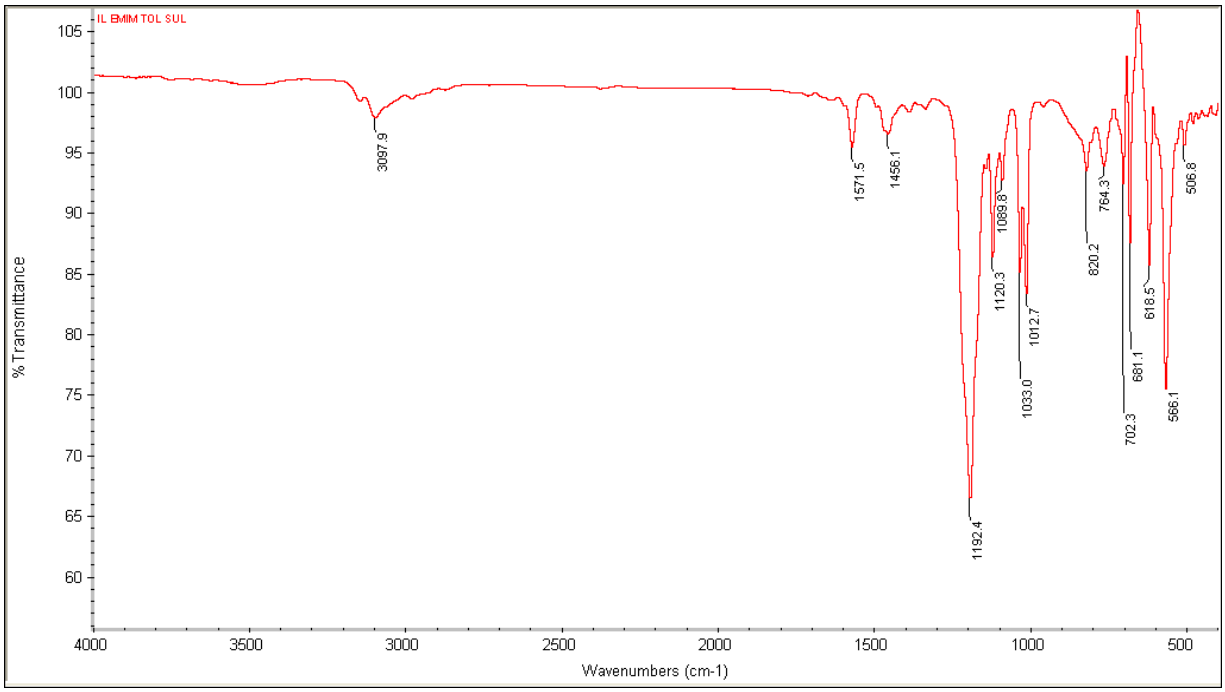

Figure 13. The FTIR spectra of 1-ethyl-methylimidazolium toluenesulfonate (ETS) ionic liquid synthesized from sodium toluenesulfonate and 1-ethyl-methylimidazolium acetate.

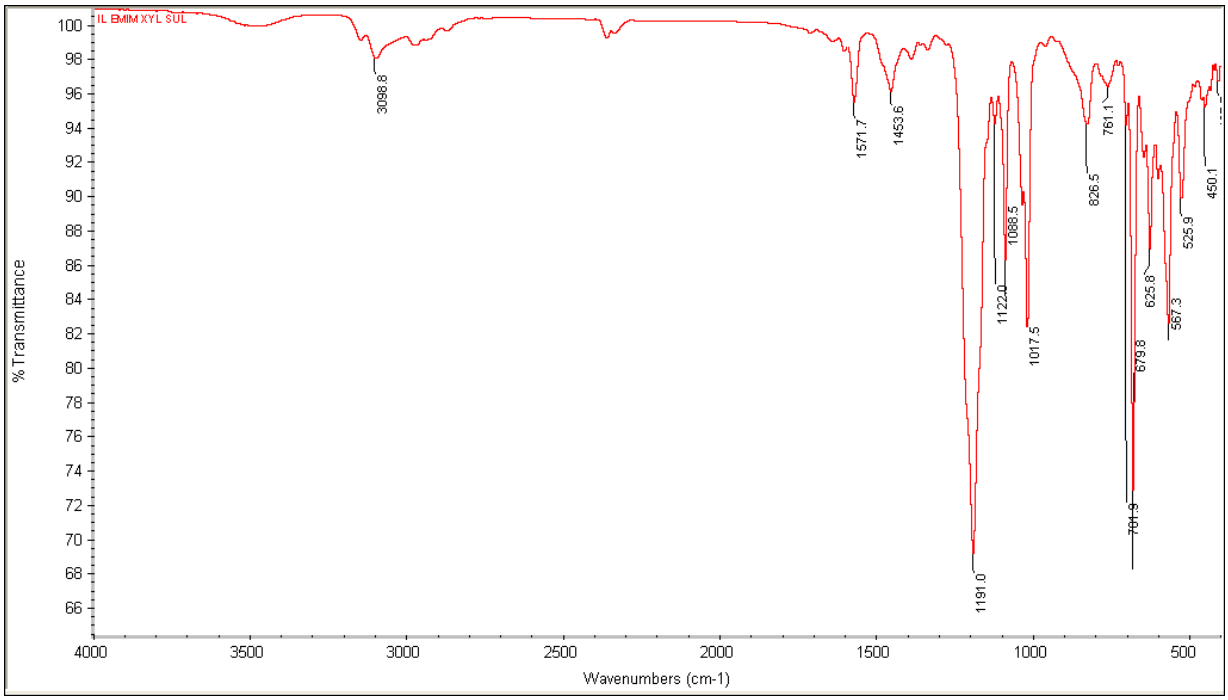

Figure 14. The FTIR spectra of 1-ethyl-methylimidazolium xylenesulfonate (EXS) ionic liquid synthesized from sodium xylenesulfonate and 1-ethyl-methylimidazolium acetate.

A symmetric stretching frequency from the sulfonate portion of the anion is seen at 1195 cm^{-1} for $S(=O)_2$ and at 1122 cm^{-1} for S=O. Various strong in-plane and out-of-plane C-H bending absorptions were found from 1069 through 761 cm^{-1} and out-of-plane ring C=C bending were found from 725 through 563 cm^{-1} in all ILs from the study. All values are in agreement with the FTIR frequency bands from literature.[1]

Table 6. Absorption bands (cm^{-1}) of EBS, EEBS, ETS and EXS from all four FTIR spectra are assigned to their characteristic absorption origins.

Absorption Band (cm^{-1})	EBS	EEBS	ETS	EXS	Band Origin
3500	*	*	*	*	Hetero-aromatic N-H stretching vibration
3100	*	*	3097	*	Aromatic C-H stretching
1572	*	*	*	*	Hetero-aromatic ring stretching vibrations (C=C and C=N)
1444	*	*	1456	*	Skeletal bands or ring stretching vibrations (C=C and C=N)
1352	*	*	*	*	Asymmetric S=O stretching
1195	*	*	1192	1191	Symmetric stretching frequency of $S(=O)_2$
1122	*	*	1120	1120	Stretching vibrations of S=O
1069	*	*	1089	1088	In-plane C-H bending
1033	*	*	*	*	In-plane C-H bending
1017	*	*	1012	*	In-plane C-H bending
997	*	*	–	–	Out of plane C-H bending
848	*	–	820	826	Out of plane C-H bending
761	*	*	*	*	Out of plane C-H bending
725	*	*	702	702	Out of plane ring C=C bending
697	*	*	681	679	Out of plane ring C=C bending
611	*	*	618	625	Out of plane ring C=C bending
563	*	*	566	567	Out of plane ring C=C bending

*Denotes that the IL has the band mentioned in the respective Absorption band column

2.2.1.3. Conclusion

The absorption bands at 3500 and 3100 cm^{-1} show the presence of a heteroaromatic ring with N-H stretch and aromatic C-H stretching respectively. Along with the bands at 3500 and 3100 cm^{-1}, vibrations at 1574 and 1444 cm^{-1} give the evidence of the presence of aromatic imidazolium and benzene rings. Presence of the S-O and $S(=O)_2$ stretching frequencies at 1352 and 1195 cm^{-1} respectively support the presence of sulfonate group in the compound. Absence of any absorption at 1700 cm^{-1} shows an absence of C=O group in the compound, showing complete elimination of acetate by-product formed in the synthesis of ILs. The data interpreted from FTIR spectra is further confirmed with ^1H NMR data in section 4.3.

2.2.2. ^1H NMR Spectral Analysis of Ionic Liquids

Nuclear magnetic resonance spectroscopy is another form of molecular spectroscopy.[1] Under a particular magnetic field, a sample can absorb electromagnetic radiation in a specific radio-frequency region (RF), which is a function of certain nuclei in the molecule.[1] All the protons with the same frequency of absorption create an equivalent proton environment which gives rises to characteristic peaks in the spectra. The density of the electron cloud shielding the proton varies with the chemical environment, giving

rise to differences in the chemical shift positions. The number of protons on adjacent carbons and their extent of shielding sensitively effect a proton environment. This phenomenon creates splitting of the absorption peaks in NMR spectra depending on the proton chemical-shift environment. The chemical shift and splitting of the absorption peaks in the NMR spectra have been exploited to interpret the structural data.

2.2.2.1. Experimental

The ^{1}H NMR spectroscopy was employed to investigate the structure of EBS, EEBS, ETS and EXS IL's based on their ^{1}H chemical shifts from the spectra. All ILs are synthesized according to the protocol in section 2.2. These studies were done on a Bruker Advance 400 MHz solutions spectrometer (Billerica, MA) equipped with a QNP 5-mm probe at 295 K. Tetradeuteromethanol (CD_3OD) with 99.96 % isotopic purity from Sigma-Aldrich was used as a solvent. The ^{1}H NMR spectra were recorded on a 512 scan mode at a 90° pulse angle with 2-sec pulse delay. The ^{1}H NMR experimental spectra were analyzed on Topspin 1.3 software.

2.2.2.2. Results and Discussion

The study of the ^{1}H NMR spectra clearly shows that the chemical shifts (δ) are sensitively affected by the composition of the chemical system.[2-5] Higher δ values

indicate that the proton is more de-shielded (downfield shift) as a result of a lower electron-density environment. The Table 7 shows chemical shifts assigned to the proton environments in the cation and anion structures from Figure 16.

The ^{1}H NMR spectra of EBS, EEBS, ETS, and EXS ILs are plotted in the Figure 15. Chemical structures and proton chemical environment numbering of the cation and anions being used in this study are shown in Figure 16. The Solvent tetradeuteromethanol (CD_3OD) showed two prominent chemical environments in the ^{1}H NMR spectra of EBS, EEBS, ETS, and EXS ILs. The proton from the hydroxyl group of methanol-d_4 showed a chemical shift of 3.35 ppm and the second chemical shift was due to the equivalent protons from the methyl group at 4.90 ppm.

The ^{1}H environments for H1-H7 are similar for all the four ILs as all have 1-ethyl-3-methylimidazolium cation. The H1 proton showed the largest chemical shift irrespective of the anion type between the four ILs. The H1 proton is the most acidic proton on imidazolium and is highly deshielded, hence it shows a large downfield chemical shift with a value of 8.94 ppm in all four ILs.[6] As there are no protons on the carbon adjacent to the H1

proton, the peak at 8.94 ppm shows no splitting and is a singlet.

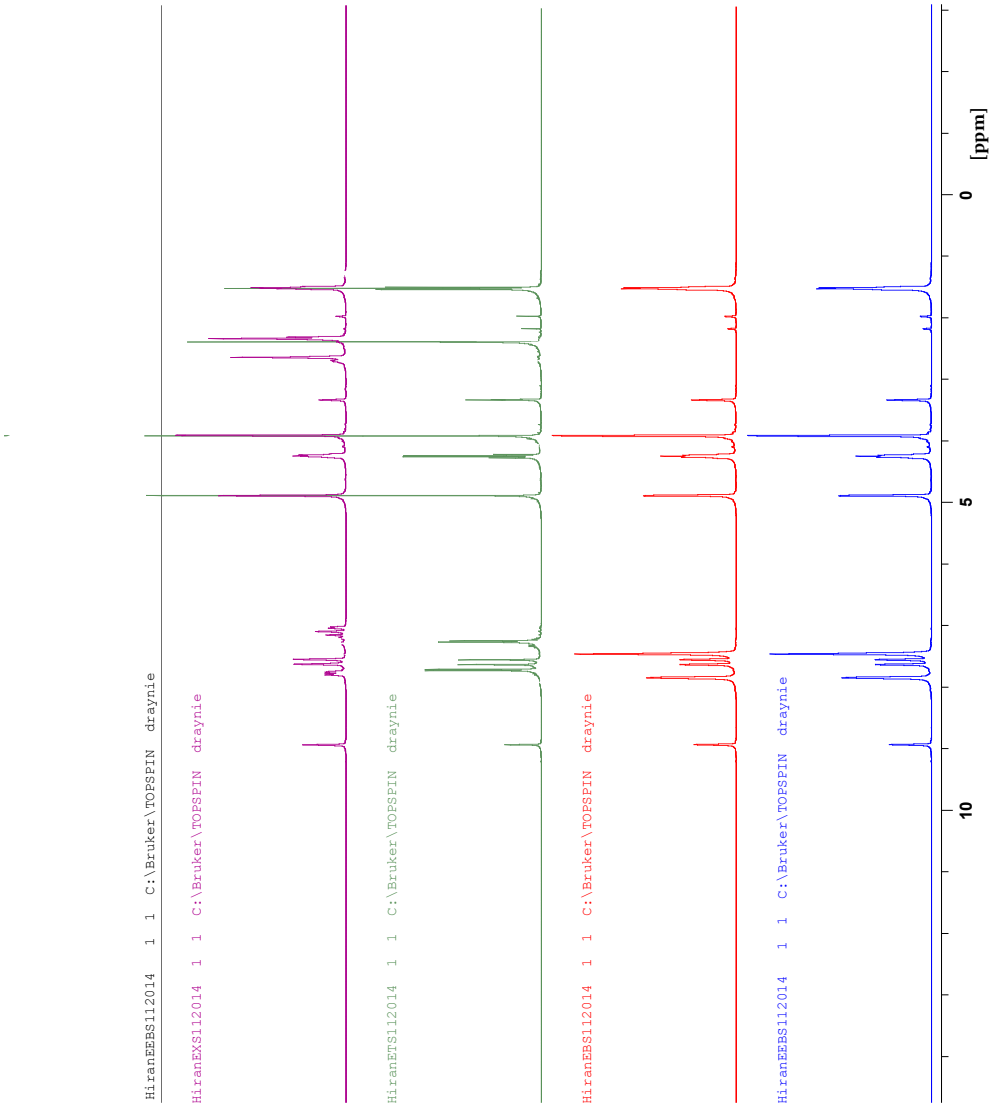

Figure 15. Stacked ^{1}H NMR spectra of EBS, EEBS, ETS and EXS ILs from top to bottom respectively. This proton NMR spectra has been analyzed on a 400 MHz NMR spectrometer.

The H2 and H3 protons on the imidazolium show a slight difference in the chemical shift of 0.09 ppm due to the presence of unequal chemical environments on the nitrogens adjacent to them. The H2 and H3 protons show a chemical shift of 7.55 and 7.64 ppm respectively. As both the proton environments have one adjacent proton to them, they both show a doublet splitting. However, only a partial doublet is seen due to insufficient resolution of the NMR. Better resolution of the peaks is expected if run on a higher magnetic field than 400 MHz.

The H6 proton environment consists of the three protons from the methyl group with two adjacent hydrogens on a pro-chiral carbon. Therefore, the H6 proton shows a triplet splitting due to the protons from the prochiral carbon. The H6 is the most shielded proton environment in imidazolium cation with a chemical shift of 1.53 ppm.

The H4 and H5 proton environments are from a CH_2 group, where the carbon is attached to nitrogen and another carbon apart from its two hydrogens. Hence, this makes the carbon bearing the H4 and H5 protons a pro-chiral carbon, contributing an unequal chemical environment to H4 and H5 positions. There is a slight difference in the proton environment between H4 and H5 due to the prochiral carbon which accounts for a 0.33 ppm chemical shift. The chemical

shifts for H4 and H5 protons are 4.25 and 3.92 ppm respectively.

Table 7. Chemical shift values assigned to the peaks in ^{1}H NMR spectra of EBS, EEBS, ETS and EXS ILs. The numbering in the first column H1-H10 (^{1}H NMR chemical shifts) corresponds to the numbering from the structures in Figure 16.

1H-NMR Chemical Shifts	**EBS (ppm)**	**EEBS (ppm)**	**ETS (ppm)**	**EXS (ppm)**
Solvent	3.35, 4.90	3.35, 4.90	3.35, 4.90	3.35, 4.90
H1	8.94	8.94	8.94	8.94
H2	7.55	7.55	7.55	7.55
H3	7.64	7.64	7.64	7.64
H4	4.25	4.25	4.25	4.25
H5	3.92	3.92	3.92	3.92
H6	1.53	1.53	1.53	1.53
H7	1.97	1.97	1.97	1.97
$H7^{1}$	2.18	2.18	2.18	2.18
H8	7.85	7.85	7.72	7.75
H9	7.46	7.46	7.25	7.10
H10	7.46	7.46	2.40	2.29

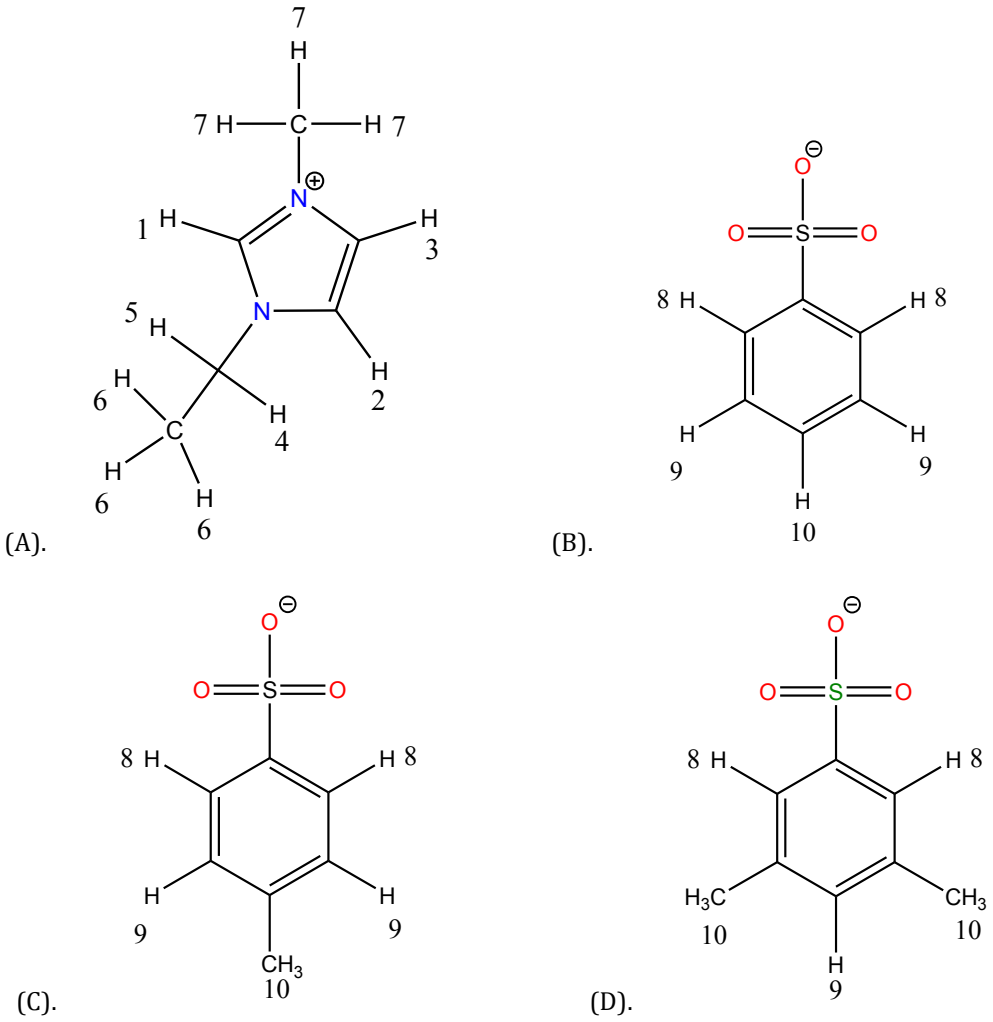

Figure 16. Chemical structures and hydrogen chemical environment numbering of the cation and anions being used in this study. The numbering on all ions is for the different chemical shifts to which the respective protons belong. The common cation ion used in all four ILs is the (A). 1-ethyl-3-methyl imidazolium. The anions used are (B). Benzenesulfonate, (C). Toluenesulfonate and (D). Xylenesulfonate.

The H7 proton environment is from the methyl group on imidazolium. No splitting is seen due to the absence of adjacent hydrogen atoms. The H7 protons show a chemical shift of 1.97 ppm. There is a ghost peak $H7^1$ seen in the NMR spectra of EBS, EEBS, ETS and EXS, which is around half the size of H7 peak. This peak may be attributed to a change in the chemical environment of H7 peak due to the influence of the protons from anion.[7] There is no splitting seen either in H7 or in $H7^1$ protons. The $H7^1$ peak is very suppressed in the EXS IL NMR spectra as is very hard to differentiate it from the baseline unless largely expended. The reason for this can be due to a specific arrangement of anions around the cation that prevents influence on the H7 proton environment in EXS.[8] The $H7^1$ environment can be further confirmed experimentally by performing 2D NMR studies.

There are three proton environments in the anions of EBS, EEBS, ETS and EXS ILs represented by H8, H9 and H10 as shown in Fig C. The H9 and H10 in EBS and EEBS are represented by a chemical shift of 7.46 ppm with a single peak. The H9 and H10 peaks may be differentiated as two different environments using a higher magnetic field than 400 MHz as used here. In ETS, the H9 proton environment shows a chemical shift at 7.25 ppm as a doublet. The H9 ^1H

in EXS is furthermore shielded when compared to EBS, EEBS and ETS ILs, hence it shows up at 7.10 ppm.

The H10 proton chemical environment arises from a single methyl group at para position on the benzenesulfonate anion in ETS with a chemical shift of 2.40 ppm. The H10 proton environment with 2.40 ppm chemical shift corresponds to the two methyl groups at the meta positions in xylenesulfonate anion in EXS.

2.2.2.3. Conclusion

The different ^{1}H environments on the EBS, EEBS, ETS and EXS ILs have been investigated to determine the structures and purity of the compounds. The proton chemical shift values assigned to the imidazolium are in good agreement with the literature values[2-5], however, there is not much ^{1}H NMR data available on the anions being studied. All chemical shifts found in the NMR spectra have been assigned to their respective protons based on the differences in their chemical environments. The data from FTIR and NMR compliment the structures of anions and cation from Figure 16 being studied in this work.

2.3. Physical characterization of the IL's

2.3.1. Viscosity of Ionic Liquids Using Rheometer

Viscosity is an important parameter to be considered during design and optimization of ILs. The knowledge of this physical property is essential when using ILs as solvents such as in this study. The viscosities of imidazolium ionic liquids are generally at least 1-3 orders of magnitude higher than the conventional organic solvents.[9-12] Hydrogen bonding and Van der Waals forces are two major interactions governing the viscous nature of compounds.[12] Viscous behavior of EBS, EEBS, ETS and EXS have been studied over a range of temperatures using a Rheometer.

2.3.1.1. Experimental

The ILs were vacuum dried at 70 °C for five hours using a rotary evaporator and the water content was measured using Karl Fisher titration before the viscosity measurements. The viscosity measurements were made on a Brookfield DV-III Ultra Rheometer (Middleboro, MA). A CP40 spindle with LV mode was used for the viscosity measurements. The LV mode is a spring torque model with a viscosity measurement range up to 63770 centipoise. Brookfield mineral oil (Middleboro, MA) viscosity reference standard was used for calibration of the instrument. A temperature probe from Rheometer was

connected to the water bath. An external circulating water bath was connected to the viscosity measurement chamber to control temperature. Viscosity measurements for the EBS, EEBS, ETS, and EXS IL's were measured over a range of temperatures from 25 °C through 100 °C using 0.5 mL sample volume. One data point was collected every 10 seconds throughout the measurement and the data was continuously recorded using the RheoCalc software. Dynamic viscosity of the ILs is reported in the centipoise.

2.3.1.2. Results and Discussion

The EBS, EEBS, ETS, and EXS exhibit 67, 67, 510 and 6467 cP viscosities at 25 °C respectively. As shown in Figure 17, the EBS and EEBS exhibit similar viscous behavior from 25 to 100 °C. Significant increase in the viscosity was observed with EBS, ETS, and EXS as a result of an extra methyl group (Figures 17 and 18).

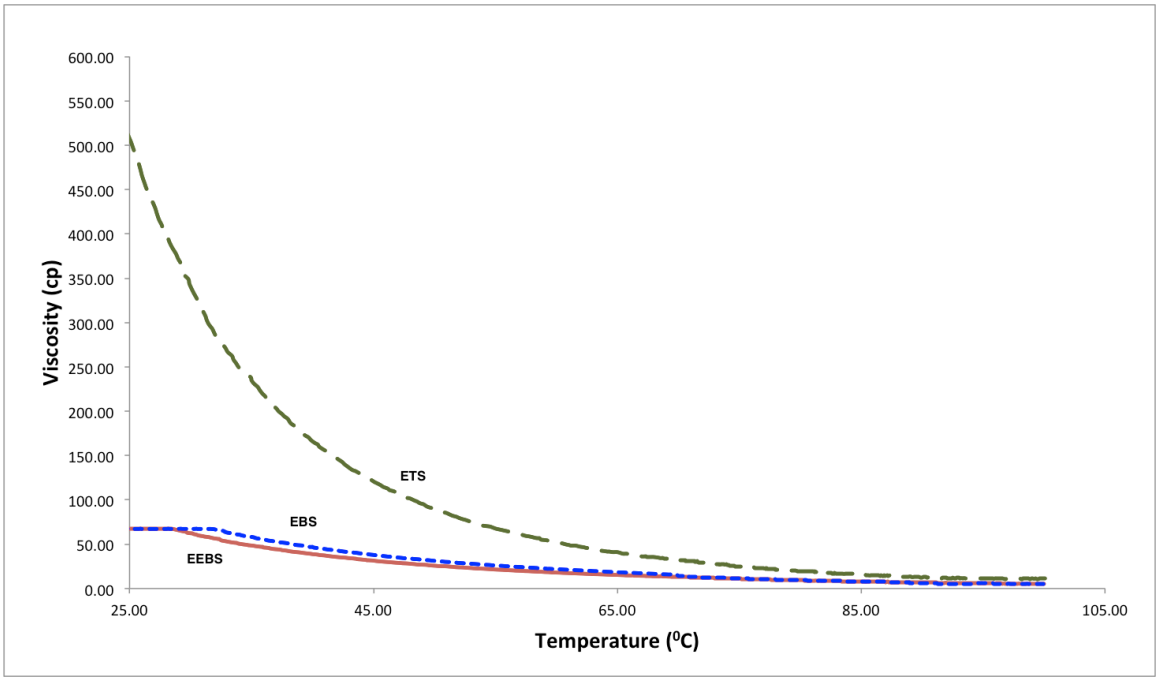

Figure 17. Viscosity of EBS, EEBS, and ETS ILs as a function of temperature from 25 to 100 °C. The viscosities of EBS, EEBS, and ETS at 25 °C are 67 cP, 67 cP and 510 cP respectively.

The viscosity of ILs is governed by hydrogen bonding and Van der waals interactions.[13] The stronger Van der waals interactions from the methyl group and increased hydrogen bonding significantly increases the viscosities of these ionic liquids. Higher viscosities of EXS and ETS when compared to EBS and EEBS can also be attributed to the asymmetry and limited mobility due to increased anion size. The Figures 17 and 18 also show the temperature dependence of the dynamic viscosity of EBS, EEBS, ETS, and EXS ILs.

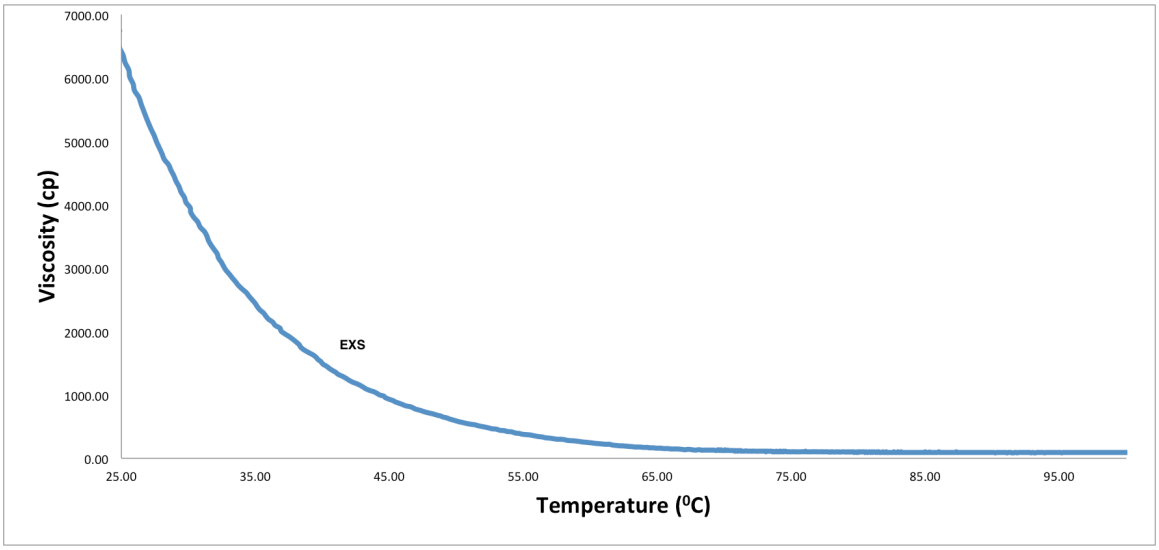

Figure 18. The viscosity of EXS as a function of temperature from 25 to 100 °C is shown in this figure. The viscosity of EXS at 25 °C is 6467 cP, which gradually decreases with increase in temperature.

2.3.1.3. Conclusion

The viscous nature of EBS, EEBS, ETS, and EXS ILs was observed to increase with increasing methylation and anion size in the following order EBS ~ EEBS < ETS < EXS.

2.3.2. Water content in Ionic Liquids

The moisture content in ILs may affect the solvent functionality of ILs such as viscosity and thermal study. Therefore, it is important to determine the water content of ILs. The ILs were vacuum dried at 70 °C for five hours

using a rotary evaporator before the Karl Fisher titration. Presence of high water content in ILs disrupts hydrogen bonding between the solvent and the solute. The main aim of this study is to determine the water content in the dry ionic liquids.

2.3.2.1. Experimental

The water content in EBS, EEBS, ETS, and EXS IL's was determined using Mettler Toledo V20 volumetric Karl-Fischer titrator (Columbus, OH). Sigma Aldrich Hydranal® Composite titrant (St. Louis, MO) was used as the reagent and Hydranal® Methanol-dry was used as the sample solvent. The titrant was added to the burette and sample to titration vessel. The instrument was zeroed by titrating unwanted moisture in the system. All samples were weighed using "weight by difference". A pre-weighed dry syringe was used to weigh 0.4 g of IL samples. Each IL was titrated with the reagent from burette while stirring. When the end point was reached, water content (in ppm) was calculated based on the amount of titrant used in the titration. Measurements were made in triplicates to calculate the standard deviation.

2.3.2.2. Results and Conclusion

The water content of EBS, EEBS, ETS and EXS was found to be 352.7±4.7, 346.7±0.6, 280.0±2.6, and 273.3±0.6 ppm. The ILs were dried before the Karl Fischer titration, hence

conclusions cannot be made on the hydrophobicity of the ILs based on this method.

2.3.3. Solvatochromic parameters of ILs

The use of ILs as extraction solvents has increased considerably in recent years due to several characteristics such as their solubilization properties, low vapor pressure and ease of their design by selecting proper cation and anion.[14, 15] The polarity of several ionic liquids have been analyzed based on a normalized scale, E^N_T using Reichardt's dye and the Kamlet Taft parameter (π^*).[16-21] The literature on polarity studies show that the most commonly used ionic liquids have polarity that lies on a scale in between acetone and Water.[21-23]

The Reichardt's normalized scale and Kamlet Taft parameters of many ILs have been examined to understand their interactions with solvatochromic probes.[21-29] Three key solvatochromic parameters can be calculated using the Kamlet Taft model, namely dipolarity/polarizability (π^*), hydrogen bond acidity (α) and hydrogen bond basicity (β).[30-33] This study focuses on calculating the E^N_T, π^*, α and β values for EBS, EEBS, ETS, and EXS ILs using the common solvatochromic probes[30-33] Reichardt's dye, 4-nitroaniline and N,N-diethyl-4-nitroaniline.

2.3.3.1. Experimental

The solvatochromic probes Reichardts's dye and 4-nitroaniline were purchased from Sigma Aldrich (St. Louis, MO), and N,N-diethyl-4-nitroaniline was purchased from Oakwood Products (Columbia,SC). A SpectraMax Spectrophotometer M2 (Silicon Valley, CA) was used for the UV-Vis measurements and all spectra were recorded at 25 °C. Falcon Microtest 96-well flat bottom plates were used for sample loading for this study. Three 96-well plates were coated with one of the three solvent probes, Reichardts's dye (RD), 4-nitroaniline (NA) and N,N-diethyl-4-nitroaniline (DENA). The probes were mixed with ethanol and added to the 96-well plates. Later, ethanol was completely evaporated leaving the probes behind in the plates. The concentration of RD, DENA and NA in each well was 14.5 μM, 8.24 μM and 11.58 μM respectively after addition of 250 μL of the ILs. The ILs were vacuum dried at 70 degrees for 5 hours using a rotary evaporator before adding them to the 96-well plates. After addition of IL's, the plates were vortexed gently using a VWR microplate vortex mixer for one hour at 25 °C and the λ_{max} was analyzed using UV-Vis.

2.3.3.2 Results and Discussion

The E_T^N solvent scale represents the overall interactions between the solvent and the dye. The Equation

1 is used to calculate the $E_T(30)$ using RD, where λ_{max} is the wavelength corresponding to maximum absorption.[34] The equation 2 has been used to calculate the normalized E_T^N value of the ILs using the $E_T(30)$ calculated from equation 1.[34] The Kamlet-Taft parameter π^* is calculated using the Equation 3, where ν_{max} is the wavelength of maximum absorbance of the dye DENA in kilokayser (1 kK = 1000 cm^{-1}).[35] The ν_0 = 27.52 kK and S = -3.182. The ν_0 is the regression value for a reference solvent system and the S is the susceptibility of spectral absorption as a result of change in dipolarity/polarizability ratio.[35]

$$E_T(30) / kcal\ mol^{-1} = \frac{28591}{\lambda_{max}\ (nm)} \quad (1)$$

$$E_T^N = \frac{E_T(30) - 30.7}{32.4} \quad (2)$$

$$\pi^* = \frac{\nu_{max} - \nu_0}{S} \quad (3)$$

The Kamlet Taft parameters α and β are calculated using equations 4 and 5, respectively.[35] The α and β parameters provide hydrogen bond-donating acidity (HBD) and hydrogen bond-accepting basicity (HBA) values of the solvents

respectively.[34] The $\nu(1)_{max}$ and $\nu(2)_{max}$ in equation 5 corresponds to the wavelengths of maximum absorbance of NA and DENA.[35]

$$\alpha = \frac{(E_T\,(30) - 14.6\,(\pi^* - 0.23) - 30.31)}{16.5} \quad (4)$$

$$\beta = \frac{(1.035\,\nu(2)_{max} - \nu(1)_{max} + 2.64)}{2.8} \quad (5)$$

The Kamlet Taft parameters of EBS, EEBS, ETS, and EXS ILs have been calculated using equations 1-5 and the E_T^N, π^*, α and β values are displayed in Table 8. All four ILs show similar values for all of the measured parameters. Based on these parameters, the EBS and EEBS ILs show the same behavior and the ETS and EXS have a common behavior. The E_T^N scale is applied to analyze the solvating ability of the ionic liquids.[36]

The E_T^N values of EBS, EEBS, ETS and EXS fall in the polar hydrogen bond-donor range.[36] This scale is sensitive to the hydrogen bond-donor ability of the cation in ionic liquid. The HBD ability of the N-H bond in imidazolium cation contributes to the E_T^N scale seen in EBS, EEBS, ETS, and EXS Ils. All three imidazolium ring protons are acidic

which makes the cation a significant hydrogen bond donor to the solute in absence of hydrogen bond-accepting anions.[38]

The π^* value is obtained from the spectroscopic shift of the DENA and is also used to describe dispersion, induction and electrostatic interactions.[36-38] The π^* is high[37] for the all four IL's and can be attributed to the higher polarizability of the aromatic rings. The high polarizability of the delocalized system on the imidazolium cation also results in an increased π^* value.

Table 8. The Kamlet-Taft solvatochromic parameters of EBS, EEBS, ETS, and EXS ILs at 25 °C.

	E_T^N	π^*	α	β
EBS	0.69	0.95	0.74	0.33
EEBS	0.69	0.95	0.74	0.33
ETS	0.75	1.08	0.75	0.42
EXS	0.75	1.08	0.75	0.42

The α value for the EBS, EEBS, ETS, and EXS ILs is 0.74, 0.74, 0.75 and 0.75 respectively and can be attributed to the imidazolium cation. This is due to the highly acidic proton present at the C2 position of the

imidazolium that has a high impact on the hydrogen bonding network.[38] The spectroscopic shifts of both NA and DENA are used to calculate the hydrogen bond basicity. Literature values show that the β value is mostly dependent on the hydrogen bond basicity of the anion in the ILs.[39] Any variation of the cation such as its chain length showed an insignificant effect on the β parameter.[39] Delocalized electron system in the anion aromatic ring makes it a weak hydrogen bond acceptor, decreasing the β parameter. Though anions in this study are weak HBA's, an increase in the β parameter has been observed from EBS and EEBS to ETS and EXS. Addition of a methyl group is responsible for the increased β parameter observed in the ETS and EXS.[39]

2.3.3.3. Conclusion

The EBS, EEBS, ETS, and EXS ILs are polar solvents which is evident by their E_T^N values and have a π^* between 0.98 to 1.08. The α and β parameters determined in this study suggest that the ILs are good hydrogen bond donors and can some times behave as hydrogen bond acceptors.[39]

2.4. References

1. Suzie, S. T.; Douglas, R. M.; Jonathan, U.; Leslie, A. E.; William, O. S. D.; Antonio F. P.; Jennifer, M. P.; Janet, L. S.; *Green Chem.* **2009**, *11*, 339-345.
2. Silverstein, R. M.; Webster, F. X.; Kiemle, D. J. *Spectrometric identification of organic compounds;* Hoboken, NJ: John Wiley & Sons, 2005.
3. Flaminia, C. M.; Cristina, P.; Olga, R.; Lorenzo, G.; Giuseppe, S.; Adolfo, L. *Chem. Phys. Chem.* **2012**, *13,* 1339-1346.
4. Jiang, W.; Wang, Y.; Voth, G. A. *J. Phys. Chem. B.* **2007**, *111,* 4812-4818.
5. Triolo, A.; Russina, O.; Fazio, B.; Triolo, R.; Do Cola, E. *Chem. Phys. Lett.* **2008**, *457,* 362-365.
6. Tokuda, H.; Hayamizulshii, K.; Susan, M. A. B. H.; Watanabe, M. *J. Phys. Chem B.* **2005**, *109,* 6103-6110.
7. Wang, P.; Zakeeruddin, S. M.; Exnar, I.; Gratzel, M. *Chem. Commun.* **2002**, 2972-2973.
8. Kolle, P.; Dronskowski, R. *Eur. J. Inorg. Chem.* **2004**, 2313-2320.
9. Mizumo, T.; Marwanta, E.; Matsumi, N.; Ohno, H. *Chem. Lett.* **2004**, *33*, 1360-1361.
10. Dean, J. A. *Lange's Handbook of Chemistry*, 15th ed. McGraw-Hill, New York, **1999.**

11. Holbrey, J. D.; Seddon, K. R. *J. Chem. Soc. Dalton Trans*. **1999**, *13*, 2133.
12. Zhang, S.; Sun, N.; He, X.; Lu, X.; Zhang, X. *J. Phys. Chem. Ref. Data,* **2006**, *35*, 4.
13. Bonhote, P.; Dias, A. P.; Papageorgiou, N.; Kalyanasundaram, K.; Gratzel, M. *Inorg. Chem*. **1996**, *35*, 1168.
14. Sun, P.; Armstrong, D.W. *Anal. Chem. Acta*. **2010**, 661 1—16.
15. Huddleston, J.G.; Visser, A.E.; Reichert, W.M.; Willauer, H.D.; Broker, G.A.; Rogers, R.D. *Green Chem*. **2001**, *3*, 156—164.
16. Reichardt, C. *Green Chem*. **2005**, *7*, 339—351.
17. Machado, V.G.; Stock, R.I.; Reichardt, C. **2014**, *114*, 10429—10475.
18. Jessop, P.G.; Jessop, D.A. *Green Chem.* **2012**, *14*, 1245—1259.
19. Khupse, N.D.; Kumar, A. *J. Phys. Chem. B.* **2010**, *114*, 376—381.
20. AbRani, M.A.; Brant, A.; Crowhurst, L.; Dolan, A.; Lui, M.; Hassan, N.H. *Phys. Chem. Chem. Phys.* **2011**, *13*, 16831—16840.
21. Crowhurst, L.; Falcone, R.; Lancaster, N.L.; Llopis-Mestre, V.; Welton, T. *J. Org. Chem.* **2006**, *71*, 8847—

8853.

22. Mellein, B.R.; Aki, S.N.V.K.; Ladewski, R.L.; Brennecke, J.F. *J. Phys. Chem. B.* **2006**, *111*, 131—138.
23. Lee, J.M.; Ruckes, S.; Prausnitz, J.M. *J. Phys. Chem. B.* **2008**, *112*, 1473—1476.
24. Fletcher, K. A.; Storey, I. A.; Hendricks, A. E.; Pandey, S. *Green Chem.* **2001**, *3,* 210.
25. Fletcher, K. A.; Pandey, S. *Appl. Spectrosc.,* **2002**, *56*, 266.
26. Dzyuba, S. V.; Bartsch, R. A. *Tetrahedron Lett.* **2002**, *43*, 4657.
27. Baker, S. N.; Baker, G. A.; Bright, F. V. *Green Chem.* **2002**, *4*, 165.
28. Huddleston, J. G.; Broker, G. A.; Willauer, H. D.; Rogers, R. D. In *Ionic Liquids: Industrial Applications for Green Chemistry*, ACS Symposium Series No. 818, **2002**.
29. Crowhurst, L.; Mawdsley, P. R.; Perez-Arlandis, J. M.; Salter, P. A.; Welton, T. *Phys. Chem. Chem. Phys.* **2003**, *5*, 2790.
30. Kamlet, M. J.; Abboud, J. L.; Taft, R. W. *J. Am. Chem. Soc.* **1977**, *99*, 6027.
31. Taft, R. W.; Kamlet, M. *J. Am. Chem. Soc.* **1976**, *98*, 2886.

32. Taft, R. W.; Kamlet, M. *J. Am. Chem. Soc.* **1976**, *98*, 377.

33. Yokoyama, T.; Taft, R. W.; Kamlet, M. *J. Am. Chem. Soc.* **1976**, *98*, 3233.

34. Reichardt, C. *Chem. Re*V. **1994**, *94*, 2319-2358.

35. Kamlet, M. J.; Taft, R. W. *J. Am. Chem. Soc*. **1976**, *98*, 377. Taft, R.; Kamlet, M. J. *J. Am. Chem. Soc*. **1976**, *98*, 2886. Kamlet, M. J.; Abboud, J. L.; Abraham, M. H.; Taft, R. W. *J. Org. Chem*. **1983**, *48*, 2877.

36. Reichardt, C. "Solvents and Solvent Effects in Organic Chemistry, 2nd ed. VCH, Weinheim, 1990; (b) Reichardt, C. *Chem. Rev.*, 1994, **94**, 2319.

37. Muldoon, M. J.; Gordon, C. M.; Dunkin, I. R. *J. Chem. Soc., Perkin Trans.* **2001**, *2*, 433.

38. Elaiwi, A.; Hitchcock, P. B.; Seddon, K. R.; Srinivasan, N.; Tan, Y.-M.; Welton T.; Zora, J. A. *J. Chem. Soc., Dalton Trans.* **1995**, 3467.

39. Crowhurst, L.; Mawdsley, P. R.; Perez-Arlandis, J. M.; Salter, P. A.; Welton, T. *Phys Chem Chem Phys.* **2003**, *5,* 2790.

CHAPTER 3

THERMAL BEHAVIOR OF 1-ETHYL-3-METHYLIMIDAZOLIUM ALKYLBENZENESULFONATE IONIC LIQUIDS

3.1 Introduction to Thermal Analysis

Thermal analysis is a set of techniques used to determine physical and chemical properties of compounds. These properties include but are not limited to glass transition, crystallization, melting, glass formation, thermal decomposition, evaporation, sublimation, and chemical reactions such as oxidation. Thermal analysis is a very important tool to understand the behavior of a compound over a range of temperatures.

Understanding thermochemical behavior of ILs can be challenging because of the weak interaction between the cation and anion. Due to this behavior, most of the ionic liquids tend to form glasses.[1,2] Most of the imidazolium ILs reported in literature show the formation of glasses and subcooling, along with a glass transition without a melting transition.[3-5] ILs with 1-alkyl-3-alkyl-imidazolium cations are well studied for their thermal properties based on the length of their hydrocarbon branch chains.[6,7] Thermal stability is a very important factor that dictates applicability of ILS for high temperatures needs.

There have been studies on ionic liquids such as 1-butyl-3-methylimidazolium iodide, [BMIM]I, which reported no phase transitions of any sort in the temperature range from -90 °C to 130 °C.[8] Only a thermal decomposition onset temperature has been described to be around 265 °C.[9] An absence or a poorly detectable exothermic crystallization transition is reported for most of the halogen-containing imidazolium ionic liquids.[10-13]

The aim of this study is to analyze physical and chemical changes in four ILs, EBS, EEBS, ETS and EXS using DSC and TG/DTA. As these ionic liquids will be mainly used in the isolation of lignin from Prairie cord grass at high temperatures, it is important to study their thermal properties in order for better solvent recovery. DSC is used to determine crystallization, melting, glass transition, and other mesomorphic changes in our ILs. Thermal stability parameters such as the decomposition and evaporation were studied using TG/DTA.

3.2 Differential Scanning Calorimetric (DSC) Analysis of Ionic Liquids

DSC thermograms are used to detect changes in physical or chemical properties of our ILs in this study as a function of temperature. There is always a change in the heat capacity of the sample where a phase transition or a

glass transition happens. This change in the heat capacity results in a difference between temperatures associated with the sample pan and the reference pan. The differential heat flow as a function of temperature difference is used to generate a signal in DSC.

3.2.1. Experimental

3.2.1.1. Materials

EMIM–ABS ionic liquids EBS, EEBS, ETS and EXS were synthesized using the procedures described in sections 2.2-2.4. The phase transitions of IL samples were analyzed using differential scanning calorimetric study on a Q-200 series DSC attached with an RCS-40 refrigeration system from TA Instruments (New Castle, DE, USA). The aluminum hermetic pans, lids and pinhole lids were purchased from TA Instruments. Fisher-brand glass pipettes were used to transfer samples into the aluminum pans.

3.2.1.2. Methods

Three sets of experiments were performed to get a better understanding of the phase transitions occurring in the EMIM–ABS ILs. In these experiments, nitrogen was used as an inert purge gas at a flow rate of 20 mL/min. Depending on the experiment, either hermetically sealed aluminum pans or hermetically sealed pinhole aluminum pans were used as the sample holders and reference pans. A

sample size of 6.0±0.5 mg was used for the analysis. Due to the high viscosity of ionic liquids, care was taken to add only a single drop of ionic liquid at the center of the pan, so that a uniform layer of the sample is obtained for the analysis at lower temperatures. Calibration of the DSC was performed using sapphire and indium standards.

The first experiment was performed to analyze crystallization (T_c), glass formation, glass transition (T_g), and other mesophasic changes from 120 °C to -45 °C at 5 °C/min negative ramp. A hermetically sealed aluminum pan was used. The second scan was a heat-cool cycle from -45 °C to 120 °C to -45 °C at 10 °C/min. A hermetically sealed aluminum pan was used for this experiment. The third scan involved an isothermal step, where the sample was kept isothermal for five minutes at 110 °C and then ramped to -45 °C with a rate of 10 °C/min. The sample was then held isothermally at -45 °C for 20 min and then heated to 300 °C with a rate of 10 °C/min. The hermetically sealed aluminum pans with a pinhole lid were used for this experiment. Different sample sets were used in the three different experiments.

3.2.2. Results and Discussion

No prominent melting (T_m), crystallization (T_c) or glass transition (T_g) phase changes were observed on simple DSC heating or cooling scans from -45 °C though 380 °C.

Hence methods were developed with repeated heat-cool cycles and isothermal time intervals to study any mesophase transitions associated with EBS, EEBS, ETS and EXS ILs.

3.2.2.1 Glass formation of ILs

Figure 19 shows the amorphous side of the ILs as it formed a melt that on cooling solidified to a glass rather than crystallizing with an exothermic phase transition. A prominent exothermic crystallization peak was not noticed when the ILs were cooled from 110 °C to -45 °C at a rate of 5 °C/min in the differential scanning calorimeter. Vitrification occurs when a liquid is cooled fast enough to by-pass crystallization.[15] The slower the cooling rate, the colder the sample can become before deviating from the thermodynamic equilibrium and hence leads to the glass formation.[16, 17]

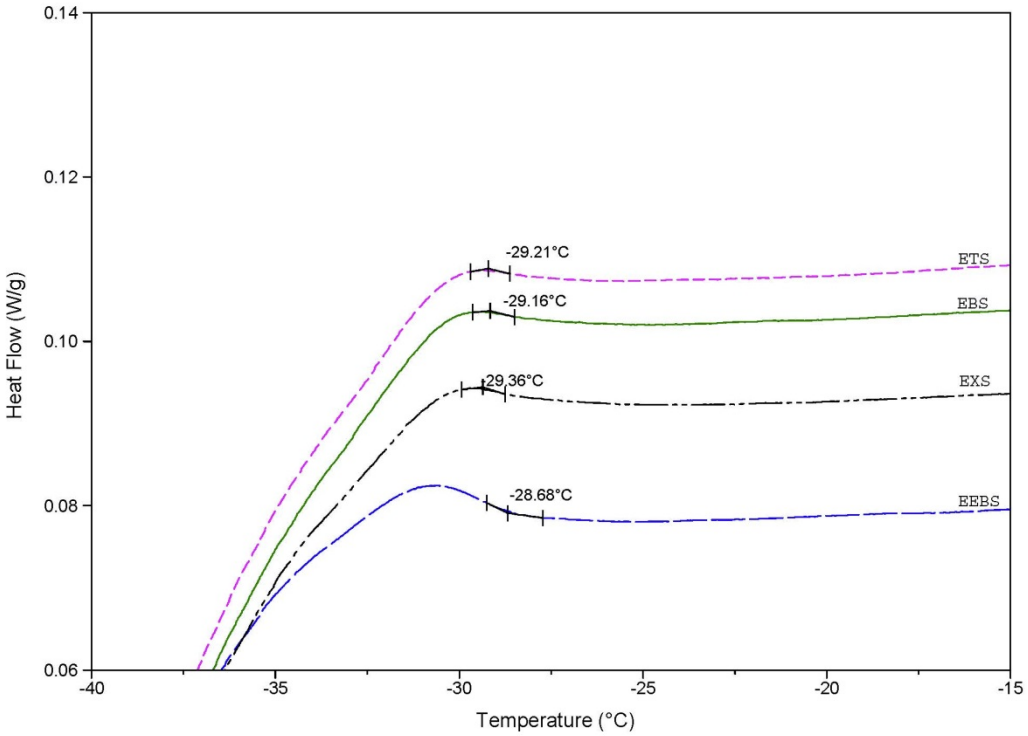

Figure 19. Glass formation of ILs during cooling from 110 °C to -45 °C at 5 °C/min in a differential scanning calorimeter. The EBS, EEBS, ETS and EXS ILs started forming glass phase around -29.16 °C, -28.68 °C, -29.21 °C and -29.36 °C respectively.

Large and less symmetrical ions in the ionic liquids being studied are likely to adopt multiple conformations[14] and lead to packing hindrance resulting in inhibited crystallization processes and lean towards glass formation. The glass formation for EBS, EEBS, ETS and EXS started

around -29.16 °C, -28.68 °C, -29.21 °C and -29.36 °C, respectively.

3.2.2.2. Liquid-crystal formation in cooling cycle of ILs

In order to analyze enthalpy relaxations which did not show up in the previous experiment, the ILs were subjected to a heat-cool-heat cycle from 110 °C to -45 °C to 110 °C with a ramp rate of 10 °C/min in DSC. An endothermic phase transition has been observed around -39 °C for EBS, EEBS, ETS and EXS ILs. For this transition at -39 °C, there is a very small change in enthalpy of 0.7 W/g for ETS and EXS, and approximately 1.2 W/g for EBS and EEBS. This mesophase transition is around 15 °C wide and is because of the formation of a solid and IL-crystal phase leading to an isotropic liquid phase.

As there is an unclear onset point for these phase transitions shown in Figure 20, peak temperature is reported instead of an onset point. For all of the ILs in this study, a liquid-crystal phase is achieved by heating from a crystalline state and also by cooling from the isotropic liquid phase during the heat-cool-heat cycle. The EBS, EEBS, ETS and EXS ILs show an exothermic shift in the baseline at -34 °C. The ETS and EXS have shown a higher magnitude of exothermic shift than the EBS and EEBS.

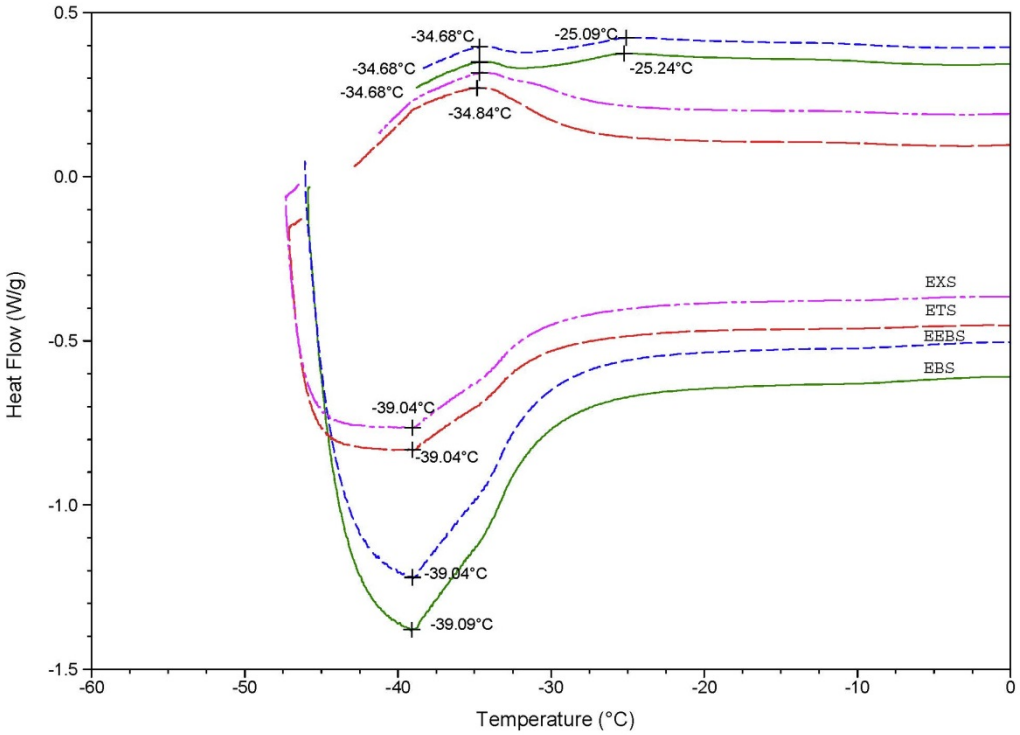

Figure 20. The second heat-cool cycle of ILs. The liquid-crystal phase transitions of EBS, EEBS, ETS and EXS ionic liquids can be observed in both heating (lower) and cooling (upper) curves. The EBS and EEBS show two exothermic shifts at -25 °C and -34 °C in the cooling (upper) curves.

As the thermogram of these ILs illustrates in Figure 21, IL's may undergo multiple phase transitions.[14] Along with the phase transition at -34 °C, both EBS and EEBS show another exothermic phase at -25 °C. Due to the weak interactions between anion and cations in ionic liquids,

they may show several packing modes for a combination. The structural flexibility of the anion-cation pair can lead to different crystalline states,[14] hence giving rise to different solid conformations and different orientation of ions towards each other as in the EBS and EEBS ILs.

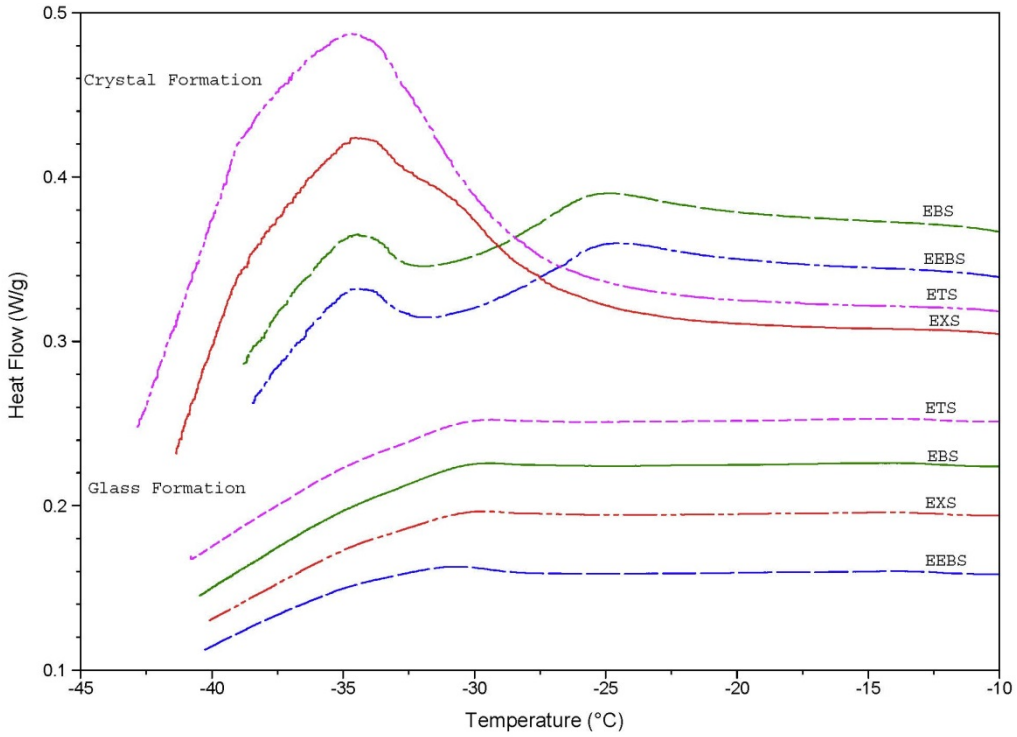

Figure 21. Comparison between two sets of DSC cooling curves showing glass formation (lower) and exothermic liquid-crystal formation (upper) of EBS, EEBS, ETS and EXS ILs.

3.2.2.3. Liquid-crystal formation in heating cycle of ILs

To further study the formation of liquid crystals in the DSC heating curve, an isothermal step was introduced. All ILs were held isothermally at -45 °C for 20 min. then heated with a ramp rate of 5 °C/min. An endothermic transition was noticed at approximately -40 °C for all ILs. This phase change is much suppressed and is around 1 °C wide with a 0.04 W/g enthalpy change. Such a minute change suggests a phase transition that is caused due to an unstable solid-liquid crystal that quickly changed its conformation in 1 °C. Due to the very low enthalpy, this phase change can be assumed to occur from an amorphous solid.

This transition at -40 °C is very small and would have been hard to notice with a large phase transition such as a melting endothermic peak in the thermogram. There is a wide endothermic baseline shift of 10 °C followed by this endothermic peak at -40 °C (Figure 22). This transition is due to a stable crystalline solid and an isotropic liquid phase that transforms into an isotropic phase without showing a melting transition.

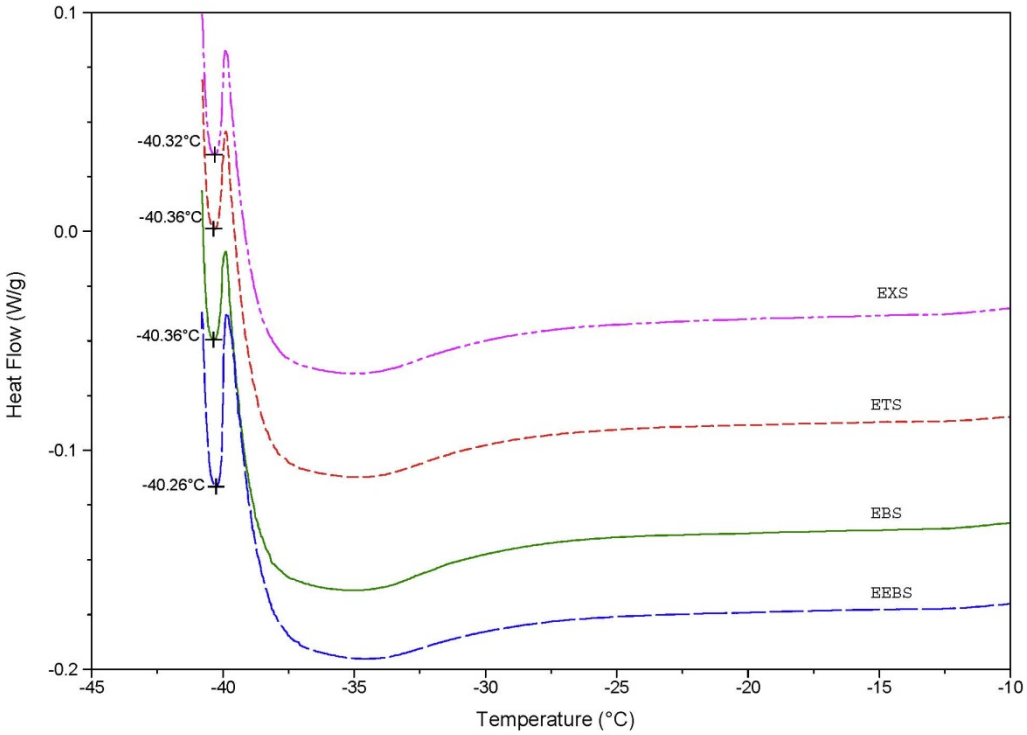

Figure 22. The DSC heating plot of EBS, EEBS, ETS and EXS ILs. The endothermic phase transition around -40 °C is seen when these ILs were held isothermally at -45 °C for 20 mins.

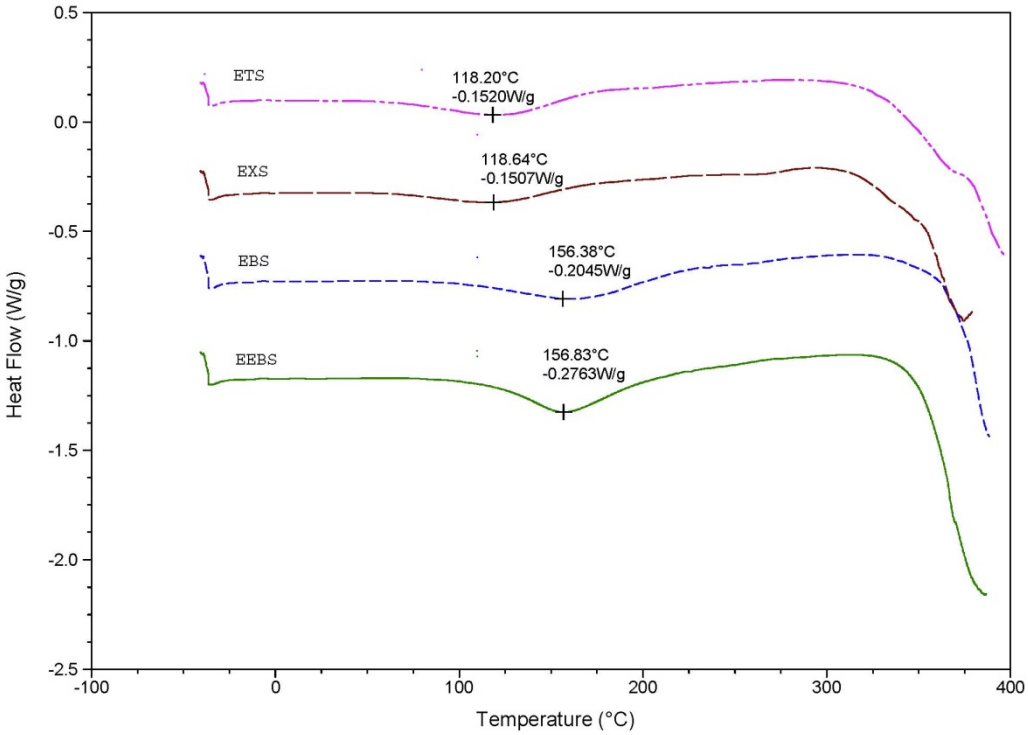

Figure 23. The change in enthalpy in DSC heating scan of ETS, EXS, EBS and EEBS ILs, showing an endothermic phase transition at 118.20 °C, 118.64 °C, 156.38 °C and 156.83 °C respectively.

As Figure 23 illustrates, a wide endothermic peak of 0.15 W/g enthalpy change for ETS and EXS occurs at 118 °C. This is a characteristic melting transition shown by sulfonate from the anions in these ionic liquids.[18] For EBS and EEBS ILs, an endothermic transition of 0.2 W/g occurs

at 156 °C. This transition can be attributed to the polymerization of sulfonate.[18] Due to the very small change in enthalpy, it might be assumed that there is only a partial polymerization, which reverts back at higher temperatures.[18]

3.2.3. Conclusion

A single cooling scan of ILs on DSC tends to form glass and did not show any other phase transition. The ILs being analyzed in this study did not revert back to the same state as before cooling. Instead, it was noticed that the repeated heat-cool cycle gave more mesophases in the ILs (Figure 21). The DSC thermogram showed melting of sulfur in ETS and EXS at 118 °C. Polymerization of sulfur was noticed in EBS and EEBS at 156 °C and this phase was evidently absent in ETS and EXS ILs. Multiple phase transitions were observed in ILs, which can be related to their structures.

The DSC-Q200 being used in the study is attached with a RCS-40 refrigerated cooling system that can only accommodate temperature range of -45 °C to 400 °C. Hence to study the glass transition or other mesomorphic phase transformations, temperatures below -45 °C need to be applied and X-ray structural analysis is necessary to get a picture of the crystal formations.

3.3. Thermogravimetric Analysis of Ionic Liquids

Thermal stability is a very vital parameter in considering the properties of solvents like ILs. It is very important to determine thermal stability of a solvent to set the appropriate temperature to avoid decomposition and or to minimize evaporation of the solvent. TGA measures loss of mass as a function of temperature. In this study, decomposition temperatures of EBS, EEBS, ETS and EXS ILs have been determined using TG/DTA. A set of carrier gas flow rates has been employed to study the decomposition or evaporation onset of ILs.

3.3.1. Experimental

3.3.1.1. Materials

The TG analysis was conducted on a TG/DTA 220 from Seiko Instruments in an inert atmosphere using N_2 (99.999% purity) as carrier gas. A platinum crucible was used to withstand high temperatures around 600 °C. The EMIM–ABS ionic liquids EBS, EEBS, ETS and EXS were synthesized using the procedures described in the sections 2.2-2.4 from the Chapter 2.

3.3.1.2. Methods

The experiments were performed at a constant heating rate of 5 °C/min from a temperature range of 30 °C to 600 °C. A sample size of 4-7 mg was used. Triplicates of the IL

samples were run to ensure reproducibility. The uncertainty arising from the experiment is largely due to the manual estimation of the onset temperature, which is ±2 °C for all measurements.

3.3.2. Results and Discussion

3.3.2.1. TG Analysis of IL's

The thermal stability of EBS, EEBS, ETS, and EXS ILs was determined by thermogravimetric analysis under N_2 flow of 100 mL/min with a temperature ramp of 5 °C/min. The onset temperature, where a significant visual mass loss reached in the thermograms was taken as a thermal decomposition onset point using the tangents method, was measured to study thermal stability of ILs. All ILs in this study exhibited a small initial weight loss due to evaporation of water from the compounds as shown in Figure 24 and Table 9. The EBS and EEBS were found to be more hygroscopic with a mass loss of 3.76% and 3.15% when compared to ETS and EBS with 1.23 and 1.22% respectively.

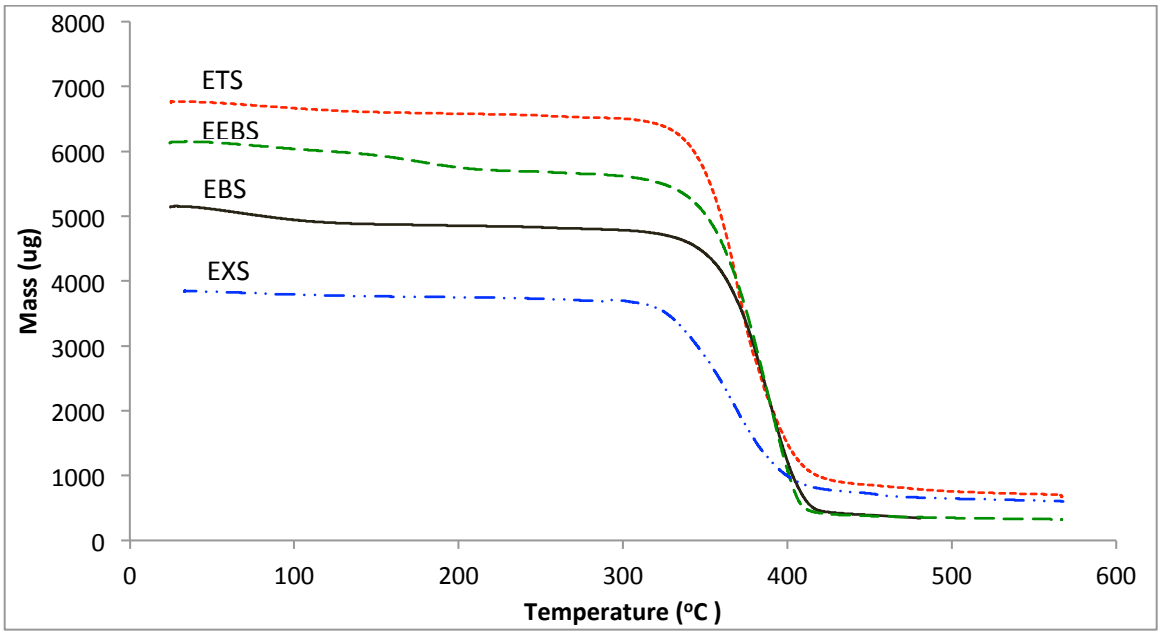

Figure 24. Thermogravimetric analysis of EBS, EEBS, ETS, and EXS ILs shows the decomposition at 349 °C, 349 °C, 331 °C and 319 °C respectively. Thermal stability of these IL tends to decrease with the increase in their molecular weight.

No significant mass loss was found as a function of temperature until the onset of decomposition. EBS and EEBS were found to be more thermally stable with decomposition onset temperatures of around 349 °C compared with ETS with the onset temperature of 331 °C. The EXS IL was found to be least thermally stable compound between the four ILs being studied, with a decomposition onset of 319 °C. The thermal stability decreased with the increase in molecular weight of the IL's.

Table 9. Thermogravimetric data showing the initial weight loss due to escape of water and the decomposition onset temperatures of EXS, ETS, EBS and EEBS ILs.

ILs	% Mass loss due to Water	Decomposition Onset Temperature (°C)
EXS	1.22	319
ETS	1.23	331
EBS	3.76	349
EEBS	3.15	348

3.3.2.2. TG heating curves with N_2 flow

The vapor pressure of ILs is extremely low but there is not enough literature available on EMIM–ABS IL's that attributes the mass loss in IL's after 300 °C to either thermal decomposition or evaporation. This experiment is to discriminate the phenomenon happening after 300 °C in EBS, EEBS, ETS, and EXS ILs as to either evaporation and/or decomposition. The rate of evaporation depends on parameters such as the type of gas, gas flow rate, filling level of the liquid sample, and the geometry of the crucible.[19] Whereas, the rate of mass loss as a result of thermal decomposition is a first-order reaction and is

independent of the type of gas, gas flow rate, or the geometry of the crucible.[19]

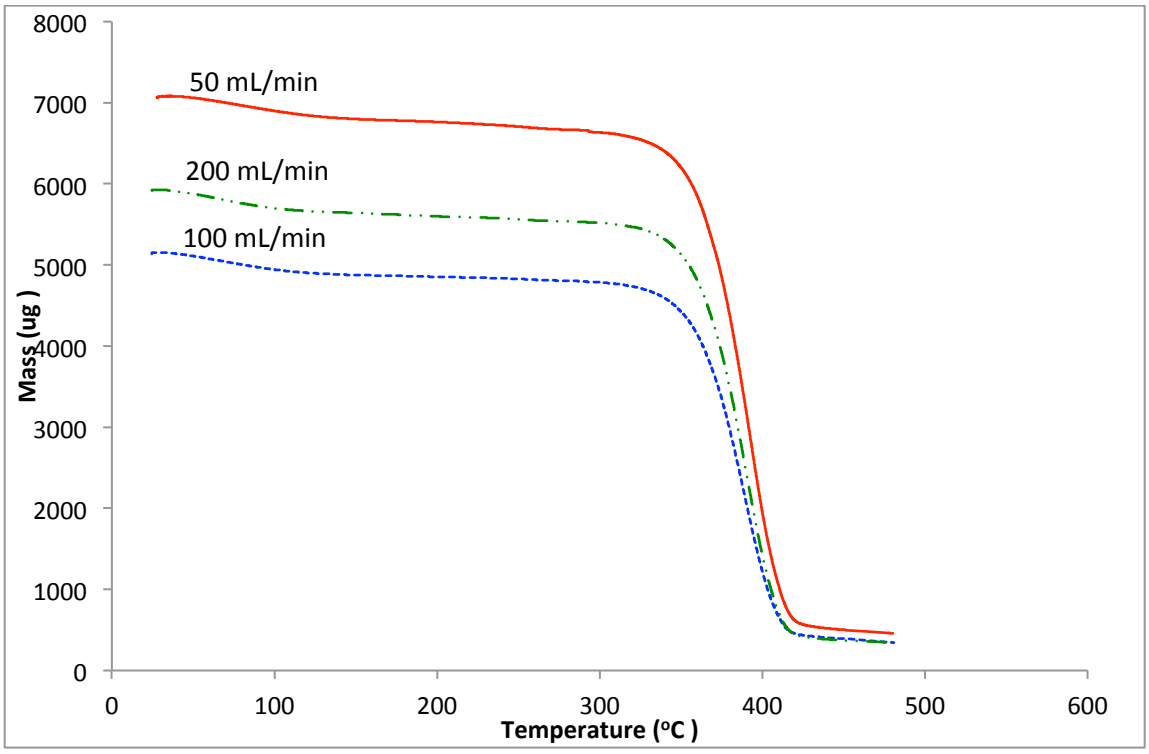

Figure 25. Comparison of mass loss occurring in EBS as a function of temperature at a N_2 flow of 50 (upper), 100 (lower) and 200 (middle) mL/min recorded from 30 °C to 480 °C with a rate of 5 °C/min.

If evaporation takes place, the rate of mass loss should vary with flow rate of the carrier gas. Whereas with decomposition, the rate of mass loss as a function of temperature would be constant with the varying flow rates of the carrier gas. As shown in Figure 25, three N_2 flow-

rates of 50, 100 & 200 mL/min have been employed to study the thermal change occurring after 300 °C in EBS. The experiment was conducted for a temperature range of 30 °C to 480 °C with a ramp rate of 5 °C/min. The results were found to be similar for all the ILs tested and the data for EBS has been presented here.

The Figures G and H illustrate the thermal behavior of EBS at carrier gas flows of 50, 100 & 200 mL/min. There was no significant change found in the thermal behavior in terms of rate of mass loss during the three N_2 flows employed on TGA for EBS, EEBS, ETS, and EXS ILs. The data from both TG and DTG curves show that the 50 (upper), 100 (lower) and 200 (middle) mL/min N_2 flows result in the same rate of mass loss for all four ILs, showing greatest mass loss (Figure 26) at 388.16 °C. This study shows that the significant transition happening on the thermogravimetric curve of ILs can be attributed to thermal decomposition rather than evaporation.

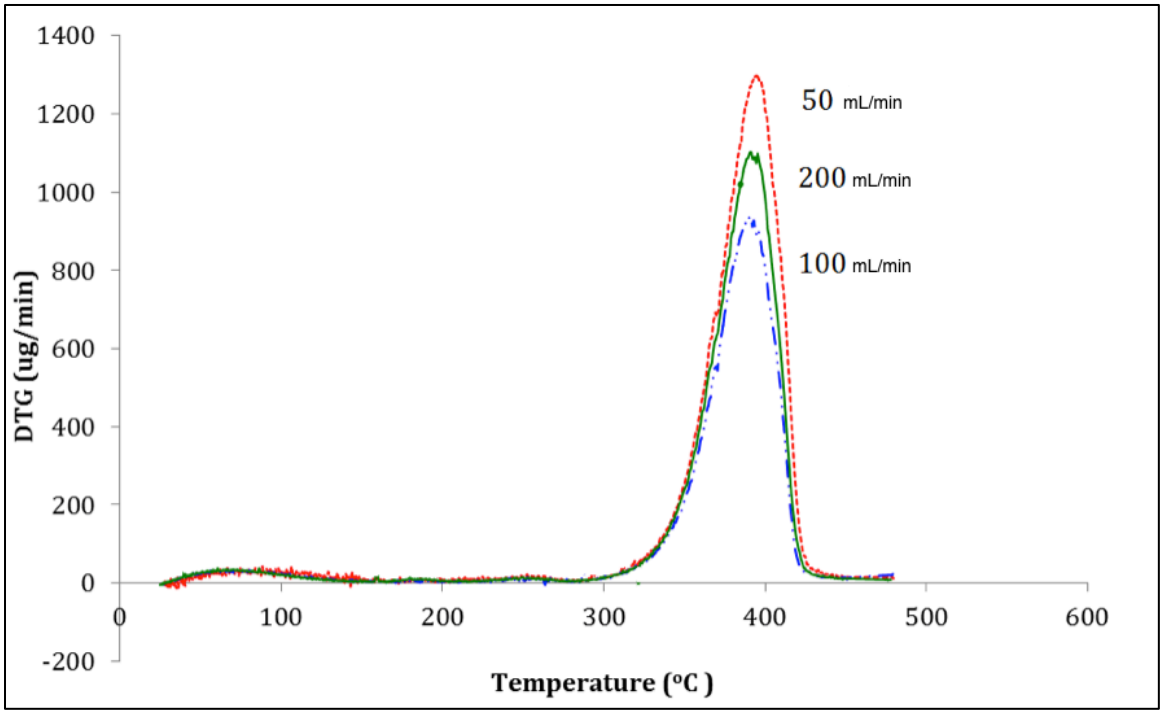

Figure 26. DTG experiment of EBS showing highest mass loss at 388.16 °C for all N_2 flows of 50 (upper), 100 (lower) and 200 (middle) mL/min recorded from 30 °C to 480 °C with a ramp rate of 5 °C/min.

3.3.3. Conclusion

There was no significant mass loss with respect to temperature until after 300 °C for all ILs, except for a small weight loss due to evaporation of water. The EBS and EEBS were found to have decomposition onset around 349 °C, which is higher than the decomposition onset of ETS and EXS at 331 °C and 319 °C respectively. Therefore, based on the structures the ILs being studied, it may be concluded that the addition of methyl group on the benzene ring of anion decreased the thermal stability of the ETS and EXS ILs due

to change in symmetry and orientation.[6] Studying the thermal behavior of ILs at different N_2 flow rates showed no change in the rate of mass loss for EBS, EEBS, ETS, and EXS ILs. Hence, the significant mass loss after 300 °C is attributed to thermal decomposition phenomenon.

3.3.4. References

1. Blokhin, A. V.; Paulechka, Y. U.; Kabo, G. J. *Thermochim. Acta.* **2006**, *445,* 75-77.
2. Blokhin, A. V.; Paulechka, Y. U.; Strechan, A. A.; Kabo, G. J. *J. Phys. Chem. B.* **2008**, *112,* 4357-4364.
3. NGO, H. L.; LeCompte, K.; Hargens, L.; McEwen, A. B. *Thermochim. Acta.* **2000**, *357-358,* 97-102.
4. Bonhote, P.; Dias, A. P.; Papagerogiou, N.; Kalyanasundaram, K.; Gratzel, M. *Inorg. Chem.* **1996**, *35*, 1168-1178.
5. McEwen, A. B.; NGO, H. L.; LeCompte, K.; Goldman, J. L. *J. Electrochem. Soc.* **1999**, *146,* 1687-1695.
6. Anthony, J. L.; Maginn, E. J.; Brennecke, J. F. *J. Phys. Chem.* **2001**, *105,* 10942-10949.
7. Bhagour, S.; Solank, S.; Hooda, N.; Sharma, D.; Sharma, V. K. *J. Chem. Thermodyn.* **2013**, *60,* 76-86.
8. Endo, T.; Kato, T.; Nishikawa, K. *J. Phys. Chem.* **2010**, *114,* 9201-9208.
9. Huddleston, J. G.; Visser, A. E.; Reichert, W. M.; Willauer, H. D.; Broker, G. A.; Rogers, R. D. *Green Chem.* **2001**, *3,* 156-164.
10. Paulechka, Y. U.; Blokhin, A. V.; Kabo, G. J.; Strechan, A. A. *J. Chem. Thermodyn.* **2007**, *39,* 866-877.

11. Paulechka, Y. U.; Kabo, G. J.; Blokhin, A. V.; Shaplov, A. S.; Lozinskaya, E. I.; Vygodskii, Ya. S. *J. Chem. Thermodyn.* **2007**, *39,* 158-166.

12. Nishikawa, K.; Wang, S.; Katayanagi, H.; Hayashi, S; Hamaguchi, H.; Koga, Y.; Tozaki, K. *J. Phys. Chem.* **2007**, *111,* 4894-4900.

13. Nakakoshi, M.; Shiro, M.; Fujimoto, T.; Machinami, T.; Seki, H.; Tashiro, M.; Nishikawa, K. *Chem. Lett.* **2006**, *35,* 1400-1401.

14. Anja-Verena, M. *Australian J. of Chem.* **2010**, *63,* 544-564.

15. Tumbull, D. *J. Non-Cryst. Contemp Phys.* **1969**, *10,* 473.

16. Mishima, O.; Calvert, L. D.; Whalley, E. *Nature.* **1985**, *314,* 76.

17. Bruning, R.; Samwer, K. *Phys. Rev. B.* **1992**, *46,* 318.

18. Ralf, S.; Sabine, P. S.; Gabriele, H. *Anorg. Allg. Chem.* **1984**, *7,* 42.

19. Heym, F.; Bastian, J. M. E.; Christoph, Kern.; Andreas, J. *Phys. Chem. Chem. Phys.* **2010**, *12,* 12089-12100.

CHAPTER 4

GENOTOXICITY AND CYTOTOXICITY OF 1-ETHYL-3-METHYLIMIDAZOLIUM ALKYLBENZENESULFONATE IONIC LIQUIDS

4.1. Introduction to Toxicity

Recently, ILs are emerging as green alternatives to conventional organic solvents for industrial applications. Due to the high solubility of various organic and inorganic compounds in ILs and excellent catalytic ability in a wide range of organic reactions, such as oxidations, Diels-Alder, Friedel-Crafts, and others, they are evolving as the choice of solvents.[1] Negligible vapor pressure, which minimizes the loss of solvent and decreases worker exposure, is the major reason attributed to the ILs for being green solvents.[2]

First-generation ILs were designed primarily based on low volatility, whereas the second-generation designer ionic solvents were targeted to have a desired chemical structure.[3] Extensive literature is available for the physical and chemical characterization of various ILs but their potential toxicity is being ignored.[2-4] The third-generation ILs are being designed to have specific biological properties to make them truly task specific.[4] Studies on aquatic and terrestrial organisms show that the

lipophilic nature of the cation is directly correlated to the toxicity of the IL.[5]

Most of the other toxicity studies done to analyze cell viability using enzyme assays, such as AMP deaminase and acetyl cholinesterase, also support the concept of direct correlation of the cation lipophilicity with the toxicity of IL.[6,7] Further studies have shown potential eco-toxicological hazards of ILs on the cellular and subcellular systems in both bacteria as well as higher-level organisms.[8]

The significance of the anion contribution was also evaluated in some microorganisms such as *Selenastrum capricornutum*, a freshwater alga.[8] The toxicities of tetrabutylphosphonium and tetrabutylammonium ionic liquids containing bromide were observed to decrease with increased incubation period. Whereas, 1-butyl-3-methylimidazolium and 1-butyl-3-methylpyridinium bromide, showed an increase in toxicity with an increase in incubation period.[8] This study on *Selenastrum capricornutum* estimates toxicity of ionic liquids containing bromide anion to be two to four orders of magnitude higher than those of organic solvents such as methanol, 2-propanol and dimethylformamide.[8] There are studies showing toxicity of ionic liquids on marine

organisms, when the ILs are released into water either by accidental spills or effluent discharges.[9-11]

Although ionic liquids are considered to be eco-friendly, it is important to investigate their toxic effects on the environment. Therefore, this chapter focuses on various bioassays to analyze the cytotoxicity and genotoxicity of the EMIM–ABS ILs to get a deeper understanding of biological effects, which is critical for designing ILs.

4.2. Cytotoxicity of Ionic Liquids

The cytotoxicity of the EMIM–ABS ILs was evaluated using the LDH (lactate dehydrogenase) and MTT (3-(4,5-dimethylthiazol-2-yl)-2,5-diphenyltetrazolium bromide) assays. Cells exposed to a toxic compound can react in a number of ways. The LDH and MTT are two *in vitro* procedures used to investigate cytotoxicity, where, LDH assay measures the amount of LDH released into the culture medium from disruption of cells and MTT measures the redox activity.

4.2.1. Lactate Dehydrogenase (LDH) Assay

Apoptosis and necrosis are two major ways that can account for cell death in living organisms. Apoptosis involves a series of signal transduction pathways that are highly regulated leading to the cell death. This process results is an articulated breakdown of the cell, leading to the membrane-bound apoptotic bodies.[12] Necrosis is caused by

a traumatic event which results in an injury to the cytoplasmic organelles such as the mitochondria, leading to rapid lysis of the cell.[13]

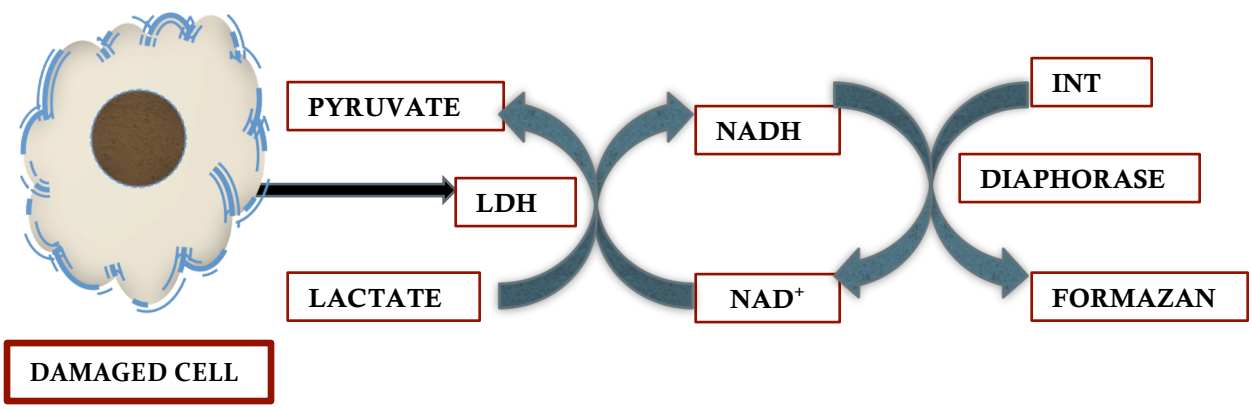

Figure 27. Schematic diagram of the lactate dehydrogenase assay mechanism.[12]

The process behind cell death in LDH is not certain and literature is inconclusive if apoptosis, necrosis, or a combination of both is actually responsible for the cell lysis. However, independent of the mechanism, the LDH assay indicates a clear end point of the membrane integrity when LDH leaks from the cytosol into the cell culture. Hence LDH is a good choice of an indicator to determine cell viability.

LDH is a cytosolic enzyme and this assay is based on the endogenous activity of LDH in cells. Once a cell is damaged either by apoptosis or necrosis caused by a toxic

chemical, LDH is released into the culture medium. The catalytic activity of LDH in culture medium is monitored indirectly to determine the LDH activity per cell.

Once a cell is lysed, a two-step coupled reaction system takes place as shown in Figure 27. In the first reaction, LDH catalyzes the energetically unfavorable oxidation of pyruvate from lactate and thereby reduction of NAD^+ to NADH.[14] Followed by the second step, where diaphorase (Dase) catalyzes the favorable conversion of the newly formed NADH and p-iodonitrotetrazolium violet (INT) to NAD^+,[14] catalyzing the reduction of INT to formazan, which is a highly colored compound. Formazan strongly absorbs at around 500 nm and its concentration is directly proportional to the amount of LDH released from a lysed cell.

4.2.1.1. Experimental

An LDH cytotoxicity assay kit was purchased from Cayman Chemicals (Ann Arbor, Michigan, USA). After receiving the cytotoxicity assay kit, LDH diaphorase, LDH INT, and LDH standards from the kit were stored at -20 °C. LDH NAD^+ and lactic acid (100X concentration) were stored at 4 °C. RPMI 1640 serum-free medium, sterile 96-well plates and sterile pipette tips were purchased from Fisher.

Monkey kidney cells were seeded in 96-well plates at a density of 10^5 cells/well in 120 μL of culture medium (RPMI without fetal bovine serum). The cells were cultured in a CO_2 incubator for 48 hours at 37 °C with various ILs. The concentrations of each ionic liquid used are 0.5, 1.0, 2.5, 5.0, 10.0 and 20.0 mM. The cell-based assay buffer tablet from the kit was dissolved in 100 mL distilled water and was stored at room temperature. The LDH diaphorase from the vial was reconstituted with 150 μL of assay buffer and was stored at -20 °C. Ten mL of the LDH reaction solution (for each 96-well plate) was prepared using 100 μL each of NAD^+, lactic acid, INT, and diaphorase in 9.6 mL of the assay buffer. The reconstituted diaphorase was placed on ice while in use.

The LDH standard stock is highly unstable and has to be stored at -80 °C when not in use. The LDH standard from the assay kit was reconstituted in 1.8 mL of assay buffer. Serial dilution was performed in culture medium to get a set of six LDH standards for the calibration curve. The sixth test tube with the culture medium without any LDH standard was used as a blank. The LDH standards were run in duplicate and the ionic liquid dilutions were run in triplicate.

The standard and sample plate formats were properly recorded to avoid confusion. After 48 hours of incubation, the 96-well cell-culture plates were centrifuged at 400x g for five minutes. One hundred μL of supernatant from each well from the first plate is transferred into appropriate wells on a new 96-well plate. The LDH standards (100 μL) are also added to the appropriately labeled wells in the second plate. One hundred μL of reaction solution was added to each well and the plates were incubated for 30 minutes at room temperature with gentle shaking. All pipetting was done using a multi-channel repeating pipette for higher precision and constant incubation times. The absorbance of all plates was read at 500 nm with a plate reader (Molecular Devices SPECTRAmax M2 ROM v2.1 plate reader) after 30 minutes of incubation.

4.2.1.2. Results and Discussion

Absorbance of the blank was subtracted from absorbance values of the other cells and a standard curve was constructed based on absorbance at 500 nm as a function of LDH concentration. The equation of the line is determined from the standard curve and the y-intercept is used in deriving total LDH activity. The equation for the line is $Y= (4.00x10^{-5})x - 0.0197$ with a correlation coefficient of 0.9966. The magnitude of the analytical background response

is measured using six replicates of the experimental blank and calculating the standard deviation (σ) of these responses. The slope (s) is derived from the calibration curve of the analyte. The LOD (3.3*σ/S) and LOQ (10*σ/S) of the LDH assay are determined to be 0.037 μU/mL and 0.111 μU/mL respectively.

LDH activity is calculated as the ratio of absorbance minus y-intercept of the sample, and the slope from the standard curve. The cytotoxicity was calculated based on the total LDH activity (μU/mL) in the sample after the assay. A single LDH unit (U) is the amount of LDH required to catalyze 1 μmol of substrate per minute. The following formulas, equations 1 and 2, were used to calculate the total LDH activity,

1. $LDH\ Activity\ (\mu U) = \frac{Absorbance - y\ intercept}{slope}$

2. $Total\ LDH\ Activity\ \left(\frac{\mu U}{mL}\right) = LDH\ Activity - Sample\ volume\ assayed.$

Unlike the studies shown by Ranke et al.[15] attributing the toxicity of ILs to cation, this study considers the role of anions toward toxicity. The Figure 28 shows the EC_{50} values of the 1-ethyl-3-methylimidazolium benzenesulfonate (EBS), 1-ethyl-3-methylimidazolium ethylbenzene (EEBS), 1-

ethyl-3-methylimidazolium toluenesulfonate (ETS) and 1-ethyl-3-methylimidazolium xylenesulfonate (EXS) ionic liquids. The EC_{50} for the 1-ethyl-3-methylimidazolium acetate (EMIM–AC) is 4.12±0.14 mM. A decrease in the EC_{50} was observed with the change in anion from acetate to benzenesulfonate. The EC_{50} for EBS and EEBS were found to be 3.24±0.03 mM and 3.36±0.18 mM respectively.

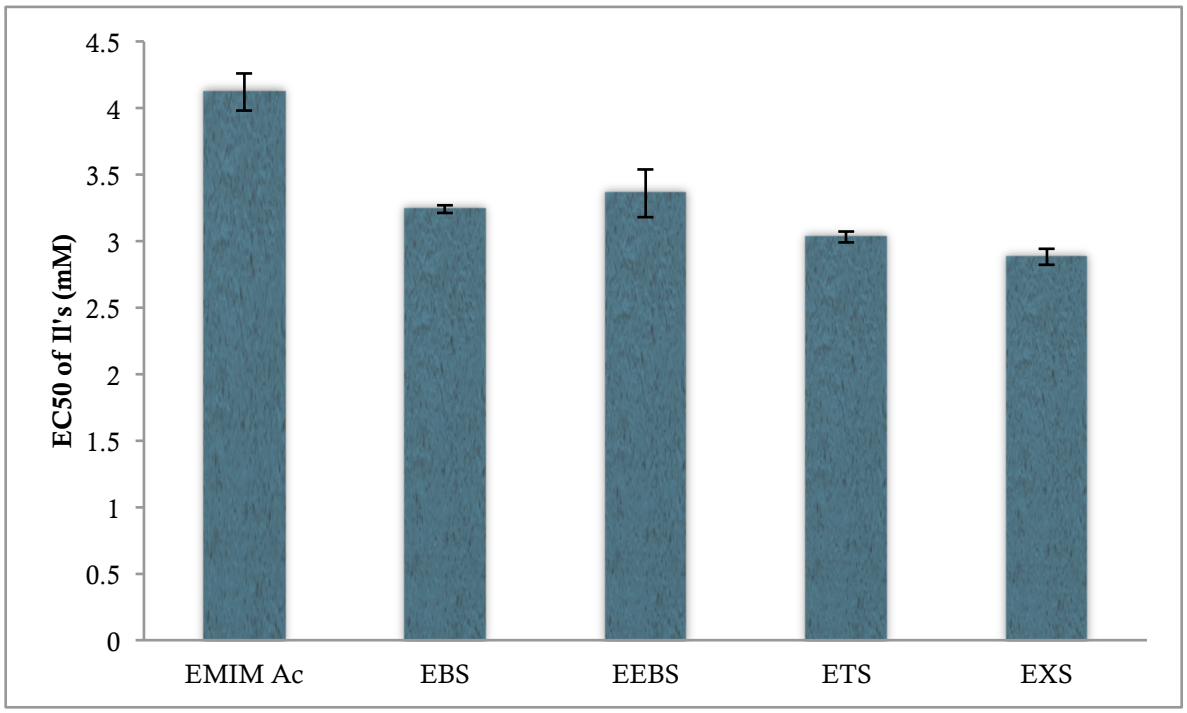

Figure 28. EC_{50} of the EBS, EEBS, ETS, EXS and EMIM-AC ILs using the LDH assay. A decrease in the EC_{50} was observed with the change in anion from acetate to benzenesulfonate.

A slight decrease in the EC_{50} values was also observed with addition of one or two methyl groups on the

benzenesulfonate anion as in case of ETS and EXS. The EC_{50} of ETS and EXS were found to be 3.03±0.04 mM and 2.88±0.06 mM respectively. A variation in EC_{50} values of the EMIM–ABS ILs was noticed when the 1-ethyl-3-methylimidazolium cation was kept constant in all ILs while changing the anion.

The addition of a methyl group on the anion has decreased the EC_{50} of EMIM–ABS ILs, in turn increasing their cytotoxicity. This study shows that the anion plays a vital role in deciding the fate of ILs and the toxicity of EMIM–ABS ILs depends on the associated anion. The literature shows the evidence of similar studies with 1-n-butyl-3-methylimidazolium cation, where the toxicity was reported as a result of the associated anions.[16] Cytotoxicity results were obtained for the 1-n-butyl-3-methylimidazolium cation associated with chloride, tetrafluroborate and hexafluorophosphate anions. The lowest effect concentrations were found for the tetrafluroborate, whereas strongest inhibition was exhibited by the hexaflurophosphate.[16]

4.2.1.3. Conclusion

The results of this study show a cytotoxic effect of EMIM–ABS ILs against the monkey kidney cells. Moreover, addition of methyl groups on anions showed a change in the

cytotoxicity of the EMIM–ABS ILs. Addition of methyl groups to anion resulted in an increase in cytotoxicity.

4.2.2. MTT (3-(4,5-dimethylthiazol-2-yl)-2,5-diphenyltetrazolium bromide) Assay

The MTT assay is a cell-based method used for screening the cytotoxicity of compounds. Like LDH, MTT can be used to test molecules for their cytotoxic effects on cell proliferation and cell death.[17] The MTT is used as an end-point determination assay to look at the number of viable cells remaining at the end of the experiment.

MTT has a positively charged quaternary tetrazole ring with four nitrogen atoms (Figure 29) that would facilitate its transfer through the plasma membrane into the cytoplasm or outside of the inner mitochondrial membrane of the cell.[17] After the cellular uptake, the colorless tetrazolium structures are reduced to brightly colored formazan due to the disruption of tetrazole rings by intracellular NADPH-oxidoreductases.[18]

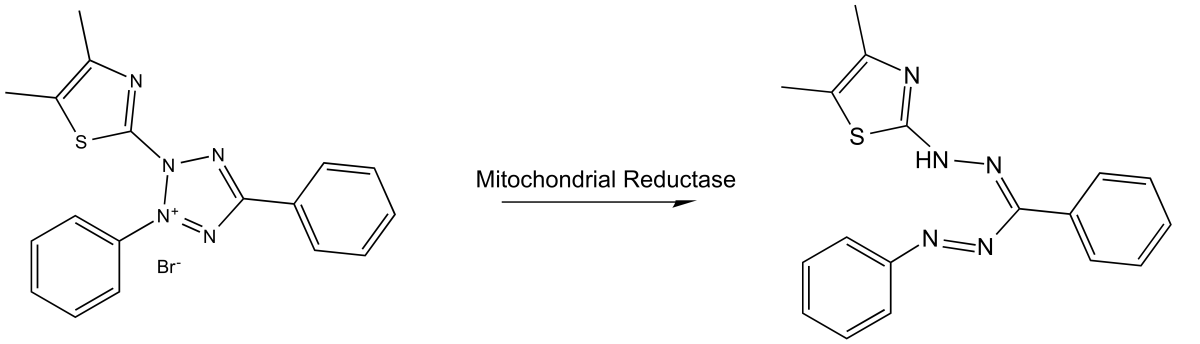

3-(4,5-dimethylthiazol-2-yl)-2,5-diphenyltetrazolium bromide
(MTT)

(*E*,*Z*)-5-(4,5-dimethylthiazol-2-yl)-1,3-diphenylformazan
(Formazan)

Figure 29. Most cellular MTT reduction occurs outside of inner mitochondrial membrane of a cell, resulting in the formation of insoluble formazan crystals.[18]

4.2.2.1. Experimental

The MTT cytotoxicity assay kit was purchased from Cayman Chemicals. RPMI 1640 medium, sterile 96-well plates and sterile pipette tips were purchased from Fisher. Monkey kidney cells were seeded in 96-well plates at a density of 10^3 cells/well in 200 μL RPMI culture medium (RPMI without fetal bovine serum). The cells were cultured in a CO_2 incubator for 24 hours at 37 °C with various ILs. The concentrations of each ionic liquid used are 1.0, 5.0, 10.0, and 20.0 mM. Each ionic liquid sample was run in octuplicate along with blanks and a negative control. The negative control has 10 μL of the MTT stock solution added to 100 μL of medium.

After 24 hours, the fluid covering the cells is aspirated using a multichannel micropipette. Around 180 µL of the medium was removed from each well and discarded. The MTT-stock solution was prepared with 5 mg/mL of MTT in sterile water. This solution was filtered and stored at 4 °C in dark, as MTT is light sensitive. The MTT-stock solution was then diluted tenfold with RPMI 1640 medium to make up the MTT solution for cell viability determination.

To each well of the 96-well plate from previous step, 50 µL of the freshly prepared MTT solution was added. The well plate was then wrapped with aluminum foil to avoid light exposure and was incubated at 37 °C for four hours. After incubation, 150 µL of DMSO was added to each well and the plate was incubated again in a CO_2 incubator at 37 °C for around an hour. The plate was put on a micro-plate shaker for five minutes to make sure all the purple crystals were dissolved and read at 570 nm using an automated UV plate reader.

4.2.2.2. Results and Discussion

All viable cells capable of active metabolism aid in the purple color formazan formation from MTT, whereas the dead cells cannot. Intensity of the purple color is directly proportional to the number of viable cells. Hence the formation of the colored formazan acts as an end point

that can be read at absorption maxima of 570 nm. The intensity of the purple color of formazan is directly proportional to the number of viable cells, as shown in Figure 30. The negative-control absorbance value containing just the assay buffer medium with MTT was subtracted from the absorbance values of the other cells.

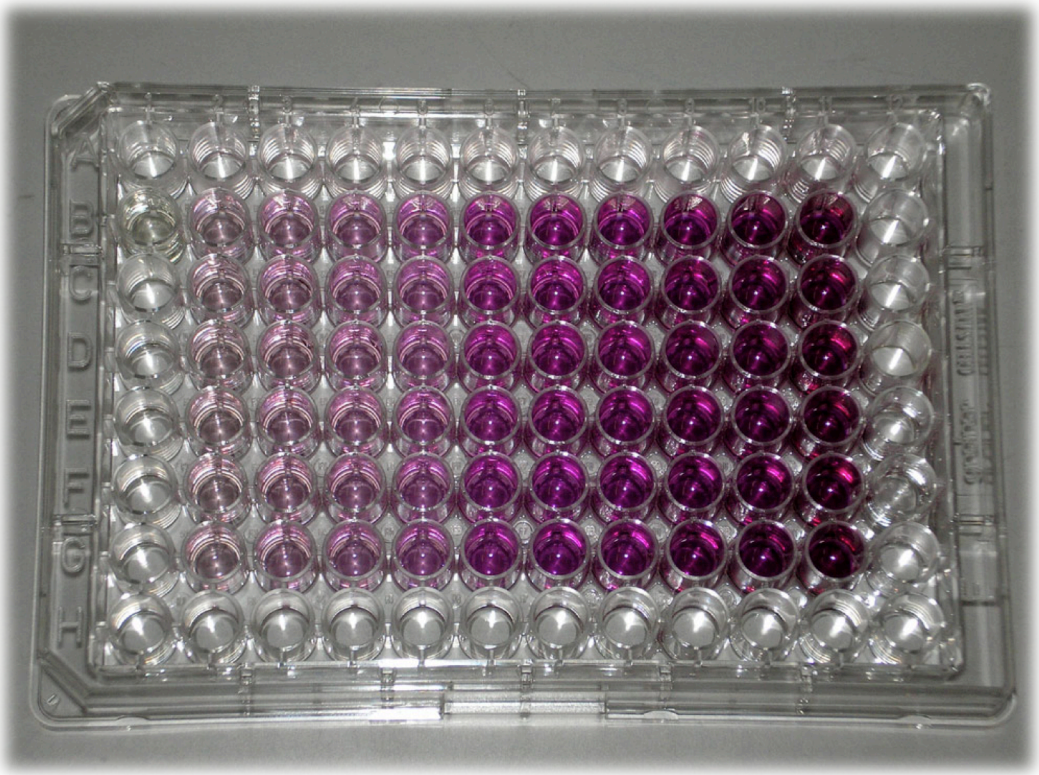

Figure 30. A 96-well plate with varying intensities of purple color from the MTT assay. Intensity of purple color is directly proportional to the number of viable cells.

The results of MTT followed a similar pattern as of the LDH assay and all EMIM–ABS ILs showed significant cytotoxicity (Figure 31). There was a change in cytotoxicity with a change in anion keeping the cation moiety constant.

The EMIM-AC had highest EC_{50} when compared to the other ILs from this study. The EC_{50} of EMIM-AC was determined to be 4.41±0.41 mM.

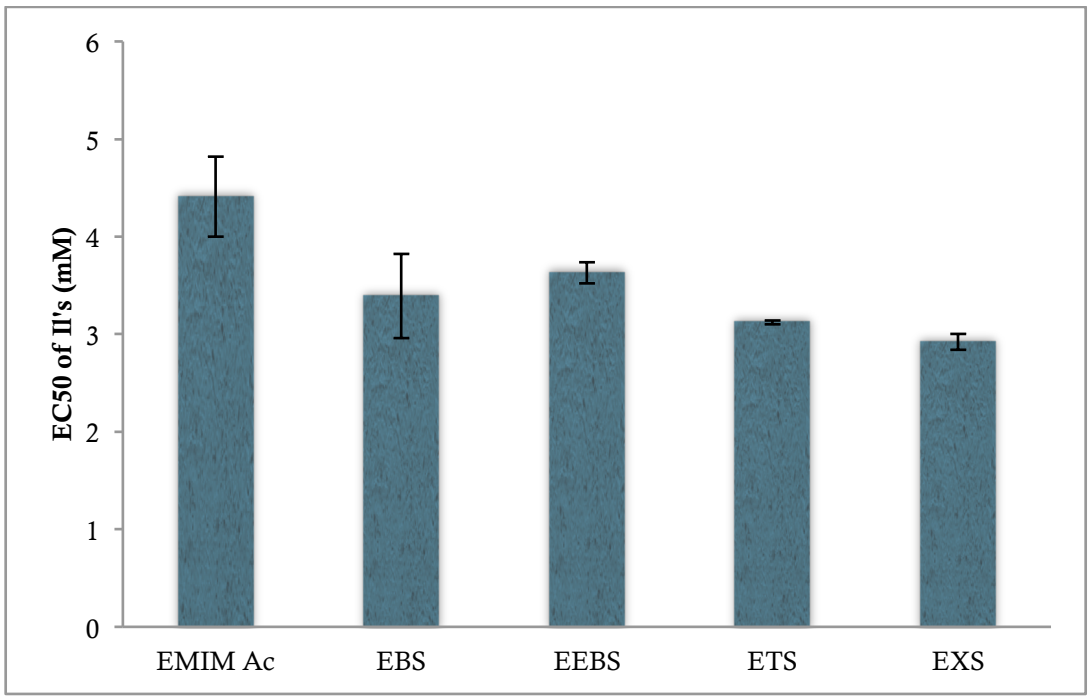

Figure 31. EC_{50} of the EMIM–ABS ILs using the MTT assay. The EMIM-AC shows the highest EC_{50} and the EXS has the highest cytotoxicity among the five compounds tested.

Replacing the acetate ion with benzenesulfonate anion on the EMIM cation resulted in an EC_{50} of 3.39±0.33 mM. The

EC_{50} of ETS and EXS were found to be 3.12±0.02 and 2.92±0.08 respectively. There is a decrease in the EC_{50} with the addition of methyl groups on the anion in ETS and EXS. This similar trend has also been noticed in the LDH assay results.

4.2.2.3. Conclusion

The findings of the MTT cytotoxicity assay are similar to the results from the LDH cytotoxicity assay. An increase in the cytotoxicity has been noticed with addition of methyl groups on the anions in ETS and EXS. Also, this study shows that the cytotoxicity varies depending on the associated anion when the cation identity is held constant.

4.3. Genotoxicity of Ionic Liquids

4.3.1. Ames Test

The genotoxicity of the EMIM-ABS ILs has been analyzed using the Ames test. This test looks for the mutation-causing ability in the compounds being tested. Specific auxotrophic strains of the bacteria *Salmonella typhimurium* are used in the Ames test.[19] The *S. typhimurium* auxotroph bacteria are produced as a result of mutation caused in phototrophic *S. typhimurium* gene encoding an enzyme required for histidine biosynthesis. As a result of mutation, the auxotroph cannot synthesize the histidine amino acid by itself. Hence, histidine has to be added to

the growth medium for the survival of *S. typhimurium* auxotroph.[19]

The strains of *S. typhimurium* auxotroph used in the Ames test are TA1535 and TA1538, and are denoted by his^- to differentiate them from phototrophic his^+ strain.[19] The auxotrophs are grown on glucose minimal-salt agar plates with only a trace amount of histidine. The auxotrophic bacteria utilize these nutrients but grow only until all the histidine is exhausted from the media. After a while, due to lack of histidine in the auxotrophic media, only the bacteria that undergo reverse mutation survive and these would be able to synthesize their own histidine. These reverse-mutated bacteria are called as revertants and mutagenic substances stimulate these reverse mutations.[19] Based on this theory, the ionic liquid samples are added to the auxotrophs and tested for their mutagenic ability to cause reverse mutations in the auxotrophic bacteria.

4.3.1.1. Experimental

The Ames test kit was purchased from Presque Isle Cultures (Erie, PA). The *S. typhimurium* culture from the test kit was inoculated in sterile tryptic soy broth and incubated at 37 °C for 24 hours before the experiment. Along with the ILs samples, a positive and a negative control were established. Each glucose minimal-salts agar tube was

supplemented with 0.3 mL of histidine/biotin stock and 0.1 mL of *S. typhimurium*. This was maintained at 50-55 °C and was poured into a sterile petri-plate to make a bottom agar plate with culture, like in Figure 32.

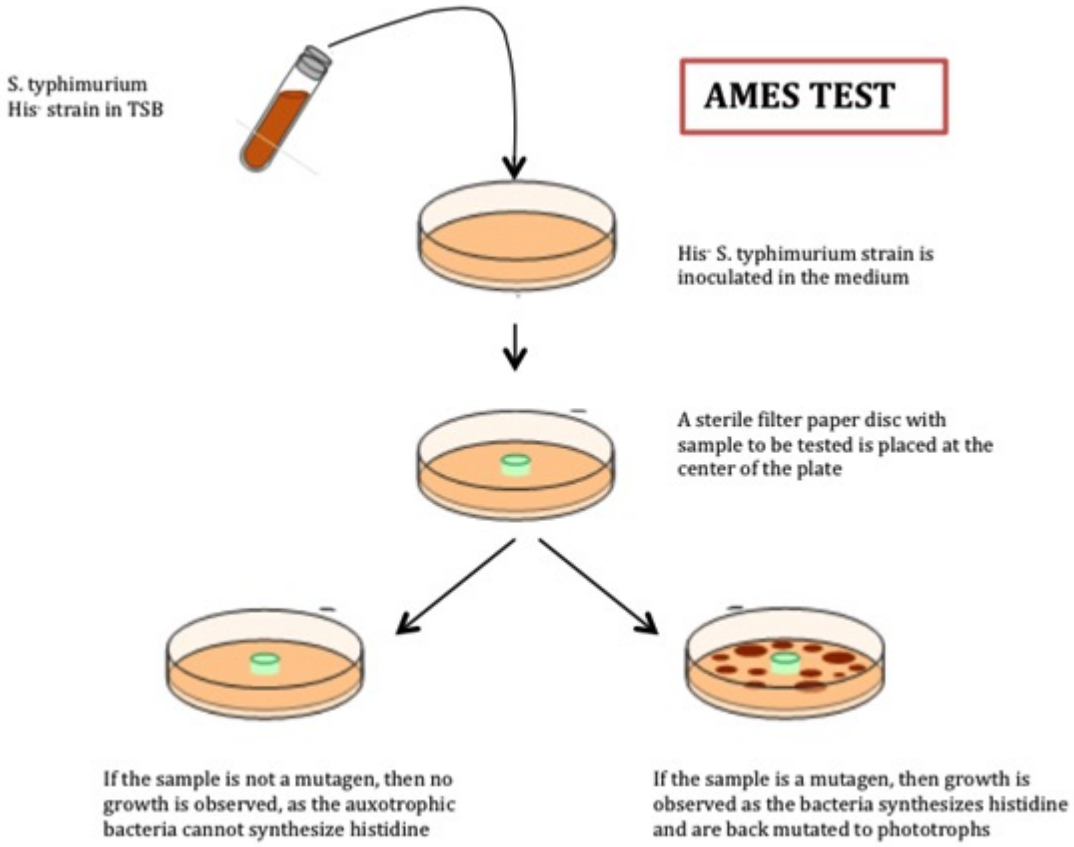

Figure 32. Genotoxicity analysis of EBS, EEBS, ETS, EXS, and EMIM-AC ILs using an Ames test. Potential carcinogens back mutate the auxotroph *S. typhimurium* bacteria to phototrophic strains that can synthesize histidine.[19]

A sterile filter-paper disc was placed on agar medium at the center of each plate. The substance to be tested is deposited on the upper edge of the disc with a sterile Pasteur pipette. In the positive-control plate, enough 4-NOPD (4-nitro-o-phenylenediamine) is deposited on the disc to saturate it. Sterile water is deposited on the disc on the negative-control plate. All of the ionic liquid samples were run in triplicate and were incubated for 48 hours at 37 °C.

4.3.1.2. Results and Discussion

The results of the Ames test were determined based on the number of revertant colonies per plate (RCP) after the incubation period. The higher the number of back-mutated or revertant colonies in the test plate, the more mutagenic the test substance is likely to be.[19] The negative-control plate that had sterile water on the disc barely had any revertants in the plate as shown in Figure 33. Whereas, the positive-control plate with NOPD on the disc had 25.3±1.2 RCP (revertant colonies per plate).

The EMIM-AC had an insignificant number of 1.0±1.0 RCP, while all the other EMIM ILs with linear alkylbenzenesulfonate anions (EBS, EEBS, ETS, and EXS) showed genotoxicity around 10 RCP (Figure 34). The EBS,

EEBS, ETS, and EXS had 10.7±0.6, 11.0±1.0, 10.3±0.6, and 10.0±1.0 back-mutated colonies per plate respectively.

Figure 33. The genotoxicity of ILs has been analyzed using the Ames test. The NOPD (on left) and sterile water (on right) were used as the positive and negative controls respectively.

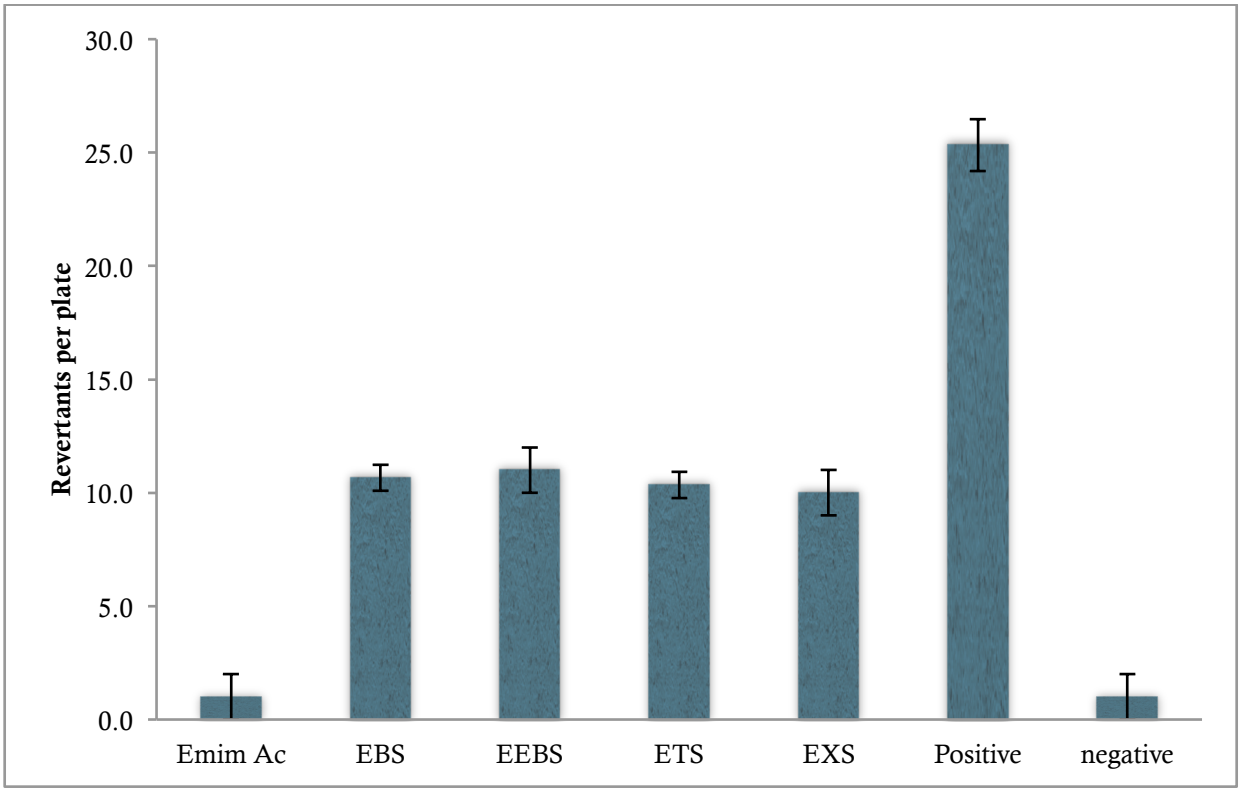

Figure 34. Genotoxicity of ILs measured by the Ames test in terms of number of revertant colonies per plate after the incubation period.

4.3.1.3. Conclusion

Among the ILs, EMIM-AC tested negative for genotoxicity through the Ames test. The other four ILs (EBS, EEBS, ETS, and EXS) showed similar results for genotoxicity. Changing the anion in EMIM ILs showed variation in genotoxicity. Unlike the results in cytotoxicity assay, there is no significant change in genotoxicity of the tested ILs with addition of extra methyl groups like in ETS and EXS, as compared to EBS.

4.4. References

1. Welton, T. *Coord. Chem. Rev.* **2004**, *248*, 2459–2477.
2. Plechkova, N. V.; Seddon, K. R. *Chem. Soc. Rev.* **2008**, *37*, 123–150.
3. Parvulescu, V.I.; Hardacre, C. *Chem. Rev.* **2008**, *107*, 2615–2665.
4. Hough, W.L.; Smiglak, M.; Rodrı guez, H.; Swatloski, R.P.; Spear, S.K.; Daly, D.T.; Pernak, J.; Grisel, J.E.; Carliss, R.D.; Soutullo, M.D.; Davis, J.H.; Rogers, R.D. *New J. Chem.* **2007**, *31*, 1429–1436.
5. Cho, C.; Jeon, Y.; Pham, T.; Vijayaraghavan, K.; Yun, Y.; *Ecotox. Environ. Safe.* **2008**, *71*, 166–171.
6. Skadanowski, A.C.; Stepnowski, P.; Kleszczyn ́ski, K.; Dmochowska, B. *Environ. Toxicol. Phar.* **2005**, *19 (2)*, 291–296.
7. Stock, F.; Hoffmann, J.; Ranke, J.; Stormann, R.; Ondruschka, B.; Jastorff, B. *Green Chem.* **2004**, *6*, 286–290.
8. Cho, C.; Jeon, Y.; Pham, T.; Vijayaraghavan, K.; Yun, Y.; *Ecotox. Environ. Safe.* **2008**, *71 (1)*, 166–171.
9. Pham, T.P.; Cho, C.W.; Yun, Y.S. *Water Res.* **2010**, *44*, 352–372.

10. Ranke, J.; Muller, A.; Bottin-Weber, U.; Stock, F.; Stolte, S.; Arning, J.; Stormann, R.; Jastorff, B. *Ecotoxicol. Environ. Saf.* **2007**, *67*, 430–438.
11. Petkovic, M.; Ferguson, J.L.; Nimal Gunaratne, H.Q.; Ferreira, R.; Leitao, M.C.; Seddon, K.R.; Rebelo, L.P.N.; Pereira, C.S. *Green Chem*. **2010**, *12,* 643–649.
12. Bursch, W.; Oberhammer, F.; Schulte-Hermann, R. *Trends Pharmnacol. Sci*. **1992**, *13*, 245-251.
13. Kerr, J. F. R.; Harmon, B. V. In *Apoptosis: The Molecular Basis of CellDeath: Current Communications on Cell and Molecular Biology*, Cold Spring Harbor LabPress, Plainview:NY, 1991; 3, pp 5-29.
14. Haslam, G.; Wyatt, D.; Kitos, P.A. *Cytotechnology* ***2000,*** *32*, 63-75.
15. Ranke, J.; Molter, K.; Stock, F.; Bottin-Weber, U.; Poczobutt, J.; Hoffmann, J.; Ondruschka, B.; Filser, J.; Jastorff, B.; *Ecotoxicol. Environ. Saf.* **2004**, *58*, 396–404.
16. Stepnowski, P.; Skladanowski, A.C.; Ludwiczak, A.; Laczynska, E. *Hum. Exp. Toxicol*. **2004**, *23*, 513–517.
17. Berridge, M. V.; Tan, A. S. *Protoplasma*. **1998**, *205*, 74–82.
18. Berridge, M. V.; Herst, P. M.; Tan, A. S. *Biotechnol. Annual Rev*. **2005**, *11,* 127-152.

19. Docherty, K.; Hebbeler, S.Z.; Kulpa Jr.; C.F. *Green Chem*. **2006,** 8, 560-567.

CHAPTER 5

ISOLATION OF LIGNIN USING IONIC LIQUIDS

Lignin is the second most abundant organic polymer found on earth. It is made up of a complex combination of phenylpropanoid structures linked by ether and C-C bonds.[1] Isolation of lignin from plant biomass is a challenge due to its structural complexity.[2] Lignin is a renewable source of energy and a potential source of biofuel that can be a good alternative to fossil fuel. It is made of phenylpropanoid units and has less oxygen content compared to cellulose.[2] Therefore, biofuel from the pyrolysis of lignin would have higher oxidative stability that would aid in achieving longer shelf life and better quality transportation fuel. This chapter focuses on lignin dissolution and lignin extraction from Prairie Cord grass.

5.1. Effect of water and temperature on lignin extraction

Dissolution of lignocellulosic biomass using ionic liquids is attributed to disruption of hydrogen bonds and coordination of anions to the hydroxyl groups of cellulose.[1-4] The process of dissolution requires low moisture content in order to avoid interference of water with hydrogen bonding ability of the ionic liquid.[3,4] There

is also research showing that addition of water is necessary for the extraction of lignin from biomass.[5,6]

The biomass is pretreated with steam to hydro-fragment the lignin polymer before actual dissolution of lignin.[6] The optimum conditions such as temperature, time and water content for extraction of lignin varies in different studies.[4-6] Extensive literature is available on dissolution of lignin using bio-mass but there is only limited research on the lignin extraction using ILs. Hence this study aims at determining the optimal temperature and water content for high lignin recovery.

5.1.1. Experimental

5.1.1.1. General Procedure for lignin extraction

This general lignin extraction procedure[6] was used for both lignin dissolution and extraction studies with varying temperatures and time according to the experimental need. Prairie cord grass (PCG) is used as the biomass feed stock. The PCG and ionic liquid were taken in a round bottom flask with a condenser and heated using an oil-heating bath with a fixed thermometer. After completion of cooking, the flask was removed from oil bath and cooled to room temperature (RT). The mixture of PCG and IL was made basic using 0.1 M NaOH to precipitate the cellulose pulp, which is filtered out using a glass fiber filter. The filtrate is a dark

yellow viscous solution, which is acidified using 1M HCl to precipitate lignin out of the solution. The lignin is filtered using a glass fiber filter and is washed with approximately 100 mL water. The lignin is then dried in an oven overnight at 60 °C.

After removal of lignin from the acidic solution, it is neutralized to pH 7.0 using 0.1 M NaOH. Water was removed using a rotary evaporator. Acetonitrile (ACN) was added to dissolve the ionic liquid, leaving salt and other plant materials as insoluble residue. The ACN was evaporated under vacuum to recover the ionic liquid. The FTIR absorption spectra were recorded using a Nicolet 380 FTIR spectrometer from Thermo-Fisher Scientific with an 8 cm^{-1} resolution with 100 scans in the range 4000-700 cm^{-1}.

5.1.1.2. Results and discussion

Three PCG samples (3 g each) were taken in a round bottom flask; raw PCG, steam-pretreated PCG and steam-pretreated PCG with 3 mL water and 15 mL EXS Il. The steam-pretreatment of PCG involved steaming of PCG sample with out direct water contact for an hour. All three PCG samples were heated at 90 °C for 3 hours and the general PCG extraction procedure (section 5.1.1.1) was followed for lignin extraction.

As shown in Figure 35, the % lignin recoveries from raw PCG, steam-pretreated PCG and steam-pretreated PCG with water are 21.88, 21.01 and 19.81 respectively. Adding water to the extraction mixture resulted in decrease of lignin recovery when compared to the other experimental PCG samples with out water. Highest lignin recovery was found in case of the raw PCG sample with out any pretreatment. Therefore, raw PCG has been used without steam treatment or addition of water in further extraction experiments.

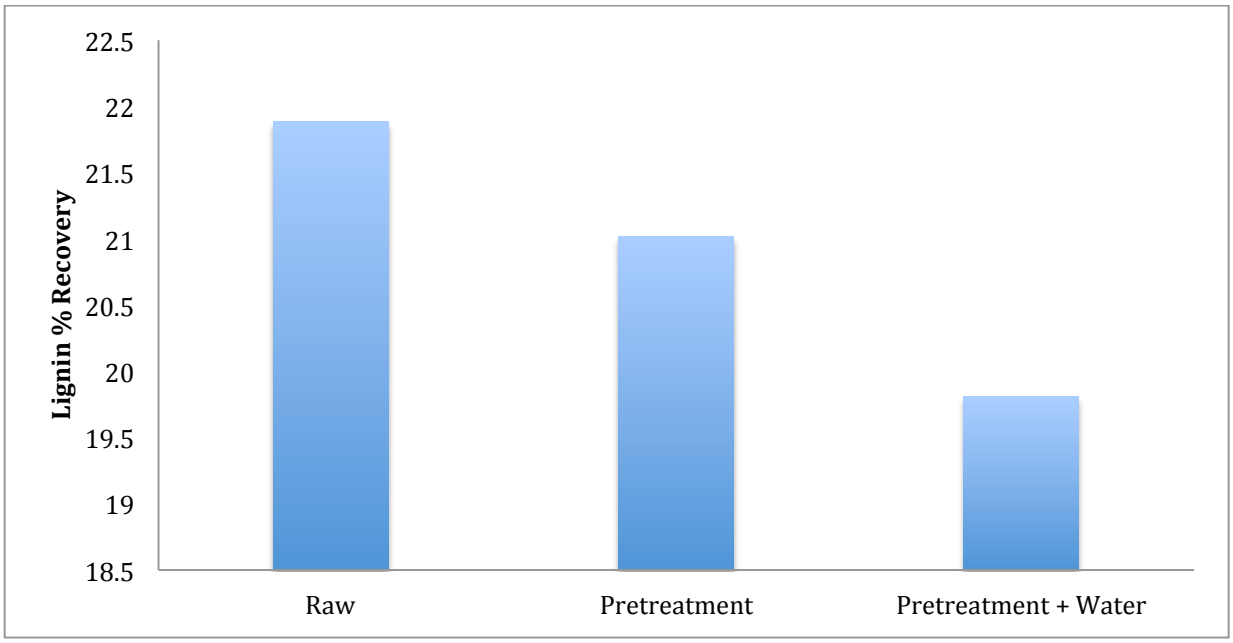

Figure 35. The % lignin recoveries for raw PCG, steam-pretreated PCG and steam-pretreated PCG with water are 21.88, 21.01 and 19.81 respectively. Highest lignin recovery was seen for the raw PCG sample with out addition of water or steam-pretreatment.

Another experiment to determine optimal temperature required for high lignin recovery was performed. Five PCG samples were cooked with 15 mL EXS IL at 70, 80, 90, 110 and 130 °C for 3 hours in similar setup. The general PCG extraction procedure (section 5.1.1.1) was followed for lignin extraction from these five PCG samples at different temperatures. The % lignin recoveries from PCG extraction at 70, 80, 90, 110 and 130 °C were 9.80, 16.91, 21.97, 21.92 and 21.75 respectively. As shown in Figure 36, the highest lignin recovery was observed at 90 °C and this temperature was maintained in all further extraction procedures using Ils.

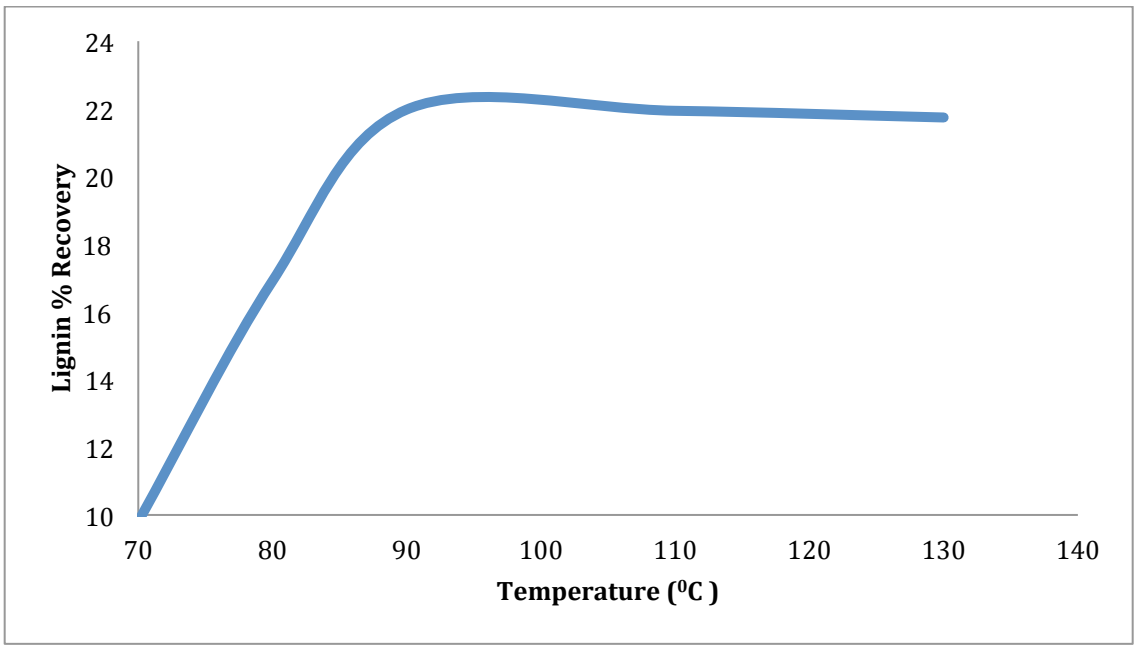

Figure 36. The % lignin recovery from PCG extraction at 70, 80, 90, 110 and 130 °C is 9.80, 16.91, 21.97, 21.92 and 21.75 respectively.

5.2. Dissolution of Lignin in 1-ethyl-3-methylimidazolium alkylbenzenesulfonate (EMIM-ABS) ionic liquids

The nature of cellulose and lignin inhibits dissolution in most solvents, thereby rendering most of the plant cell-wall area inaccessible to the solvents. Therefore, lignin dissolution experiment was conducted to analyze % recovery of free lignin dissolved in IL. Unlike the actual lignin extraction from PCG, the Il does not need to extract lignin form its co-plant material. Hence the main aim is to determine any major modifications occurring due to lignin and IL interactions. A 0.5 g lignin sample purchase from Sigma Aldrich was used for the dissolution study. The lignin sample was dissolved in 10 mL IL at 90 °C for 3 hours and the general extraction procedure from section 5.1.1.1 was followed to recover lignin from IL.

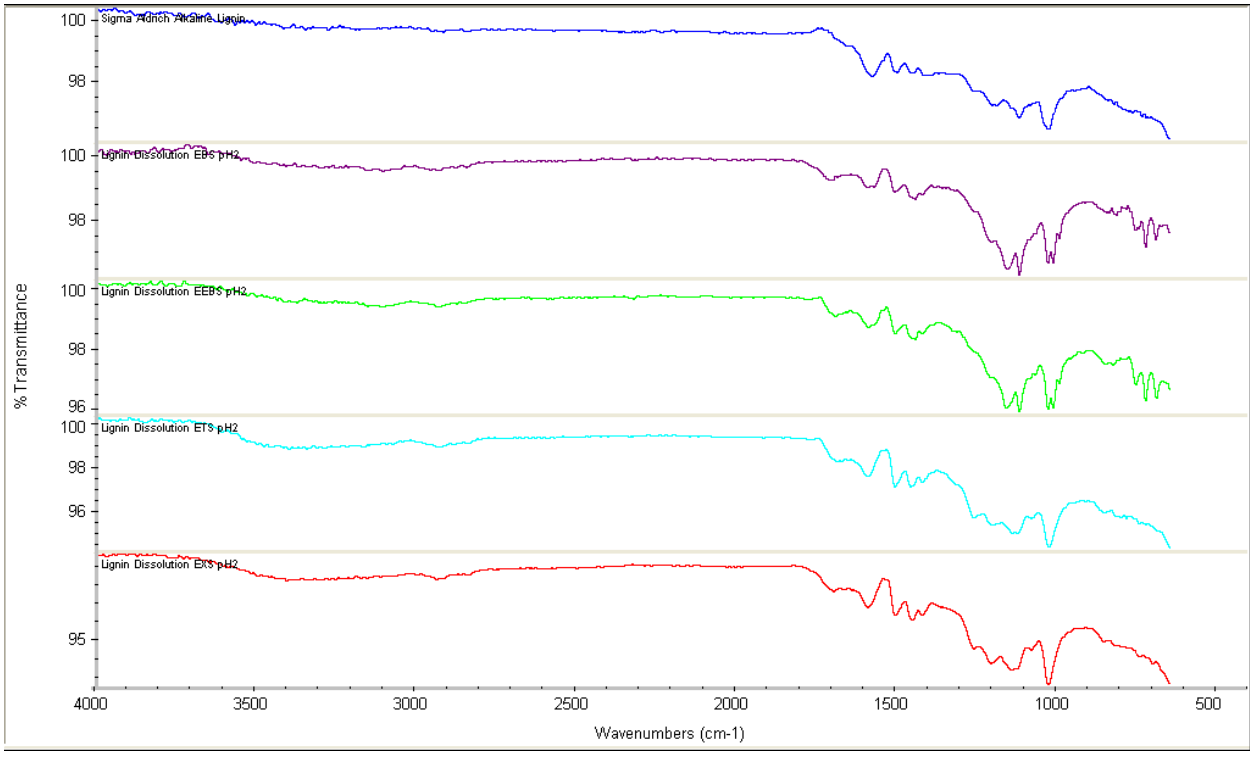

Figure 37. FTIR spectrum of recovered lignin from the lignin dissolution study with EBS, EEBS, EXS and ETS ILs.

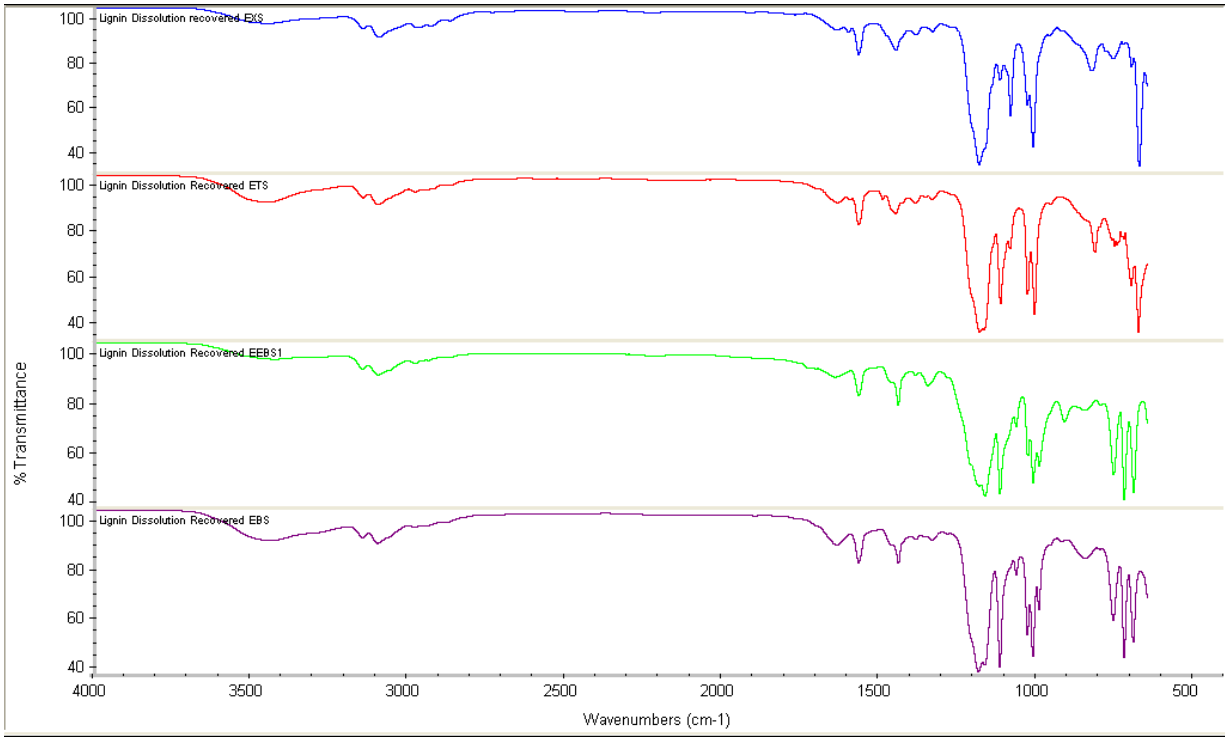

Figure 38. Infrared spectrum of recovered EBS, EEBS, ETS and EXS ILs from the lignin dissolution.

A 100 % lignin recovery was achieved from the lignin dissolved in all four ionic liquids. The Figures 37 and 38 show that no major modification was noticed in ETS and EXS recovered lignin from the dissolution study. Where as, the recovered lignin from EBS and EEBS show a small band near 1168 and larger band around 680 cm^{-1}. This band may be attributed to the symmetric SO_2 stretching and C-S stretching which is carried over from EBS and EEBS ILs to the recovered lignin.[6] All other typical lignin absorption

bands such as are intact in the recovered lignin. There are no major modifications observed in the recovered ILs.

5.3. Extraction of Lignin from PCG using EMIM-ABS Ionic Liquids

The four ILs in this research EBS, EEBS, ETS and EXS were employed to extract lignin from PCG. Around 3 g of PCG and 15 mL IL were cooked in a round bottom flask at 90 °C for 3 hours and the extraction procedure from section 5.1.1.1 was followed for lignin and IL recovery. The Figure 39 shows extraction efficiencies of the ILs. The % lignin recoveries from PCG extraction using EBS, EEBS, ETS and EXS ILs are 17.5±0.28, 17.4±0.53, 19.6±0.07 and 21.9±0.05 respectively. The recovery efficiencies of these ionic liquids are in the order EXS>ETS>EBS~EEBS of ILs. The EXS has the maximum lignin recovery from PCG, which agrees well with the literature.[4-6]

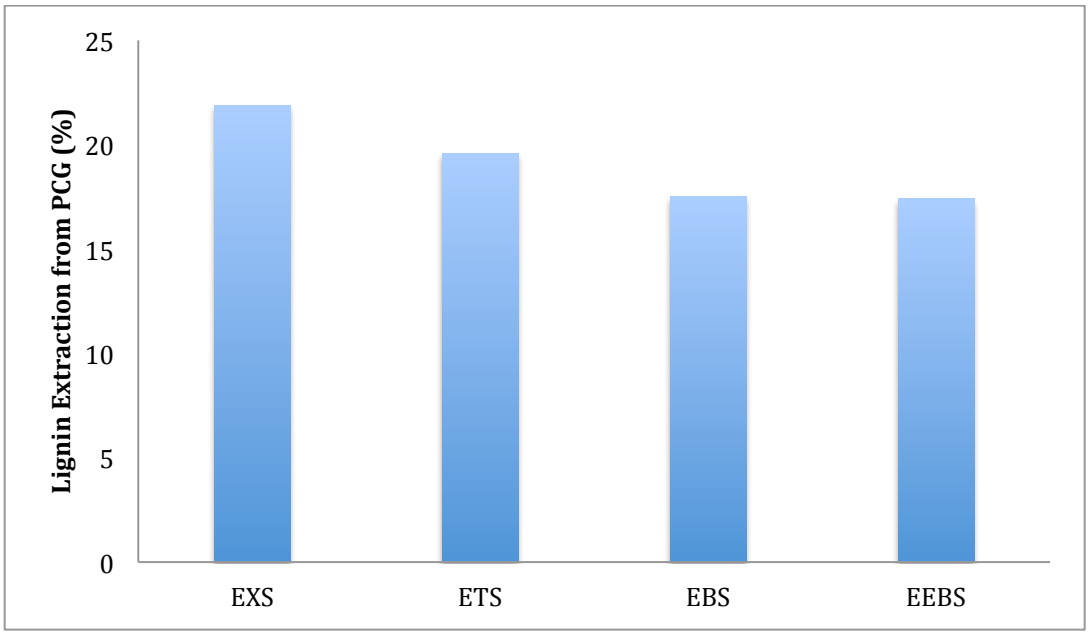

Figure 39. The % lignin isolation from PCG extraction for EBS, EEBS, ETS and EXS is 17.5±0.28, 17.4±0.53, 19.6±0.07 and 21.9±0.05 respectively.

5.3.1. FTIR of the lignin isolated from PCG

The Figures 40 and 41 show FTIR spectrum of isolated lignin and IL respectively. The tables 1 and 2 display major absorption bands from recovered lignin and recovered IL respectively. Spectra of the recovered lignins from PCG show similarities in the spectral profiles and are comparable with the earlier spectra of FTIR investigations of lignins.[7-9] The aromatic C-H in-plane deformation present at 1125 cm^{-1}, a C=O vibration of esters at 1167 cm^{-1} and a band due to aromatic C-H out of plane vibration at 834 cm^{-1}

of the PCG show the spectral features of *p*-hydroxyphenyl (H), guaiacyl (G) and syringyl (S) type lignins.[7-9]

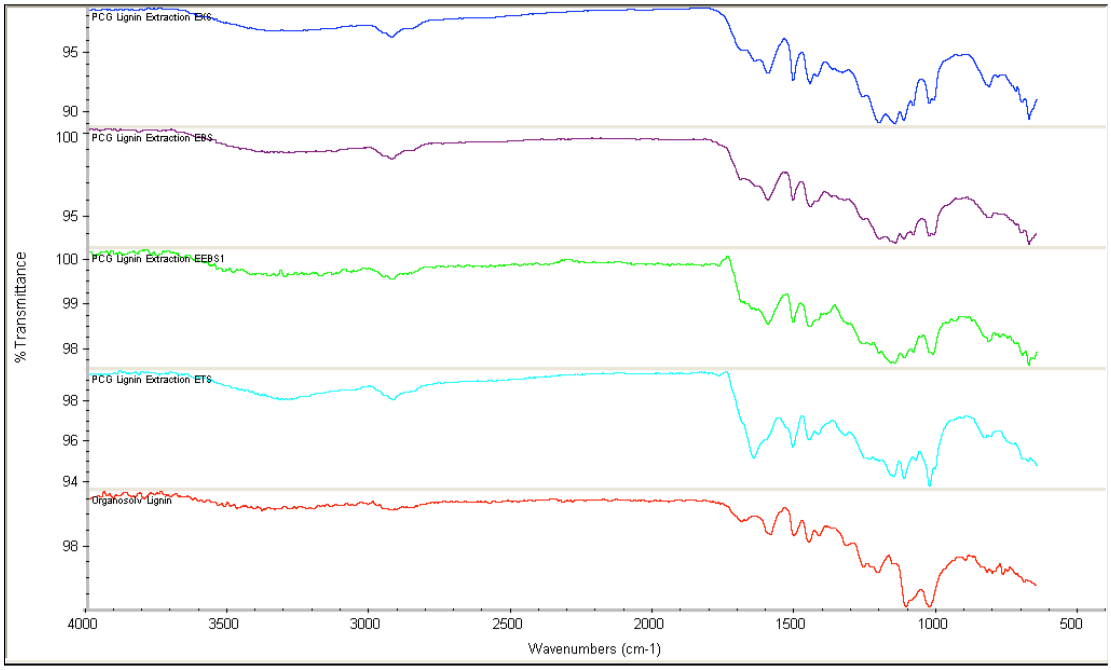

Figure 40. FTIR spectra of recovered lignin from the lignin dissolution study with EBS, EEBS, EXS and ETS ILs. An FTIR spectrum of the Organo-Solv lignin has been included as a reference lignin spectrum.

The C=O stretching frequency range between 1800-1633 cm^{-1} shows a strong absorption band of C=O for unconjugated ketones, carbonyls, and ester groups at 1737 cm^{-1} along with a C=O vibration band at 1270 cm^{-1}.[7] The band at 1500 cm^{-1} due to aromatic skeletal vibrations, the band at 1463 cm^{-1} due to C-H deformations and the band at 1330 cm^{-1} due to C-O vibration suggest the presence of guaiacyl (**G**) and syringyl

(**S**) moieties.[10] From these FTIR spectroscopic results, the recovered PCG lignin consists of the monomers of H, G, and S moieties.

Table 10. FTIR spectral absorption bands of recovered lignin from PCG extraction.

Absorption Band (cm^{-1})	**Band Origin**
3440–3200	O–H stretching
3189–3000	C–H stretching in methyl and methylene groups
1730–1700	C=O stretch in unconjugated ketone, carbonyl and in ester groups.
1670–1655	C=O stretch in conjugated *p*-substituted aryl ketones
160–1590	Aromatic skeletal vibrations plus C=O stretch
1510–1500	Aromatic skeletal vibrations; G>S
1470–1460	C–H deformations asymmetric in methyl and methylene
1430–1420	Aromatic skeletal vibrations plus C–H in plane deformations
1370–1360	Aliphatic C–H stretching in CH_3
1330–1320	S ring plus G ring condensed
1266–1270	G ring plus C=O stretch
1166	Typical for HGS lignins; C=O in ester groups conjugated
1140	Aromatic C–H in plane deformation; typical for G units
1035–1030	Aromatic C–H in plane deformation>S; C–O deformation in alcohols
858–853	C–H out of plane in position 2, 5, and 6 of G units
835–834	C–H out of plane in position 2 and 6 of S, and in all positions of H units

5.3.2. FTIR of the ionic liquids recovered from lignin extraction

As shown in Figure 41, there is no modification of the IL structure in the recovered ILS. Major absorption bands and the corresponding band origin are listed in the Table 11.

The absorption bands at 3500 and 3100 cm^{-1} show the presence of hetero-aromatic ring with N-H stretch and aromatic C-H stretching respectively. Along with the bands at 3500 and 3100 cm^{-1}, vibrations at 1574 and 1444 cm^{-1} give the evidence of the presence of aromatic imidazolium and benzene rings. Presence of the S-O and $S(=O)_2$ stretching frequencies at 1352 and 1195 cm^{-1} respectively support the presence of sulfonate group in the compound.[11,12] All values are in agreement with the FTIR frequency bands from literature.[11]

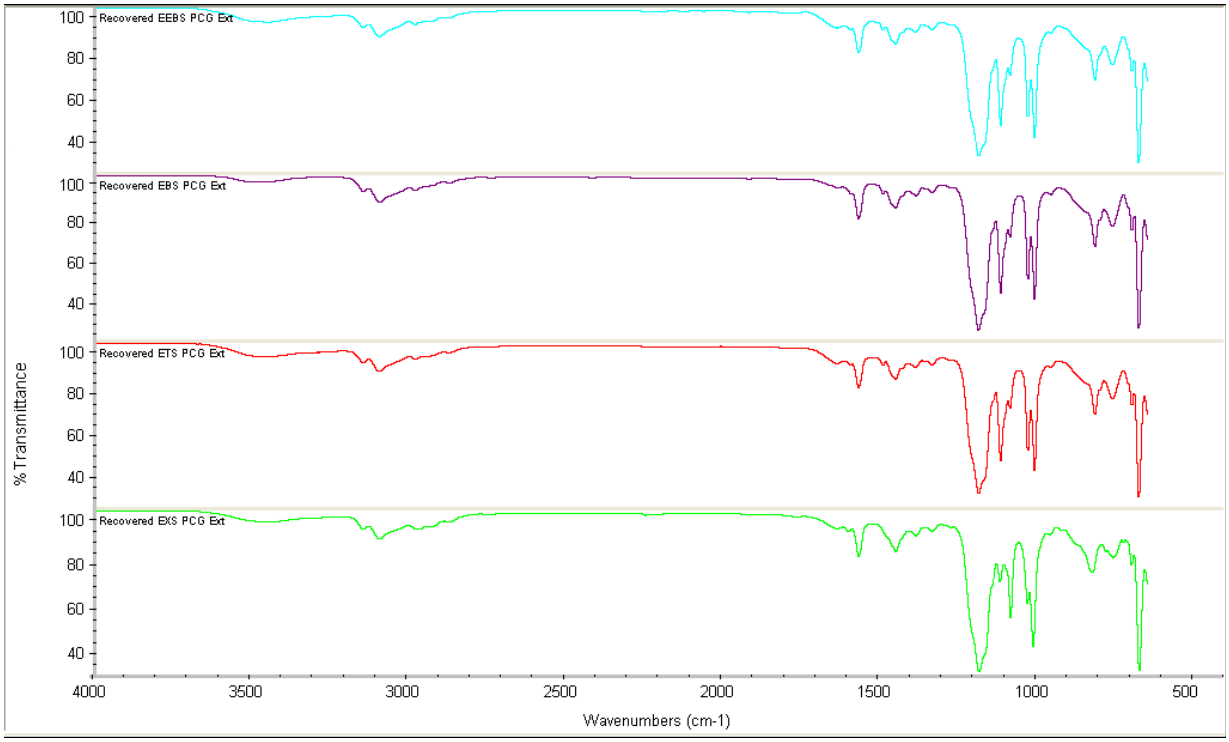

Figure 41. FTIR spectra of recovered ionic liquids EBS,EEBS, ETS and EXS from the Prairie cord grass as the biomass feed stock.

Table 11. FTIR spectral absorption bands of recovered ionic liquids from PCG extraction.

Absorption Band (cm^{-1})	Band Origin
3400-3600	Hetero-aromatic N-H stretching vibration
3000-3100	Aromatic C-H stretching
1550-1640	Hetero-aromatic ring stretching vibrations (C=C and C=N)
1444-1470	Skeletal bands or ring stretching vibrations (C=C and C=N)
1300-1352	Asymmetric S=O stretching
1150-1195	Symmetric stretching frequency of $S(=O)_2$
1100-1130	Stretching vibrations of S=O
1060-1069	In-plane C-H bending
1000-1033	In-plane C-H bending
930-997	Out of plane C-H bending
830-848	Out of plane C-H bending
600-760	Out of plane C-H bending & Out of plane ring C=C bending

5.4. Conclusion

The lignin recovery was found to be more efficient without the steam pretreatment and/or addition of water. The optimal temperature for lignin extraction is determined to be 90 °C for 3 hours. Clean lignin and IL recoveries were obtained during lignin dissolution while using ETS and EXS. This can be attributed to the symmetric SO_2 stretching and

C-S stretching which is carried over from EBS and EEBS ILs to the recovered lignin.[6] The lignin extraction efficiencies of the ILs were found to be in the following order: EXS>ETS>EBS~EEBS.

5.5. References

1. Swatloski, R. P.; Spear, S. K.; Holbrey, J. D.; Rogers, R. D. *J. Am. Chem. Soc.* **2002**, *124*, 4974–4975.

2. Fort, D. A.; Remsing, R. C.; Swatloski, R. P.; Moyna, P.; Moyna, G.; Rogers, R. D. *Green Chem.*, **2007**, *9*, 63–69.

3. Kilpelainen, I.; Xie, H.; King, A.; Granstrom, M.; Heikkinen, S.; Argyropoulos, D. S. *J. Agric. Food Chem.* **2007**, *55*, 9142–9148.

4. Myllymaeki, V.; Aksela, R. *WO Pat.* 2005/017001, 2005.

5. Upfal, J.; MacFarlane, D. R.; Forsyth, S. A. *WO Pat.* 2005/017252, 2005.

6. Suzie, S.; Tan, Y.; Douglas, R. M.; Jonathan, U.; Leslie, A. E.; William, O. S. D.; Antonio F. P.; Jennifer, M. P.; Janet, L. S.; Faix, O. *Holzforschung* **1991**, *45*, 21.

7. Derkacheva, O.; Sukhov, D. *Macromolecular Symposia* **2008**, *265*, 61.

8. Xu, F.; Sun, J.-X.; Sun, R.; Fowler, P.; Baird, M. S. *Industrial Crops and Products* **2006**, *23*, 180.

9. Tatiana, T.; Adina-Mirela Capraru; Kratochvilova, I.; Popa, V. I. *Cellulose Chemistry and Technology* **2009**, *43*, 399.

10. Jiang, W.; Wang, Y.; Voth, G. A. *J. Phys. Chem. B.* **2007**, *111,* 4812-4818.

11. Silverstein, R. M.; Webster, F. X.; Kiemle, D. J. *Spectrometric identification of organic compounds;* Hoboken, NJ: John Wiley & Sons, 2005.

Chapter 6

CONCLUSIONS AND FUTURE WORK

Lignin is the second most abundant natural polymer, which makes it a rich carbon source that can be utilized in making bio-fuel. It is difficult to isolate lignin from plant material due to its complex structural organization. A set of 1-ethyl-3-methylimidazolium alkylbenzenesulfonate ionic liquids were synthesized in this study, which can specifically isolate lignin from the plant bio-mass. Comprehensive structural, thermal and toxicological characterization was performed to understand the behavior of ionic liquids.

6.1. Synthesis of 1-ethyl-3-methylimidazolium alkylbenzenesulfonate ionic liquids

The 1-ethyl-3-methylimidazolium alkylbenzenesulfonate ionic liquids were synthesized using a metathesis reaction. Ionic couples with 1-ethyl-3-methylimidazolium acetate (EMIM–AC) and alkylbenzenesulfonate (ABS) anions were used to synthesize 1-ethyl-3-methylimidazolium benzenesulfonate (EBS), 1-ethyl-3-methylimidazolium toluenesulfonate (ETS), 1-ethyl-3-methylimidazolium xylenesulfonate (EXS). Another synthesis route was employed to synthesize 1-ethyl-3-methylimidazolium benzenesulfonate (EBS), where ethyl

benzenesulfonate was used as the anion source and 1-ethyl-3-methylimidazolium acetate as the cation parent. The 1-ethyl-3-methylimidazolium benzenesulfonate synthesized via this route was abbreviated as EEBS. The synthesis yield for EBS, EEBS, ETS, and EXS ionic liquids was determined to be 91.2 ± 1.5 %, 99.2 ± 0.2 %, 96.1 ± 0.7 %, 99.0 ± 0.5 % respectively.

6.2. Structural characterization of 1-ethyl-3-methylimidazoilum alkylbenzenesulfonate ionic liquid

The N-H absorption stretching at 3500 cm^{-1} and heteroaromatic C=C and C=N ring vibrations at 1572 and 1444 cm^{-1} were observed for all ILs in FTIR spectra. These are the characteristic absorption regions for the imidazolium cation. The absence of absorption at 1700 cm^{-1} (C=O group) shows elimination of acetate group as a by-product in the synthesized ILs. Vibration absorption between the sulfur and oxygen bonds in anions of ILs was observed at 1352 and 1122 cm^{-1} with a characteristic doublet asymmetric stretch at 1352 cm^{-1}.

The chemical shifts for all proton environments identified in the NMR spectra in this study supports the theoretical structures of IL's. The data from the FTIR and

NMR spectra indicates the complete elimination of sodium acetate from the synthesized ILs.

6.3. Physical characterization of 1-ethyl-3-methylimidazoilum alkylbenzenesulfonate ionic liquids

A significant increase in viscosity of ILs was observed with an addition of methyl group to the anion. This increase in viscosity can be attributed to stronger Van der Waals interactions and hydrogen bonding with addition of methyl group. Addition of methyl group also results in an increase in asymmetry and limited mobility due to increase in the anion size, which results in increased viscosity. The EBS, EEBS, ETS, and EXS showed 67, 67, 510 and 6467 cP viscosities at 25 °C respectively. A gradual decrease in the viscosity of ILs was noted with increase an in temperature. The water content of EBS, EEBS, ETS and EXS was found to be 352.7 ± 4.7, 346.7 ± 0.6, 280.0 ± 2.6, and 273.3 ± 0.6 ppm.

The EBS, EEBS, ETS, and EXS ILs are polar solvents which is evident by their polarity (E_T^N) values and have a dipolarity/polarizability (π^*) between 0.98 to 1.08. The calculated polarity E_T^N values of the ILs indicate that they are polar and hydrogen bond donors (HBD). The N-H bond and the three acidic ring protons on the imidazolium ring

attribute to the HBD ability of these ILs and the delocalized system on imidazolium results in high polarizability of these EBS, EEBS, ETS and EXS ILs. The hydrogen basicity (β) of these ILs range from 0.33 to 0.42, making them week hydrogen bond acceptors due to delocalized aromatic ring in anions. Addition of methyl group showed increase in the β parameter.

6.4. Thermal behavior of 1-ethyl-3-methylimidazoilum alkylbenzenesulfonate ionic liquids

Glass formation was observed when the IL's were cooled from 110 to -45 °C at 5 °C/min during the differential scanning colorimetric (DSC) analysis. Melting, crystallization or glass transition phase changes were not observed on simple DSC heating or cooling scans from -45 °C though 380 °C. Glass formation can be attributed to packing hindrance as a result of large, asymmetric ions in this study. The glass formation for EBS, EEBS, ETS and EXS started around -29.16 oC, -28.68 oC, -29.21 oC and -29.36 oC, respectively.

The ILs being analyzed in this study did not revert back to the same state as before cooling. Instead, it was noticed that the repeated heat-cool DSC cycles gave more mesophases in the ILs. Multiple phase transitions showing

several packing modes were observed in the DSC analysis of ILs due to the weak interactions between anion and cations. In the thermogravimetric analysis (TGA) of ILs, the EBS and EEBS were found to be more hygroscopic with an initial mass loss of 3.76 and 3.15% due to water when compared to ETS and EBS with 1.23 and 1.22% mass loss respectively.

TGA analysis of EBS, EEBS, ETS, and EXS ILs shows the decomposition at 349 °C, 349 °C, 331 °C and 319 °C respectively. Thermal stability of these IL tends to decrease with the increase in their molecular weight. The addition of methyl group on the benzene ring of anion decreased the thermal stability of the ETS and EXS ILs due to change in symmetry and orientation. There was no change in the rate of mass loss for EBS, EEBS, ETX and EXS ILs under different N2 flow rates. This result indicates that the significant mass loss identified in TGA analysis of ILs at the onset of mass loss around 300 °C can be attributed to the thermal decomposition behavior rather and not evaporation.

6.5. Toxicity analysis of 1-ethyl-3-methylimidazoilum alkylbenzenesulfonate ionic liquids

The EC_{50} for EBS, EEBS, ETS, EXS were found to be 3.24±0.03 mM, 3.36±0.18 mM, 3.03±0.04 mM and 2.88±0.06 mM

respectively from the lactate dehydrogenase (LDH) assay. A slight decrease in the EC_{50} values was observed with addition of methyl groups on the benzenesulfonate anion as in case of ETS and EXS. The addition of a methyl group on the anion decreased the EC_{50} of EMIM–ABS ILs, thereby increasing their cytotoxicity. This study shows that the anion plays a vital role in deciding the fate of ILs and the toxicity of EMIM–ABS ILs depends on the associated anion. The results of 3-(4,5-dimethylthiazol-2-yl)-2,5-diphenyltetrazolium bromide (MTT) Assay indicates similar results as the LDH assay, where, addition of methyl group on anion exhibited an increase in cytotoxicity. A decrease in EC_{50} with the addition of methyl groups was observed in ETS and EXS.

In contrast to the trend seen in cytotoxicity results from LDH and MTT assays, all ILs showed similar genotoxicity of 10 RCP (revertant colonies per plate). There was no notable increase in genotoxicity with an increase in methyl group on anion.

6.6. Lignin extraction from Prairiecord grass using ILs

The synthesized ILs, EBS, EEBS, ETS and EXS were used to extract lignin from Prairiecord grass (PCG). A better lignin yield was obtained using raw biomass feed stock when

compared to pretreated biomass. Adding water to the extraction mixture resulted in lower lignin recovery compared to the lignin extraction with no external water addition. The highest lignin extraction was obtained with extraction at 90 ℃ fro 3 hours. The % lignin recoveries from PCG extraction using EBS, EEBS, ETS and EXS ILs are 17.5±0.28, 17.4±0.53, 19.6±0.07 and 21.9±0.05 respectively.

The recovery efficiencies of these ionic liquids are in the order EXS>ETS>EBS~EEBS of ILs. FTIR Spectra of the recovered lignins from PCG using these ILs are comparable with the earlier spectra of FTIR investigations of lignins in this study. The lignin extraction efficiencies of the ILs were found to be in the following order: EXS>ETS>EBS~EEBS.

6.7. Future work

Unlike traditional solvents, ILs are designer solvents, which can be chemically tuned to achieve ideal ionic couples that are task specific. The IL interaction with both polar and non-polar molecules makes them good solvents. Hence methods developed in this study along with X-ray crystallography and advanced microscopy can be used to further investigate structural arrangement and mesophasic transitions of ILs. Radio-labeled carbon and

hydrogen experiments can be performed to analyze anion and cation interactions in various solute environments.

Lignin extraction procedures suggested in this study can be scaled up and the extracted lignin can be pyrolized to bio-oil. Research involving characterization of bio-oil from lignin pyrolysis and upgrading it to meet better fuel quality can be conducted. ILs have great potential to be used in research involving sensors and biomedical devices. Toxicity studies on animals and the IL metabolism fate can lead to the synthesis of eco-friendly solvents.